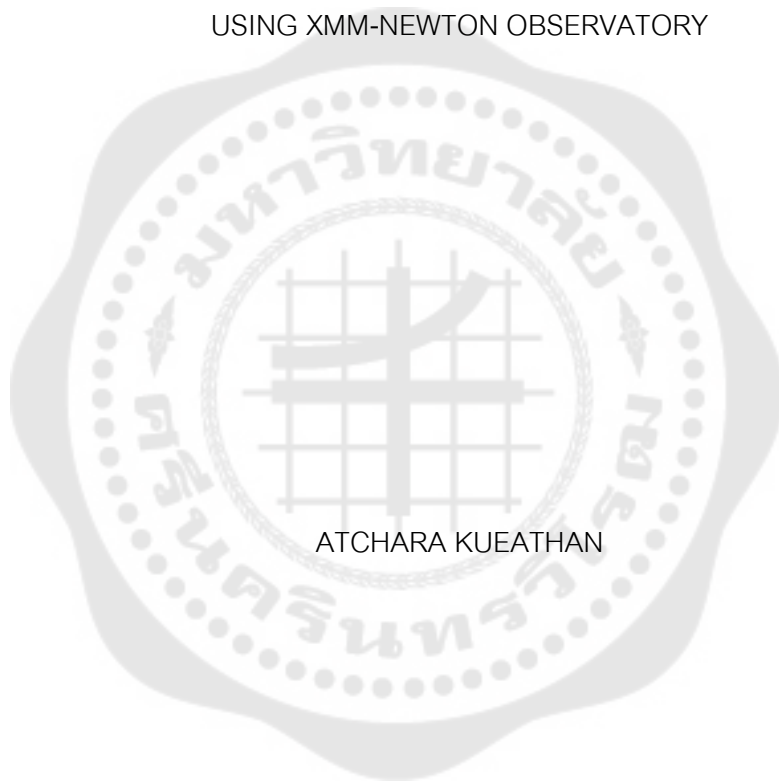




THE SEARCH FOR X-RAY EMISSION FROM AN ELECTRON/POSITRON PAIR HALO
USING XMM-NEWTON OBSERVATORY



ATCHARA KUEATHAN

Graduate School Srinakharinwirot University

2019

การค้นหาค่าการแผ่รังสีเอ็กซ์จากรากฏการณ์รัศมีคู่อิเล็กตรอน/โพสิตรอนโดยใช้สถานีสังเกตการณ์
เอกซ์เอ็มเอ็มนิวตัน



ปริญญานิพนธ์นี้เป็นส่วนหนึ่งของการศึกษาตามหลักสูตร
วิทยาศาสตร์มหาบัณฑิต สาขาวิชาฟิสิกส์
คณะวิทยาศาสตร์ มหาวิทยาลัยศรีนครินทรวิโรฒ
ปีการศึกษา 2562
ลิขสิทธิ์ของมหาวิทยาลัยศรีนครินทรวิโรฒ

THE SEARCH FOR X-RAY EMISSION FROM AN ELECTRON/POSITRON PAIR HALO
USING XMM-NEWTON OBSERVATORY



ATCHARA KUEATHAN

A Thesis Submitted in Partial Fulfillment of the Requirements
for the Degree of MASTER OF SCIENCE
(Physics)

Faculty of Science, Srinakharinwirot University

2019

Copyright of Srinakharinwirot University

THE THESIS TITLED
THE SEARCH FOR X-RAY EMISSION FROM AN ELECTRON/POSITRON PAIR HALO
USING XMM-NEWTON OBSERVATORY

BY
ATCHARA KUEATHAN

HAS BEEN APPROVED BY THE GRADUATE SCHOOL IN PARTIAL FULFILLMENT
OF THE REQUIREMENTS FOR THE MASTER OF SCIENCE
IN PHYSICS AT SRINAKHARINWIROT UNIVERSITY

(Assoc. Prof. Dr. Chatchai Ekpanyaskul, MD.)
Dean of Graduate School

ORAL DEFENSE COMMITTEE

..... Major-advisor Chair
(Dr.Wasutep Luangtip)	(Dr.Utane Sawangwit)
..... Co-advisor Committee
(Dr.Anant Eungwanichayapant)	(Asst. Prof. Dr.Patipan Utayarat)

Title	THE SEARCH FOR X-RAY EMISSION FROM AN ELECTRON/POSITRON PAIR HALO USING XMM-NEWTON OBSERVATORY
Author	ATCHARA KUEATHAN
Degree	MASTER OF SCIENCE
Academic Year	2019
Thesis Advisor	Dr. Wasutep Luangtip
Co Advisor	Dr. Anant Eungwanichayapant

The electron/positron pair halo is a physical phenomenon formed by electromagnetic cascades. It initiates when the very high energy gamma-rays emitted from Blazar interact with cosmic infrared background (CIB), to produce electron/positron pairs; the produced electron/positron pairs could up-scatter the cosmic microwave background (CMB) reproducing the gamma-rays. Thus, the cascade process of producing the electron/positron pairs appear as a halo around the central blazar. Indeed, given the presence of the ambient intergalactic magnetic field, the electron/positron pairs could emit X-ray light via synchrotron process providing another opportunity to detect the halo. In this research, we search for the X-ray emission from the halo of the candidate source - Blazar H1426+428 - using the observed X-ray data from *XMM-Newton* observatory. The Monte Carlo simulation was adopted to compute the X-ray Spectral Energy Distributions (SEDs) in order to predict the X-ray emission of the Blazar H1426+428's pair halo, and used these SEDs as a source model for simulating the spectra of the halo virtually observed by *XMM-Newton*. The results of the X-ray SEDs of H1426+428 suggest that the region that could provide the best opportunity to detect electron/positron pair halos is the outer region of the *XMM-Newton*'s field of view. After that, we extracted X-ray spectra of the halo from the annulus, source-free regions around the Blazar, following the best halo detecting area suggested by previous simulated results. The X-ray contaminations from the Blazar and the point sources in the field were also excluded during this step. The extracted spectra were fitted using the physical model which took into account the emissions from the known cosmic X-ray emissions and instrument background. The unresolved flux of 10^{-13} erg/cm²/s¹ were detected in the analyzed regions, and it was argued that, at least, some fraction of the flux might be emissions from the pair halo.

Keyword : Electron/positron pair halo, XMM-Newton observatory, Blazar, H1426+428, Electromagnetic Cascades

ACKNOWLEDGEMENTS

This thesis has been funded by the Science Achievement Scholarship of Thailand (SAST) and the Theoretical High-Energy Physics and Astrophysics group (THEPA).

I would like to thank my chair examiner, Dr. Utane Sawangwit.

I am very grateful to a number of people, who have been instrumental in getting this thesis to completion. Some, however, deserve special mention:

My advisors – Dr. Wasutep Luangtip and Dr. Anant Eungwanichayapant who gave unfailing support.

Asst. Prof. Dr. Patipan Utayarat - who always support and inspired me throughout the course my master studies.

My mum and dad – who will be happy pleased when I start a job with a salary.

William Duggan – who taught me the positive stuff.

Nutt Thanaboonrungrach – the bad fryer, the best person to travel with.

Grittichon Chanilkul – simply but he is Grittichon.

Wararat Treesukrat – the best friend ever.

Pachara Threetanya – the best brother who encouraged me.

Surasak Loekkesee – who spent a lot of time listening me when I was stressful.

ATCHARA KUEATHAN

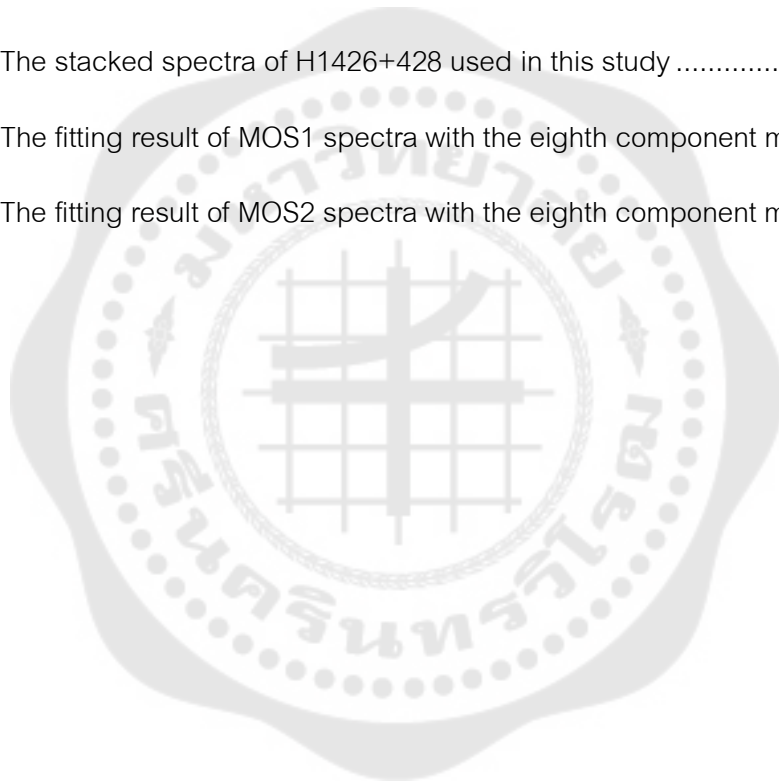
TABLE OF CONTENTS

	Page
ABSTRACT.....	D
ACKNOWLEDGEMENTS.....	E
TABLE OF CONTENTS.....	F
LIST OF TABLES.....	H
LIST OF FIGURES.....	I
CHAPTER 1 INTRODUCTION.....	1
An electron/positron pair halo.....	1
The synchrotron radiation of pair halo.....	4
The physical model of pair halo.....	6
The <i>XMM-Newton</i> observatory.....	9
Aims of this work.....	12
CHAPTER 2 LITERATURE REVIEW.....	14
CHAPTER 3 SIMULATION OF X-RAY SEDs.....	19
Introduction.....	19
Source selection.....	20
An X-ray Spectral Energy Distribution from an electron/positron pair halo.....	23
Simulation of <i>XMM-Newton</i> spectra.....	26
Discussion.....	30
Conclusion.....	34
CHAPTER 4 X-RAY SPECTRAL ANALYSIS.....	35
Introduction.....	35

Observations and data reduction	35
Spectral analysis and results.....	42
Discussion	54
Conclusion.....	58
CHAPTER 5 CONCLUSION.....	59
Conclusion.....	59
Future work	61
APPENDIX.....	64
Appendix A The result of emission time distribution.	65
Appendix B The result of X-ray SEDs of H1426+428's pair halo.....	79
Appendix C Research publications.....	87
REFERENCES.....	100
VITA.....	105

LIST OF TABLES

	Page
Table 1 Summary of operating modes of EPIC MOS and pn CCDs.	10
Table 2 The count rate and total counts of H1426+428's halo observed in region A, B and C by <i>XMM-Newton</i> pn, MOS1 and MOS2 detector for 500 ks.....	27
Table 3 <i>XMM-Newton</i> observational data of H1426+428.....	38
Table 4 The stacked spectra of H1426+428 used in this study	41
Table 5 The fitting result of MOS1 spectra with the eighth component model.....	52
Table 6 The fitting result of MOS2 spectra with the eighth component model.....	53



LIST OF FIGURES

	Page
Figure 1 The unification model of AGN suggesting that the observed type of AGN depends on the angle of view.	2
Figure 2 The electromagnetics cascade diagram.	4
Figure 3 The synchrotron radiation which results in X-ray radiation of pair halo.....	5
Figure 4 The physical process of an electron/positron pair halo.....	6
Figure 5 The pair production and inverse Compton scattering mean free paths, plotted together with the electron/positron gyroradius for a magnetic field B of 10^{-9} G	8
Figure 6 The sketch of the <i>XMM-Newton</i> X-ray payload: the EPIC MOS cameras (green) and the radiator of the EPIC pn camera (violet).....	9
Figure 7 The <i>XMM-Newton</i> circular field of view and CCD chip sizes: EPIC MOS (<i>left</i>) and EPIC pn (<i>right</i>).	11
Figure 8 The example images obtained from each operating modes for the MOS cameras. <i>Top left</i> : Full Frame mode; <i>top right</i> : Large Window mode; <i>bottom left</i> : Small Window mode, and <i>bottom right</i> : Timing mode.	12
Figure 9 The X-ray SEDs and X-ray angular distribution of the pair halo in different levels magnetic field.	16
Figure 10 The VHE blazar sky map which were detected and identified by VERITAS...	20
Figure 11 The absorbed gamma-ray spectra of the blazar H1426+428.	21
Figure 12 The pair halo SED from monoenergetic source with $E_0=100$ TeV emitting within 1° along with the H.E.S.S. point source sensitivity.	22
Figure 13 The procedure to calculate the energy distributions of the electron/positron.	25
Figure 14 The example MOS observation of the H1428+428. The overlaying yellow lines divide the image into region A, B and C which are used in the simulation; the angular	

distance of each line from the centre is indicated in white. The blue dashed lines indicate the boundary of each CCD chip of MOS detector.....	26
Figure 15 <i>Top left panel:</i> The emission time distributions of H1426+428 within 0.3 degree. <i>Top Right panel:</i> The emission time distribution in region A, which covers the angular distance from 0-0.133 degrees. <i>Bottom Left panel:</i> The emission time distribution in region B, which covers the angular distance from 0.133-0.200 degrees. <i>Bottom Right panel:</i> The emission time distribution in region C which covers the angular distance from 0.200 to infinite degree and is an area outside the <i>XMM-Newton</i> field of view.....	29
Figure 16 The pair halo X-rays SEDs simulated by assuming the AGN properties following the properties of H1426+428. The simulation was divided into three regions - region A, B and C - for purpose of study of the detection (see text).	31
Figure 17 The simulated MOS1 spectra of the halo obtained from H1426+428's halo in region A, B and C.....	32
Figure 18 The simulated MOS2 spectra of the halo obtained from H1426+428's halo..	33
Figure 19 The simulated pn spectra of the halo obtained from H1426+428's halo.....	33
Figure 20 The procedure to reduce the observational data of H1426+428, which follows the instructions in the <i>XMM-Newton</i> Extended Source Analysis web page.....	37
Figure 21 The example of clean pn images.....	39
Figure 22 The example MOS image after excising point source using CHEESE script.	39
Figure 23 The comparison between analysing regions used in Chapter 3 and this chapter. <i>Left panel:</i> The overlaying yellow lines divide the observation into the region A, B and C used in the analysis in Chapter 3. The angular distance of each line from the centre is indicated in white. <i>Right panel:</i> The overlaying yellow lines divide the observation into region B1, B2 and B3 used in the analysis of this chapter; the angular distance of each line from the centre is indicated in white. The blue dashed line indicated the boundary of each CCD	42

Figure 24 The example spectra of stacked MOS1 from Region B1.....	44
Figure 25 The example spectra of stacked MOS1 from Region B1.....	45
Figure 26 <i>Top panel:</i> The model data best fitting with M1-B1 (black), M1-B2 (red) and M1-B3 (green) spectra. <i>Bottom panel:</i> The residue plot of with M1-B1 (black), M1-B2 (red) and M1-B3 (green) spectra.	48
Figure 27 <i>Top panel:</i> The model data best fitting with M1-B1-ANO (black), M1-B2-ANO (red) and M1-B3-ANO (green) spectra. <i>Bottom panel:</i> The residue plot of with M1-B1-ANO (black), M1-B2-ANO (red) and M1-B3 -ANO (green) spectra.	49
Figure 28 <i>Top panel:</i> The model data best fitting with M2-B1 (blue), M2-B2 (orange) and M2-B3 (pink) spectra. <i>Bottom panel:</i> The residue plot of with M2-B1 (blue), M2-B2 (orange) and M2-B3 (pink) spectra.	50
Figure 29 <i>Top panel:</i> The model data best fitting with M2-B1-ANO (blue), M2-B2-ANO (orange) and M2-B3-ANO (pink) spectra. <i>Bottom panel:</i> The residue plot of with M2-B1-ANO (blue), M2-B2-ANO (orange) and M2-B3-ANO (pink) spectra.....	51
Figure 30 The fitting residue obtained from the model without (top panel) and with blackbody (bottom panel) component.....	57

CHAPTER 1

INTRODUCTION

An electron/positron pair halo is a predicted phenomenon in astrophysics that could emitted electromagnetic waves, especially gamma-rays, appearing as a halo to a distance observer. Due to the prediction, almost pair halo studies focused to search for this phenomenon only in gamma-ray waveband. In fact, the studies of absorption of gamma-rays relating to the pair halo mechanism in the intergalactic medium could be one of windows to study cosmic history because the absorption of gamma-rays also contains an important information about the cosmic infrared background at each epoch, corresponding to the redshift of the central source. However, it has been proposed that an electron/positron pair halo could also emitted photons in another electromagnetic waveband – i.e. X-ray – via synchrotron radiation when the pair halo happens in the suitable level of intergalactic magnetic field (A Eungwanichayapant, Maithong, & Ruffolo, 2011). This thesis will focus on this topic by searching for the pair halo in X-ray waveband using data from *XMM-Newton* X-ray observatory, which might provide another new window to observe it. We will start this chapter with the detail of an electron/positron pair halo. Then, the synchrotron radiation and how to obtain the X-rays from an electron/positron will be discussed. Finally, the *XMM-Newton* observatory and its equipped instruments used to search for the pair halo in this thesis will be explained.

An electron/positron pair halo

It has been known since 1961 (Nikishov, 1961) that the universe in that era is opaque for gamma rays with very high energy (VHE; $E > 100$ GeV) that come from an extragalactic source: i.e. blazar, a subtype of AGN that has its jets pointing towards to the earth as presented in Figure 1. In fact, VHE gamma rays from relativistic jets of blazar (Schlickeiser, 1996) can interact with low energy photons: cosmic infrared background (CIB) and Cosmic Microwave Background (CMB). The interactions between

VHE gamma-rays and the lower energy photons results in an *electromagnetic cascade*, in which the VHE photons are converted into lower energy photons travelling further into the space as shown in Figure 2.

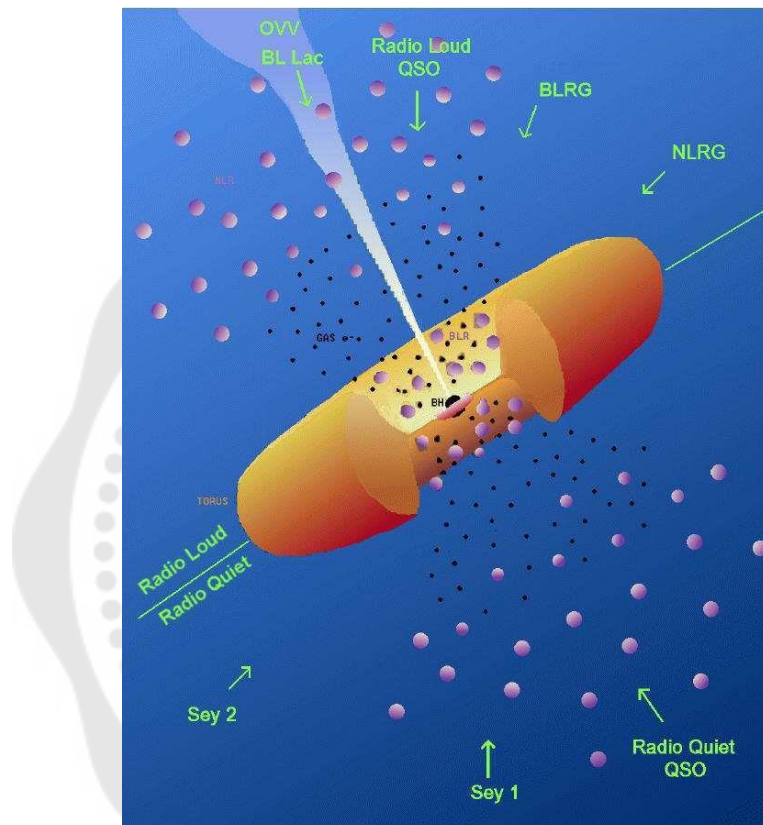


Figure 1 The unification model of AGN suggesting that the observed type of AGN depends on the angle of view.

Source: Urry and Padovani (1995) Unified Schemes for Radio-Loud Active Galactic Nuclei.

In brief, the cascade begins by the absorption of these VHE photons by CIB via pair production process so that produces electron/positron pairs. After that, the resulting electron/positron pairs could interact with the soft photon background via

inverse Compton scattering so that the soft photons become secondary gamma-ray photons which their energy is in the gamma-ray regime again. These secondary gamma photons can turn into the electron/positron pairs by interacting with the soft photon background again, similar to that of the primarily gamma-rays do. These cascades could develop continuously until the Compton up-scattered photons are not sufficiently energetic to create the next generation of electron/positron pairs. Moreover, if the Intergalactic Magnetic Field (IGMF) is taken into account, the forms of electromagnetic cascade would depend on the strength of the IGMF (B) in which the trajectory of electron/positron pair would be different, resulting in different scenarios for searching them. For a weak IGMF ($B < 10^{-14}$ G) the cascade develops and points forward direction to observer (Attila Abramowski et al., 2014). In case of a moderate IGMF (10^{-12} G $< B < 10^{-7}$ G) the electron/positron pairs that the trajectory are isotropised around the source, resulting in an extended isotropic emission of photons around the central source, defined as an electron/positron pair halo. In this case, the photons would take much longer time to reach the observer, comparing to that of the direct photons from the source (FA Aharonian, Coppi, & Völk, 1993). Finally, for a strong IGMF intensity ($B > 10^{-7}$ G), the synchrotron cooling becomes dominant the Compton cooling so that no secondary gamma rays are produced (R. Gould & Rephaeli, 1978) because the gyroradius (R_{gyro}) of electron/positron is much less than the inverse Compton scattering (IC) mean free path (λ_{IC}). Therefore, to detect the pair halo, ones may focus only on an electron/positron pair halo that occurs in the moderate IGMF since the pair halo photons would take much longer time to reach the observer and also look like a quasi-spherical halo around the source.

Since this effect has been theoretically proposed, the search for electron/positron pair halo has been attempted in gamma-ray waveband by several groups. Until now, the electron/positron pair haloes have been still only a theoretically prediction, and the detection has not been successful yet.

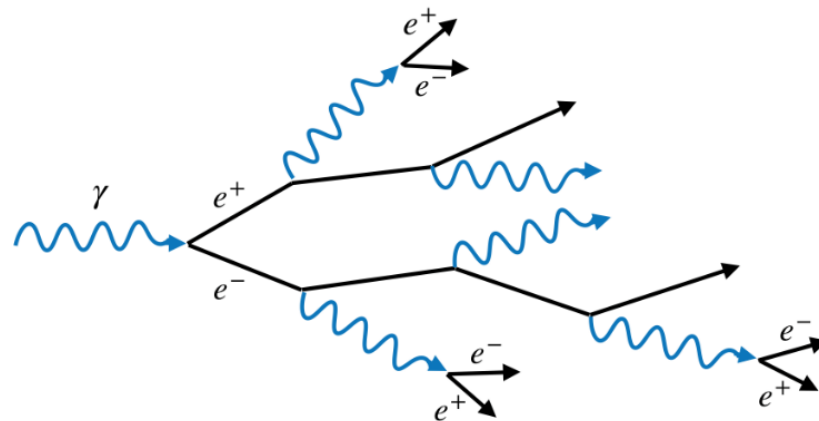


Figure 2 The electromagnetics cascade diagram.

Source: Maithong (2012). X-Ray distributions from pair halos around extragalactic sources.

However, the search for the pair halo has still been one of the challenging topics and, up to now, there has been an attempt to observe it in gamma-ray regime by many groups. However, as explained above, the electron/positron pair halo might not radiate the gamma-rays only, but could also radiate the X-ray photons as well via the synchrotron radiation, since the produced electron/positron could gyrate in IGMF (we will explain the physics of the radiation process generating this X-ray emission in next section). Therefore, in this work, we will search for an electron/positron pair halo in X-ray regime, instead of searching in the gamma-ray regime. In fact, this work would make a new way to confirm the existence of an electron/positron pair halo using the *XMM-Newton* X-ray observatory.

The synchrotron radiation of pair halo

In previous section, it was explained that when the IGMF is taken into account, the trajectory of electron/positron pair could be different. In fact, if a sufficiently level of

IGMF presented in the area of the halo, the synchrotron photons could be radiated so that are defined as synchrotron radiation of pair halo.

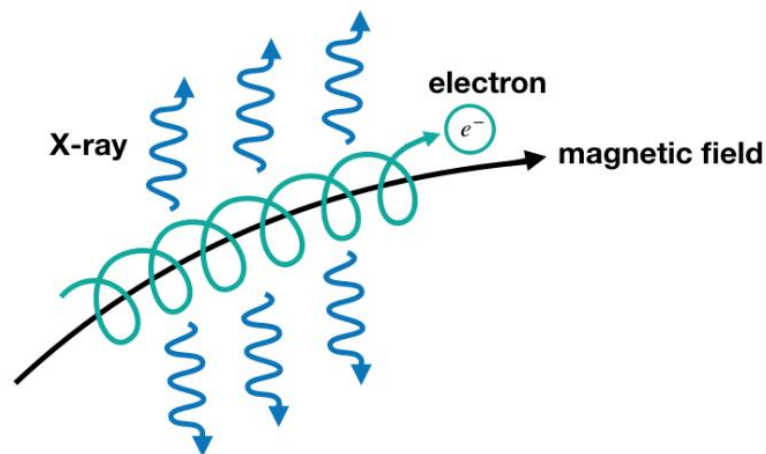


Figure 3 The synchrotron radiation which results in X-ray radiation of pair halo.

Source: Maithong (2012). X-Ray distributions from pair halos around extragalactic sources.

Generally, synchrotron radiation - which is responsible for non-thermal emission i.e. emission from charged particles such as from electron and positron, occurs when a charged particle was move at relativistic speed in magnetic field (Figure 3). Indeed, the charge particle is forced to move circularly around the field line appearing as a helical path. As a result, the accelerating charged particle emits electromagnetic radiation. The term “synchrotron” refers to an emission that is radiated along the direction in which the particle is moving. The synchrotron photons from the halo are emitted electromagnetic wave especially in X-ray band providing the window to observe the emission of an electron/positron in X-ray band. In this thesis, the Monte Carlo simulation will be adopted for computing the energy distribution of an

electron/positron pair halo and the result will be used to calculate the spectra energy distribution (SED) of X-ray from a pair halo following the physical model of pair halo which we will discuss in next section.

The physical model of pair halo

An electron/positron pair halo model was proposed in 1993 by Aharonian, Coppi and Völk (FA Aharonian et al., 1993); this was the first model concerning about the effect of the IGMF on electromagnetics cascade of VHE gamma rays from the extragalactic source.

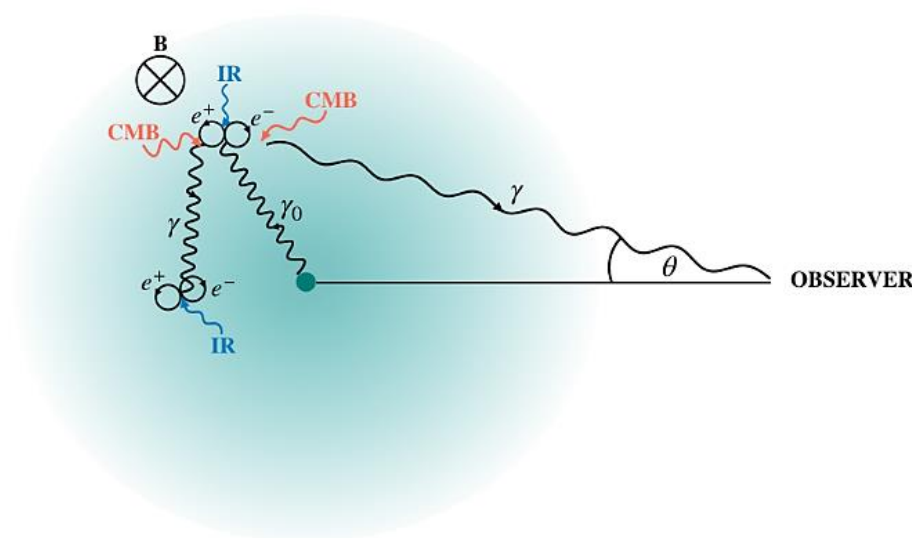


Figure 4 The physical process of an electron/positron pair halo.

Source: Eungwanichayapant (2003). Giant pair halos surrounding non-thermal extragalactic objects.

This physical model of electron/positron pair halo is schematically shown in Figure 4. In brief, it begins by the extragalactic source - i.e. blazar – emitting VHE

gamma-ray photons (Anant Eungwanichayapant, 2003). These VHE photons are absorbed by an ambient soft photon (e.g. from the CIB (Stecker, De Jager, & Salamon, 1992; Tkaczyk, Wdowczyk, & Wolfendale, 1975) and CMB (R. J. Gould & Schröder, 1966)); indeed, the absorption depends on the energy of VHE gamma photon. In the case of gamma rays with energies greater than several hundred TeV, they could interact with CMB photons and produce electron/positron pair via pair production process. In contrast, for a gamma photon with energy lower than hundred TeV, it could produce a pair production via a collision of gamma photons and CIB photons via IC process instead. Normally, the density of the lower energy gamma photons is higher than that of the higher energy photons. This means that most electron/positron pairs are produced via pair production process from the collision with CIB photon. The first generation of electron/positron pairs could then interact with the same types of background photons via IC process; as a result, the background photons - which is dominated by CMB rather than CIB since it has a much higher density than the CIB - could be up-scattered to become secondary gamma-ray photons.

If the electromagnetic cascade occurs in the sufficiently strong magnetic field ($|B| \approx 10^{-9}$ G), the gyroradius (R_{gyro}) of electron/positron energies E_e could be determined as $R_{\text{gyro}} = 100 \text{ pc} \left(\frac{E_e}{100 \text{ TeV}} \right) (10^{-9} \text{ G} / |B|)$ (Anant Eungwanichayapant, 2003). Figure 5 shows the pair production and inverse Compton scattering mean free paths plotted together with an electron/positron gyro radius for magnetic field $|B|$ of $\approx 10^{-9}$ G (Anant Eungwanichayapant, 2003). At $E_e \approx 100$ TeV, the inverse Compton scattering (IC) mean free path (Λ_{IC}) is $\approx 1 \text{ kpc}$. Obviously, the mean free path of gyro radius is lower than that of inverse Compton scattering: i.e. $R_{\text{gyro}} \ll \Lambda_{\text{IC}}$. This means that after electrons/positrons are produced via pair production, they could gyrate several times before interacting with soft photon via inverse Compton scattering producing the isotopically secondary gamma-ray photons. The up-scattered secondary gamma rays could continually produce a new generation of an electron/positron pairs, resulting in the electromagnetic cascade of the gamma-rays. This cascade could develop until the gamma rays of final generation have insufficient energy which is less than the threshold

energy: $E_{\text{eth}} = m_e^2 c^4 / E_e$ (Anant Eungwanichayapant, 2003). As a result, after several cascade generations, there are a large number of electron/positrons distributed isotropically around a VHE gamma-ray source. Importantly, these pairs would produce electromagnetic waves – especially in X-ray waveband - which might be observed by an observer from the earth.

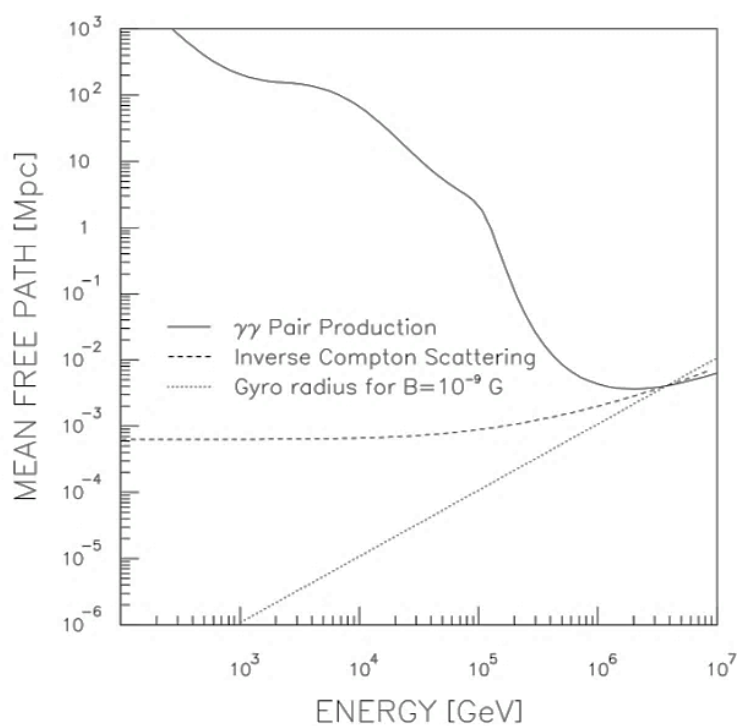


Figure 5 The pair production and inverse Compton scattering mean free paths, plotted together with the electron/positron gyroradius for a magnetic field B of 10^{-9} G

Source: Eungwanichayapant (2003). Giant pair halos surrounding non-thermal extragalactic objects.

The *XMM-Newton* observatory

X-ray Multi-Mirror Mission is one of the most successful astronomy missions (also known as *XMM-Newton* observatory). It was launched by the European Space Agency (ESA) on December 10th, 1999. It carries a telescope that offers a great observation in X-ray waveband, including with one optical monitoring telescope. A key aspect of the designed *XMM-Newton* observatory was the simultaneous operation of 6 coaligned instruments as shown in Figure 6: the three EPIC (European Photon Imaging Camera) imaging X-ray cameras which consisted of two types of X-ray payload; EPIC MOS and EPIC pn cameras, the two RGS (Reflection Grating Spectrometer) and the OM (Optical Monitor). In this thesis, the analyzed data was obtained from the EPICs and so the principals of this instrument will be explained here. However, more information on OM and RGS could be found on the *XMM-Newton* User's Handbook webpage.

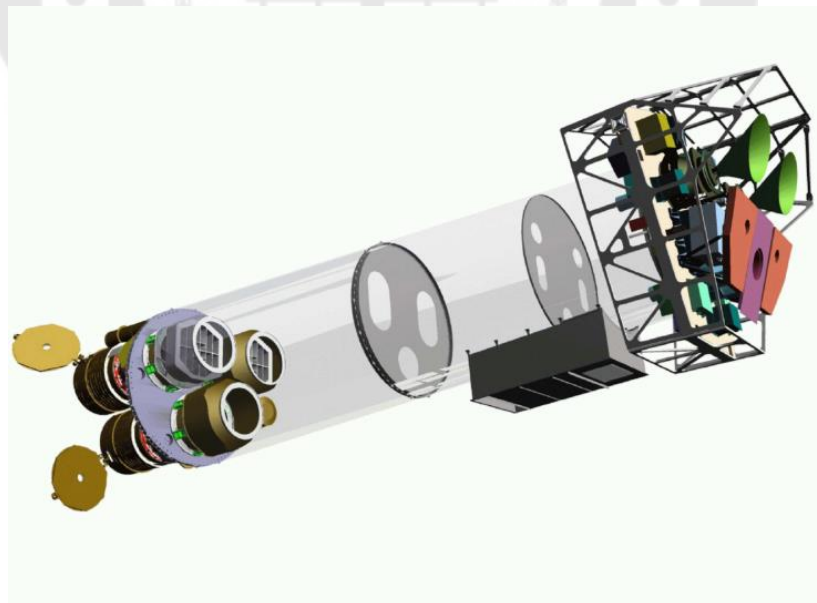


Figure 6 The sketch of the *XMM-Newton* X-ray payload: the EPIC MOS cameras (green) and the radiator of the EPIC pn camera (violet).

Source: The *XMM-Newton* community support (2019). *XMM-Newton* user's handbook.

As we explained above that the EPIC imaging X-ray cameras are a set of three X-ray CCD cameras (Strüder et al., 2001; Turner et al., 2001). One camera, pn CCDs, which the CCDs were referred to as the pn camera was produced by the implanted junction semiconductor technology. The other camera that the camera contains two MOS CCD arrays are known as the MOS camera; two of MOS detectors were produced by the Metal-Oxide-Semiconductor technology. Two MOS cameras were installed behind the X-ray telescopes that are equipped with the RGS. The pn camera was installed at the focus as the third of the X-ray telescope. The telescopes field of view (FOV) of the EPIC cameras perform the sensitive imagine observations around $30'$ of FOV with the energy range from ~ 0.15 to ~ 15.0 keV with moderate spectral resolution ($E/\Delta E \sim 20 - 50$). The geometry of the two EPIC MOS and pn detectors is shown in Figure 7. This EPIC MOS consists of seven chips in which each CCD is not co-planar, but they are offset concerning each other which is following the slight curvature of the focal plane of the Wolter telescopes. For the EPIC pn, the camera is a single silicon wafer with 12 CCD chips integrated.

Table 1 Summary of operating modes of EPIC MOS and pn CCDs.

Operating mode	Image area in pixel (in arcmin)		Time resolution	
	MOS	pn	MOS	pn
Full Frame	600 × 600 (11" × 11")	376 × 384 (26" × 27")	2.6 s	73.4 ms
Large Window	300 × 300 (5.5" × 5.5")	198 × 384 (26" × 13.6")	0.9 s	47.7 ms
Small Window	100 × 100 (1.8" × 1.8")	64 × 64 (4.4" × 4.4")	0.3 s	5.7 ms
Timing	100 × 600 (1.8" projection)	64 × 200 (4.4" projection)	0.3 ms	7 μ s

All EPIC CCDs was operated by in the photon counting mode with a fixed so that created difference modes of EPIC X-ray image. The mode of EPIC X-ray image dependent on a frame time to read out of frequency which allows several modes of data acquisition. Both MOS and pn cameras consist of 4 modes: Full Frame mode, Large Window mode, Small Window mode, and Timing mode which the image area and time resolution are showed in Table 1. In addition, the example image from each mode of MOS camera is illustrated in Figure 8. In the case of Full Frame mode, all pixels of all CCDs are read out and thus the full field of view (FOV) is covered. In contrast, in the Large Window and Small Window modes, the CCDs of cameras can be read out only by a fraction of CCDs chip. Finally, in the Timing mode, spatial information is maintained only in one dimension, along the column RAWX axis.

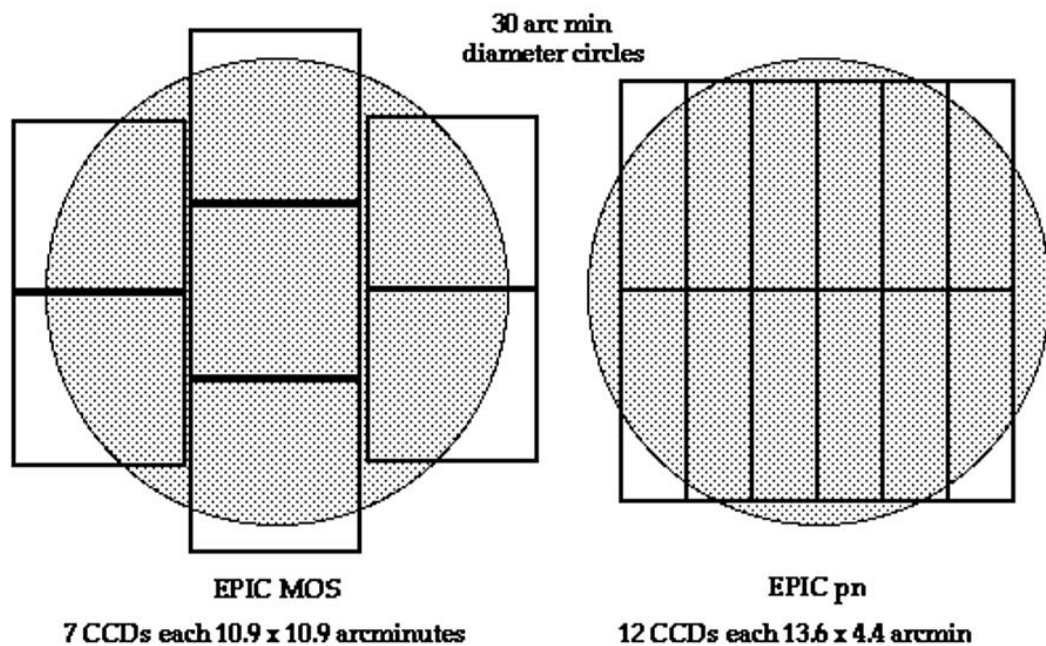


Figure 7 The *XMM-Newton* circular field of view and CCD chip sizes: EPIC MOS (left) and EPIC pn (right).

Source: The *XMM-Newton* community support (2019). *XMM-Newton* user's handbook.

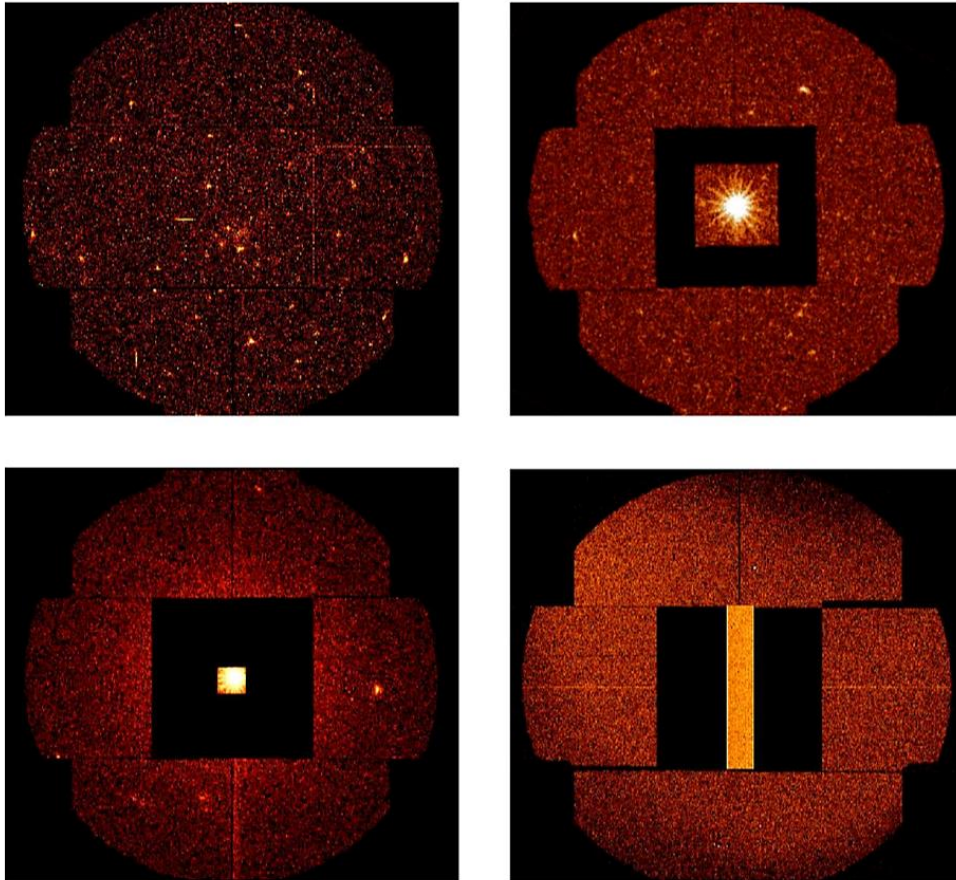


Figure 8 The example images obtained from each operating modes for the MOS cameras. *Top left*: Full Frame mode; *top right*: Large Window mode; *bottom left*: Small Window mode, and *bottom right*: Timing mode.

Source: The *XMM-Newton* community support (2019). *XMM-Newton* user's handbook.

Aims of this work.

An electron/positron pair halo is an interesting topic in astronomy; In fact, it has been searched for only in the gamma-ray wave band. However, since an electron/positron pair halo could also emit electromagnetic wave in the other waveband – i.e. X-ray - via synchrotron radiation. In this thesis, we will attempt to search for a pair halo in X-ray waveband using the *XMM-Newton* observatory; this is a new window for

searching the halo. We will use the Monte Carlo simulation to produce the spectral energy distributions (SEDs) of an electron/positron pair and then compute the X-ray SEDs of pair halo. Moreover, these X-ray SEDs will be used as a model to simulate the X-ray spectra which we could obtain if we observe the halo using the *XMM-Newton*'s instruments. Finally, we will analyse the real X-ray data obtained from *XMM-Newton* observatory for detecting the pair halo.

The thesis is laid out as follows. In Chapter 2, we will talk about historical studies of an electron/positron pair halo. In Chapter 3, we will focus on how to choose candidate source and how to simulate the X-ray SEDs; we will also estimate the observed X-ray spectra which might be obtained from *XMM-Newton* observatory in this chapter. After that, in Chapter 4, we will analyse the observed X-ray data of candidate source by a physical model to estimate whether we could detect the pair halo emission? Finally, in Chapter 5, we will summarise the key results found in this thesis.

CHAPTER 2

LITERATURE REVIEW

As being described in the previous chapter, an electron/positron pair halo could be formed by electromagnetics cascades via two interactions, i.e. the pair production and IC scattering. The produced electron/positron pairs could gyrate in the extragalactic magnetic fields several rounds so that they emit the X-ray light. In fact, this phenomenon has been the theoretical prediction. The first model of an electron/positron pair halo was proposed in 1993 by Aharonian et al. (Aharonian et al., 1993) in which the model predicts that the halo should emit the gamma photons. According to the model, the spectral energy distributions (SEDs) of the gamma-rays from pair halos were calculated to predict the signal of the pair halo. Later, the first attempt to observe the pair halo was performed in 2001. The High-Energy Gamma Ray Astronomy (HEGRA) team (Aharonian et al., 2001) attempted to detect the gamma rays from the pair halo of the studied AGN - the blazar Mrk501 - using the Cherenkov telescopes. Since it was reported that Mrk501 is an extragalactic source that could emit gamma-ray with energy of \sim PeV (10^{15} eV), so one could expect to obtain an isotropic halo emission around this source following the proposed halo model. However, no detection was claimed from the work. The pair halo had been studied continually until, in 2006, the size of electron/positron pair halo was calculated by A Eungwanichayapant, Aharonian, & Völk, 2006. They reported that the halo could be \sim 10 Mpc in diameter and should appear to enclose the central AGN; in addition, it was predicted that the gamma rays which have energy in the range of 0.1 - 10.0 TeV could be emitted from the halo (i.e. Aharonian et al., 1993). Later, in 2009, the angular distribution of the gamma ray emission was calculated by Eungwanichayapant and Aharonian (Eungwanichayapant & Aharonian, 2009) so that the detectable distance of the AGN possessing the halo has been proposed: i.e. $z \sim 0.129$. Furthermore, they also proposed the impacts of the primary gamma-ray, the redshift of the source, and the flux of the extragalactic

background light on the observation of pair halo. A year later, Ando and Kusendo (Ando & Kusenko, 2010), reported the detection of the electron/positron pair halo from the AGN which has a magnetic field of ~ 1 fG. This work claimed the evidence of detection of such a gamma-ray halo emission obtained by analysing the stacked images of the 170 brightest AGNs, which the data were obtained from the 11-month source catalogue of the Fermi Gamma-Ray Space Telescope; they found the excess flux, comparing to the Point Spread Function (PSF), in the surface brightness profile of the nearby AGN emitting high energy gamma-ray photons with the statistically significant level of 3.5σ (99.95% confidence level), suggesting the detection of the extended flux from the halos. Furthermore, they also reported that the halo might occur in the IGMF $|B_{\text{IGMF}}|$ of $\approx 10^{-15}$ G. In fact, the ability to constrain the IGMF would be very useful for the studies of gamma-rays and charged-particles in which potentially opens a new window to study the origin of cosmological magnetic fields. However, the results was argued by Neronov (Neronov, Semikoz, Tinyakov, & Tkachev, 2011) in later year; they indicated that the angular distribution of the gamma-ray of the stacked AGNs is consistent with the angular distribution of the gamma-ray around the Crab pulsar, in which the latter is an ideal point source for Fermi Gamma-Ray Space Telescope. This has made an argument that the detection of excess flux occurring from an electromagnetic cascade of TeV photons in the intergalactic space might be a mistake. In fact, the work compared the angular distribution of the gamma-ray around the stacked AGNs with the PSF of Fermi Gamma-Ray Space Telescope and then confirmed that the detection of an excess flux above the PSF was caused by an instrument effect; the detection is artificial due to systematic errors of the telescope instruments.

In 2011, the SEDs and angular distribution of the halo in the X-ray waveband were proposed by Eungwanichayapant and Aharonian (A Eungwanichayapant et al., 2011). Indeed, the model has predicted that the electromagnetics cascades creating electron/positron pairs halo do not emit only the gamma-rays, but could also emit X-ray photons via synchrotron radiation, in case that the cascade happens in the sufficiently strong magnetic field. Thus, this is the first

proposed that the X-ray emission of the halo emission of the AGN and could provide another method to detect the halo. However, there has been no group attempting to search for the pair halo in the X-ray regime yet.

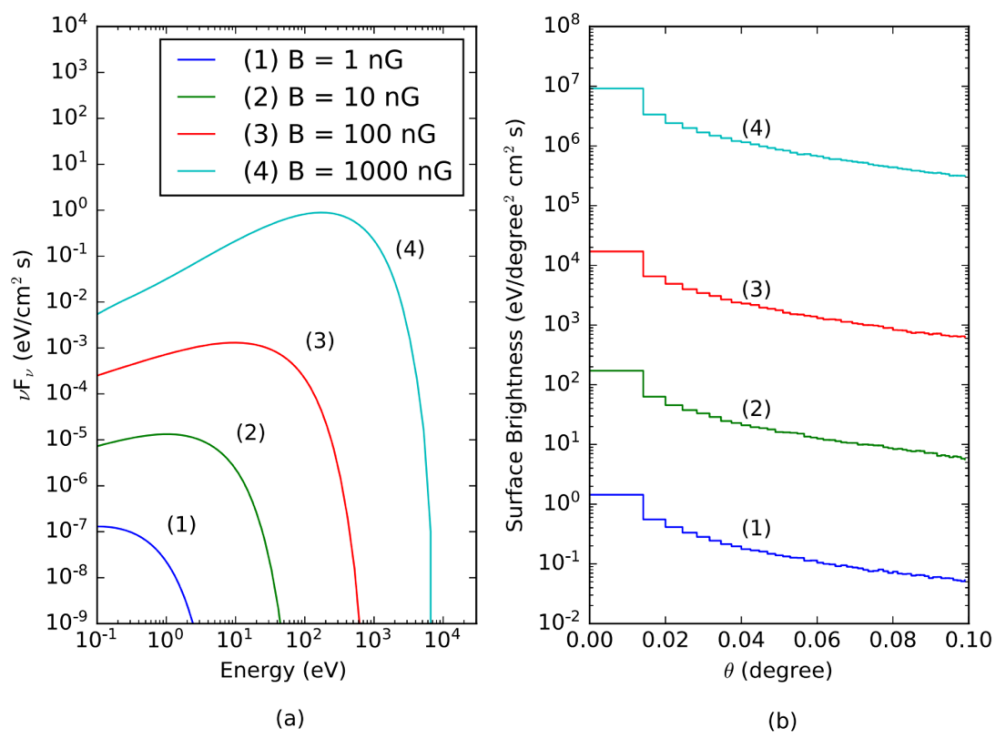


Figure 9 The X-ray SEDs and X-ray angular distribution of the pair halo in different levels magnetic field.

Source: Eungwanichayapant, Luangtip, Maithong and Ruffolo (2019). X-rays from electron/positron pair halos.

In 2015, Fernandez Alonso and his team (Alonso, Supanitsky, & Rovero, 2015) simulated the SED and angular distribution of pair halo in the gamma-ray waveband using the Monte Carlo simulation; they computed the electromagnetics

cascades of pair halo of the blazars 1ES0229+200 at different values of the IGMF. Indeed, this blazar has the redshift (z) of 0.1 so that the source is within an ideal distance for searching the pair halo emission. The result from this study provided the prediction of the detection of pair halo using future gamma-ray telescopes. At about the same time, another group also reported that the TeV source which is the low redshift blazar ($z < 0.5$) might give more chance to detect the pair halo if this halo was presented in the low IGMF ($\sim 10^{-17} - 10^{-15}$ G) (Chen, Buckley, & Ferrer, 2015). This work also reported the results of the search for gamma-ray pair halos from the stacked 24 BL Lac objects data obtained from the Fermi Large Area Telescope. The result is interesting in which they reported the marginal, positive signal of the halo emission (p-value ~ 0.01) for the extended emission against the point-source hypothesis. The result from this work hinted that some low redshift AGN residing in stronger ambient magnetic fields might be candidate sources for observing the pair halos. Given above information, an electron/positron pair halo was mostly proposed and observed in gamma-ray regime.

However, the X-ray emission of the pair halo has been recently proposed by Eungwanichayapant et al. (A Eungwanichayapant, Luangtip, Maithong, & Ruffolo, 2019). The work proposed that the current and near future X-ray observations could reveal the existence of an electron/positron pair halos occurring with some ranges of physical parameters. In brief, they computed the X-ray SEDs and X-ray angular distribution of the halo occurring with different levels of IGMF and initial seed gamma-ray energy as illustrated in Figure 9, and then check whether the halo emission would be detected by current X-ray observatories -*XMM-newton*, *Chandra*- and the future X-ray observatory which is *Athena*. A very exciting results from this work has showed that the current X-ray missions, *XMM-Newton*, could obtain a positive signal from the pair halos created under some physical conditions. For a magnetic field of $\sim 1 \mu\text{G}$, the X-ray of pair halo could be observable if a seed gamma-ray energy is ≥ 50 TeV. However, for a pair halo with the seed gamma-ray energy of 100 TeV, it would be observable if the magnetic field is ≥ 300 nG. Therefore, it is obvious that the halos are predicted to emit the observable X-ray light but no one has been attempted to detect it yet. In this work,

we will perform the very first search for the X-ray emission of the halo from the data obtained from one of the best current generation X-ray observatories: *XMM-Newton*.



CHAPTER 3

SIMULATION OF X-RAY SEDs

Introduction

An electron/positron pair halo was theoretically predicted to emit gamma-rays so that the observational searches for the pair halos have also been performed only in the gamma ray regime. Albeit there has been no evidence to confirm an existence of the pair halos yet, this phenomenon has been searched continuously and so it is a challenging topic in gamma-ray astronomy. However, the pair halo has also predicted to emit X-ray photons via synchrotron radiation (A Eungwanichayapant et al., 2011), which we have already described in the previous chapter. Therefore, in this chapter, we will compute the X-ray Spectral Energy Distributions (SEDs) of the pair halos using the Monte Carlo simulation of the electron magnetic cascades which are triggered by intrinsic gamma-rays from AGN. This intrinsic gamma photon properties were assumed following properties of candidate source - the blazar H1426+428 - which we expected to obtain the electron/positron pair halo photons; in addition, a magnetic field and redshift (z) are also used as an initial parameter to simulate the SEDs. The SED results will show the flux and distribution of X-ray photons which should possibly be obtained from the pair halos. Then, we will use these SED results as an emission model to simulate the observed spectra which should be obtained from *XMM-Newton* observatory.

To describe the SED simulation process and show how we simulated the pair halo spectra of the candidate source to estimates the possibility of the halo detection, this chapter is laid out as follows. In Source selection section, we describe the important properties of H1426+428. Then, the next section will explain how we simulated the SEDs of X-ray from H1426+428 and the results will be presented. Subsequently, the SEDs generated from the previously section will be used as the emission model of the

H1426+428 halo in Simulation of *XMM-Newton* spectra section. Finally, we will discuss and conclude in the light of the results obtained in Discussion and Conclusion section.

Source selection

It was previously suggested that the electron/positron pair halos are created from extragalactic, energetic TeV sources such as active nuclei (AGNs) (Coppi & Aharonian, 1997; Costamante, Aharonian, Ghisellini, & Horns, 2003). One type of AGN which might hosts pair halos is the blazar since it is known that they could emit the gamma-rays. In fact, the blazars which have been identified as an TeV source are shown in Figure 10 (Ong & Collaboration, 2014), so that we might expect these blazars to associate with the pair halo emission.

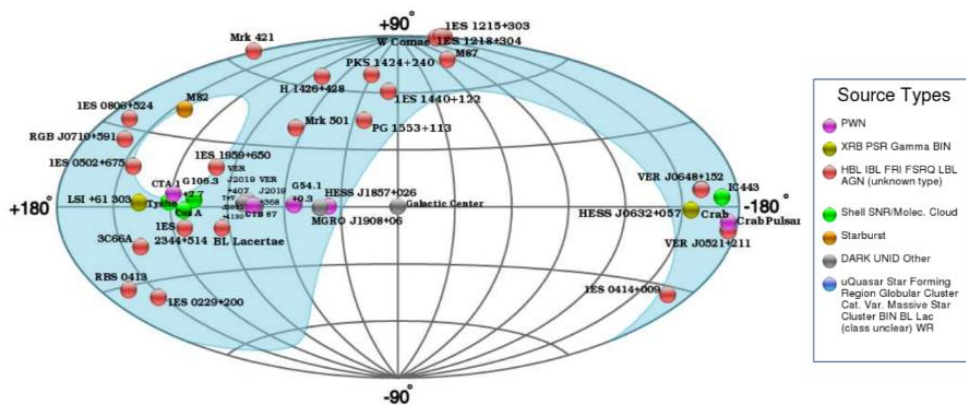


Figure 10 The VHE blazar sky map which were detected and identified by VERITAS.

Source: Ong & Collaboration (2014). Highlights from VERITAS on VHE Gamma-ray Sources in our Galaxy.

Nevertheless, we should not expect that the halos of all identified TeV sources would be observable because, technically, the full detection of electron/positron pair halos should be obtained from the ones which have suitable angular size, i.e. not too big or too small. In fact, if the blazars are too close to us, we might be able to observe only some fraction of the pair halos. In contrast, for the blazars that are too far, we might completely detect the entire halos of these blazar; however, the source should be too faint so that the flux levels are substantially below the detector sensitivity limit. Therefore, we will consider only some TeV sources which have suitable angular size.

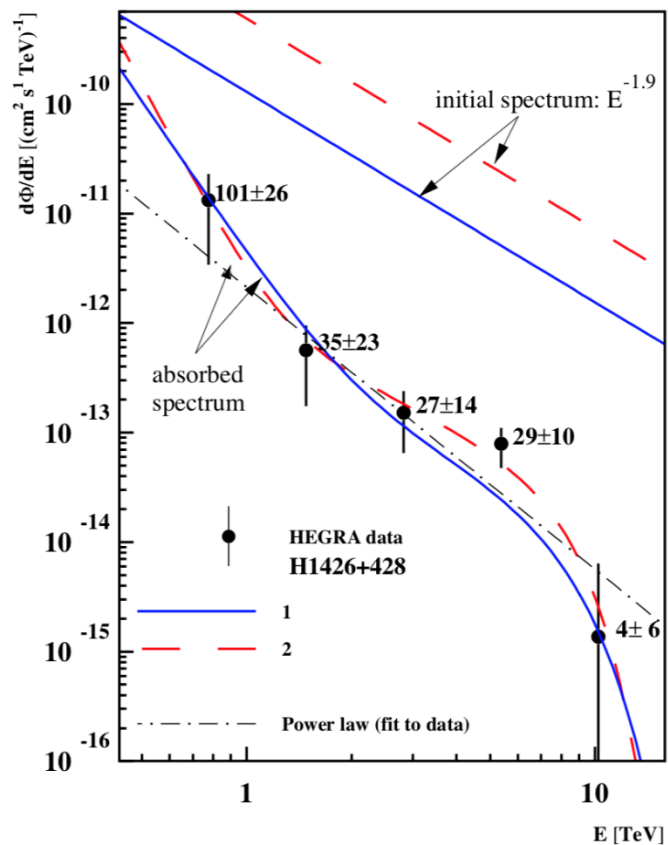


Figure 11 The absorbed gamma-ray spectra of the blazar H1426+428.

Source: Aharonian (2001), TeV gamma rays from the blazar H1426+428 and the diffuse extragalactic background radiation.

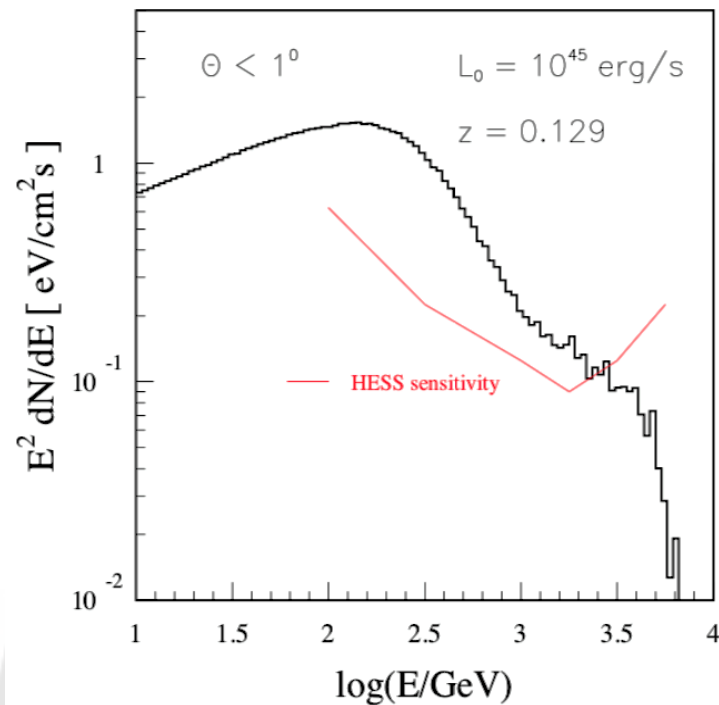


Figure 12 The pair halo SED from monoenergetic source with $E_0=100$ TeV emitting within 1° along with the H.E.S.S. point source sensitivity.

Source: Konopelko (2001), Stereo imaging of the VHE gamma-rays with HEGRA & H.E.S.S.

H1426+428 is a one of the promising candidates for detecting a pair halo (Anant Eungwanichayapant, 2003). With the redshift (z) of 0.129, the intergalactic absorption can trigger the cascade so that forms a pair halo around the AGN with suitable angular size for detection. In fact, signals indicating intergalactic absorption of photons from H1426+428 have been reported (F Aharonian et al., 2002) so that this provided a piece of evidence to argue that the source might contain an observable pair halo. Figure 11 shows the absorbed gamma-ray spectra of the blazar H1426+428 which could be the signal that the electromagnetic cascade is created. In addition, in Figure 12, the pair halo SED from monoenergetic source with seed gamma ray energy (E_0) =

100 TeV and angular size of 1° is plotted along with the sensitivity limit of the IACT array (FA Aharonian, Konopelko, Völk, & Quintana, 2001), i.e. H.E.S.S. The plot shows the characteristic of the pair halo SED of source with luminosity $\sim 10^{45} \text{ erg} \cdot \text{s}^{-1}$ located at $z = 0.129$; it is clear that the pair halo flux density lies above the H.E.S.S. sensitivity limit, especially at energy below ~ 3.2 GeV indicating that the pair halo should be detectable if the gamma ray luminosity of the source is $\geq 10^{45} \text{ erg} \cdot \text{s}^{-1}$ (J. D. Finke, Razzaque, & Dermer, 2010). Indeed, the gamma luminosity of H1426+428 is $\sim 10^{45} \text{ erg} \cdot \text{s}^{-1}$ or higher (D. Finke, 2010) since the source is believed to emit gamma-rays within a small solid angle, possibly as small as $10^{-2} - 10^{-4} \text{ sr}$, with a relativistic jet pointing towards the observer. Recently, this object has been observed the absorption feature in the gamma-ray spectra (Abdalla et al., 2017) so that it has been expected to have the gamma ray pair halo (A Abramowski et al., 2013). Therefore, H1426+428 was chosen to be our candidate source for searching the pair halo in this work. In the simulation, most parameters for simulation will be obtained from the properties of H1426+428; we will explain this in the next section.

An X-ray Spectral Energy Distribution from an electron/positron pair halo

In this section, we simulated the X-ray SEDs expected to be obtained from the H1426+428's halo which is our candidate source. H1426+428 was discovered by HEAO1 (Johnson, Cruddace, Ulmer, Kowalski, & Wood, 1983; Wood & Hutchinson, 1984) in the X-rays waveband (2 – 6 keV) and classified as a BL Lac object in 1989 (Remillard et al., 1989). This source has a cosmological redshift of 0.129 and emits a luminosity around $10^{45} \text{ erg} \cdot \text{s}^{-1}$. Given the source properties obtained from the literature, we simulated the X-ray SEDs using the following parameters (Atchara Kueathan, Luangtip, Maithong, & Eungwanichayapant, 2018): the monoenergetic, intrinsic gamma ray photon energy of 100 TeV, magnetic field of $1 \mu\text{G}$ and a source luminosity of $10^{45} \text{ erg} \cdot \text{s}^{-1}$. In this research, the Monte Carlo simulation method was adopted to calculate the SEDs following the model of Eungwanichayapant in 2011 (A

Eungwanichayapant et al., 2011). All electromagnetic cascades from the candidate source were simulated to get the emission time distribution following the algorithm of the cascade development using the procedure shown in Figure 13 (Anant Eungwanichayapant, 2003). Then, the obtained emission time distributions were used to calculate the energy distribution of the electrons/positrons and, subsequently, the results were converted to the energy distributions of the X-ray photons of the pair halo.

However, the emission time distribution was simulated only within 0.3 degree which is a suitable angular size for observation of the halo since this are, approximately, the size of *XMM-Newton* field of view. In addition, we are still aware that we might get a strong contamination of the direct X-rays flux from the central of AGN. To reduce the effect of this, we separated the region of observed X-rays observatory into three regions which are region A, B and C as shown in Figure 14. Region A which is the inner region out of three regions that covers the angular distance from 0 – 0.133 degrees. This is the area that we would obtain the strong contamination of X-ray emission from the AGN so that the X-ray flux in this region could be dominated by the X-ray emission from the AGN. Next, region B which is the middle region covers the angular distance from 0.133 – 0.200 degrees. In this part is still in the field of view of *XMM-Newton* but we propose that it should be sufficiently far from the central AGN emission so that we could ignore the central AGN X-ray emission. In the last region, region C covers the angular distance from 0.200 to infinite degree in which this is the area outside the telescope's field of view. Therefore, the emission time distributions were simulated for these three regions; the emission time of each individual region is shown in Figure 15 and the detail of results is shown in Appendix A.

After that, the obtained emission time distributions were used to compute the SEDs of electron/positron and then were converted into the X-ray SEDs; the simulated SED results of these three regions are shown in Figure 16. In fact, the results of these X-ray SEDs are quite similar for all regions (excepting for the normalization); indeed, the main flux contributions come from the region A which is closer to central AGN than region B and C (see more details in Appendix B which shown the result of the

X-ray SEDs of electron/positron pair halos). Moreover, considering the shape of X-ray SEDs, one can see that the X-ray SED from all of regions is dominated in the energy band of $10^1 - 10^3$ eV.

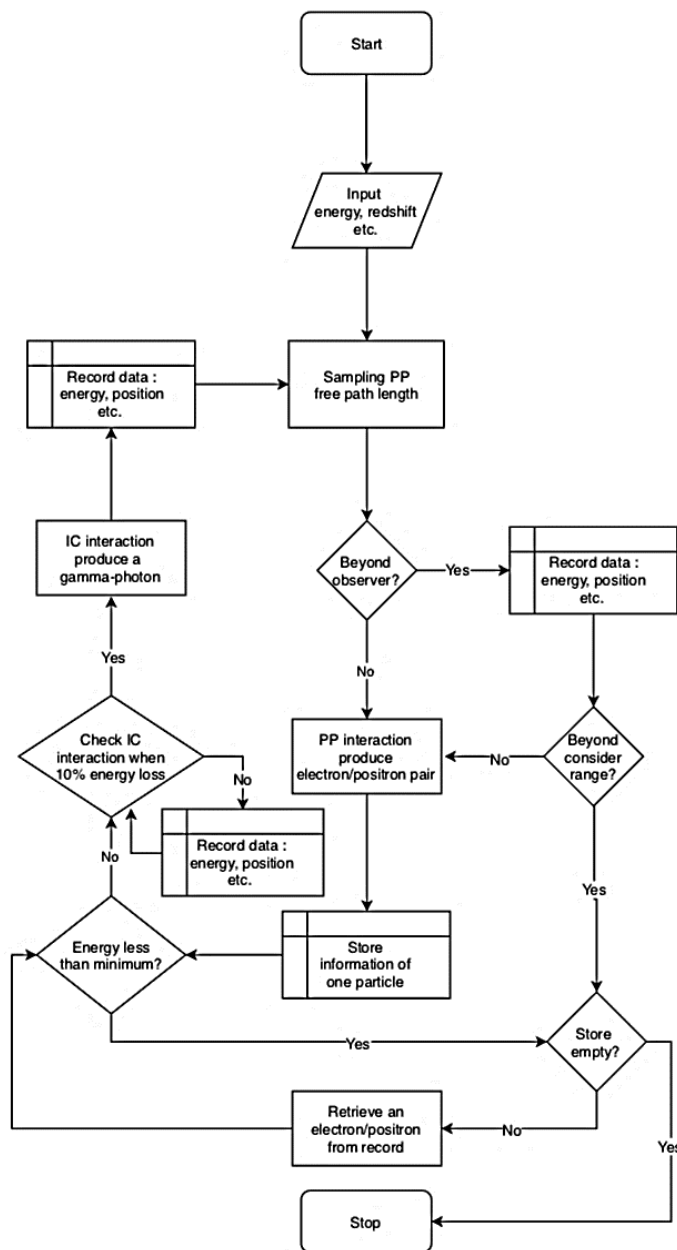


Figure 13 The procedure to calculate the energy distributions of the electron/positron.

Source: Eungwanichayapant (2003), Giant pair halos surrounding non-thermal extragalactic objects.

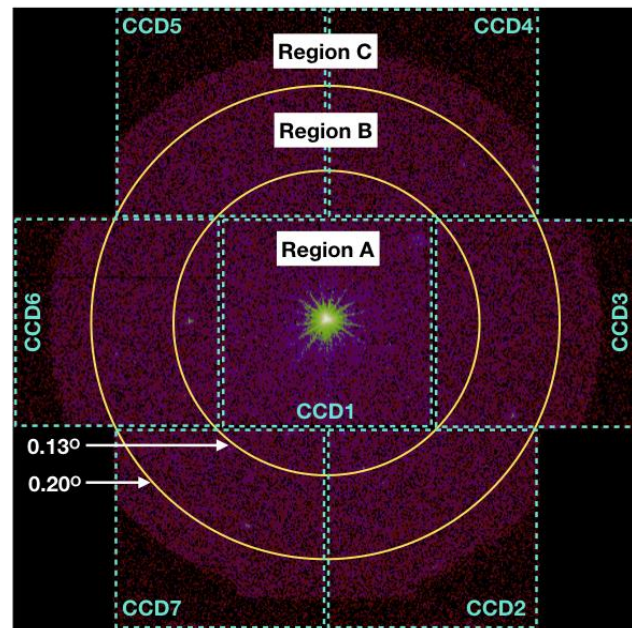


Figure 14 The example MOS observation of the H1428+428. The overlaying yellow lines divide the image into region A, B and C which are used in the simulation; the angular distance of each line from the centre is indicated in white. The blue dashed lines indicate the boundary of each CCD chip of MOS detector.

Simulation of *XMM-Newton* spectra

We also examine whether the pair halo X-ray emission theoretically proposed in the previous section would be detected by the current generation X-ray observatory - *XMM-Newton* - since it has been suggested by the recent work that *XMM-Newton* could give a signal of the pair halo occurring under the physical conditions which are similar to the properties of our candidate source (A Eungwanichayapant et al., 2019). To detect an electron/positron pair halo with *XMM-Newton* observatory, we need to know whether the halo signal is above or below the sensitivity limit of the instrument. To know this, we need to simulate the count rate and total counts of halo photon detected in the instrument's bandpass. In this work, we simulated the observed count rate by X-ray spectral fitting package (XSPEC) version 12.9.2 and used the X-ray SED data which obtained from

previous section as the source spectra of H1426+428's halo. To simulate the observed *XMM-Newton* spectra, we converted the SED data into the appropriate FIT file format (i.e., XSPEC table models) to make them readable by XSPEC. In addition, we also accounted for foreground Galactic extinction by adding the absorption column (N_H) of $1.11 \times 10^{20} \text{ atom} \cdot \text{cm}^{-2}$ along the line of sight into the simulation to make the model more realistic for the *XMM-Newton* observations. The absorption column value was estimated using the tool N_H Column Density. In brief, the N_H value is approximated from the galactic absorption along the line of sight to the source H1426+428; the right ascension (RA) and declination (DEC) of the blazar H1426+428 is $\alpha_{J2000} = 14^{\text{h}}28^{\text{m}}32^{\text{s}}$ and $\delta_{J2000} = +42^{\circ}40'20''$, respectively. Therefore, the multiplicative models of N_H absorption and X-ray SEDs were used as a basis for simulating the observed spectra. Here, the *XMM-Newton* spectra were simulated which using the XSPEC command *fakeit* for all three *XMM-Newton* detectors: pn, MOS1 and MOS2. The Ancillary Response File (ARF) and the Response Matrix File (RMF) of each instrument used here were released on January 12th, 2017 which both of ARF and RMF were obtained from the observatory's official webpage. To get more information from the simulation, we also proceeded to calculate the X-ray counts of an electron/positron pair halo assuming the 500 ks of required source exposure time; this are the moderate value of long exposure time that ones could be awarded in the *XMM-Newton* large program proposal.

Table 2 The count rate and total counts of H1426+428's halo observed in region A, B and C by *XMM-Newton* pn, MOS1 and MOS2 detector for 500 ks.

Regions	Count rates (cts \cdot s $^{-1}$)			Expected counts		
	pn	MOS1	MOS2	pn	MOS1	MOS2
A	3.938×10^{-3}	7.780×10^{-4}	7.780×10^{-4}	2700	480	490
B	8.700×10^{-4}	1.880×10^{-4}	1.800×10^{-4}	580	90	90
C	1.040×10^{-4}	2.200×10^{-5}	2.400×10^{-5}	70	10	15

The simulated spectra of each instrument with the corresponding observed count rate of the H1426+428, which are virtually observed that might be obtain by the *XMM-Newton* observatory are illuminated in Figure 17, Figure 18 and Figure 19 for MOS1, MOS2 and pn, respectively. As we expected, the simulated spectra also shown that the observed halo flux from region A is highest while that of regions B and C are relatively in the middle and lowest, respectively. This is what we should expect since the halo flux should be reduced as a function of the distance from the central AGN following the results from the previous section. Moreover, since the effective area of *XMM-Newton* is reduced as a function of off-axis angle (the distance from the focal point on detector), this effect could increase the reduction of the halo flux at region B and C, comparing to region A. Thus, by assuming that the H1426+428 is observed by the *XMM-Newton* observatory using pn, MOS1 and MOS2 detectors for 500 ks, the count rate and total photon counts of region A, B and C are shown in Table 2. For region A, which is the region closest to the central AGN, we could get a total photon counts from pn detector around 2,700 photons, while ~ 580 photons and 70 photons could be obtained from region B and C, respectively. For each MOS detector, we could get ~ 500 photons for region A, ~ 90 for region B and $\sim 10 - 15$ photons for region C.

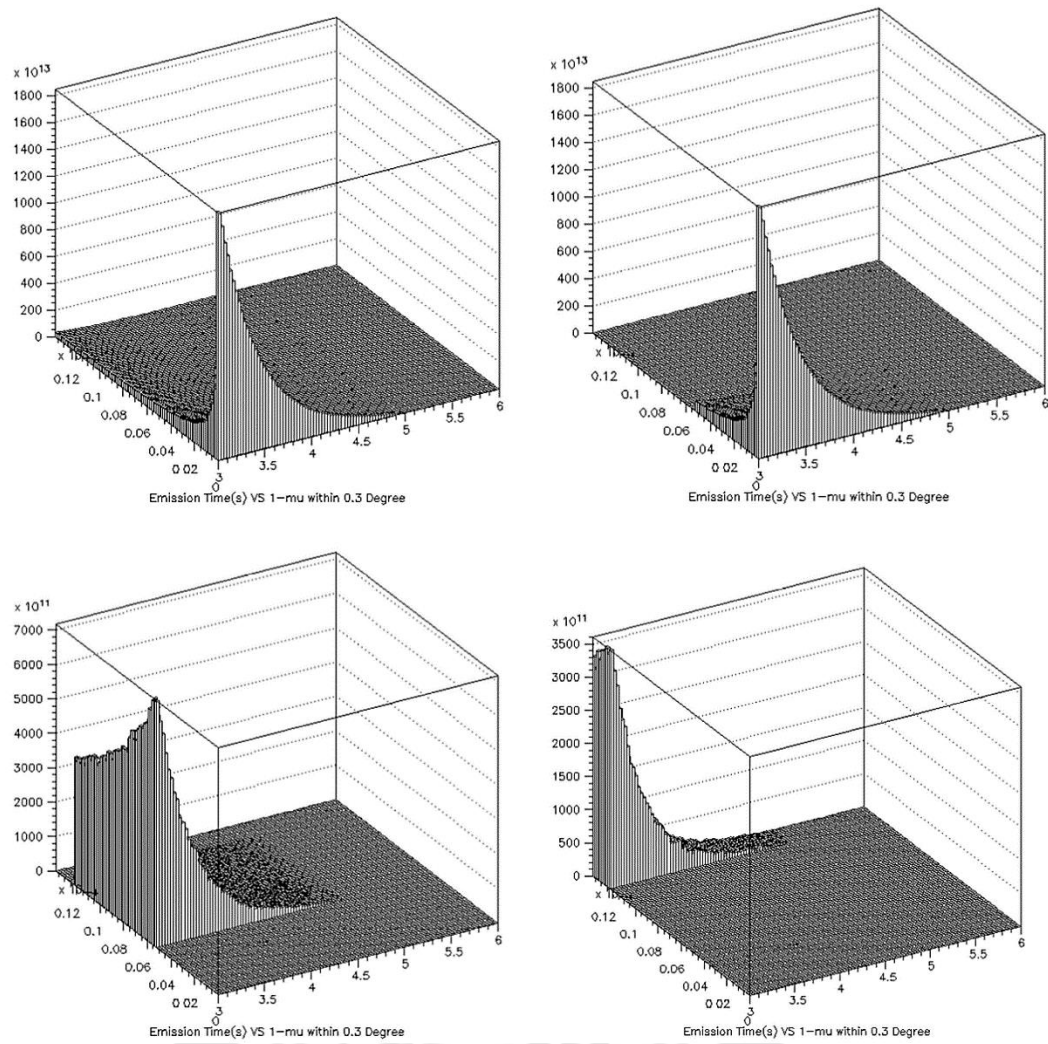


Figure 15 *Top left panel:* The emission time distributions of H1426+428 within 0.3 degree. *Top Right panel:* The emission time distribution in region A, which covers the angular distance from 0-0.133 degrees. *Bottom Left panel:* The emission time distribution in region B, which covers the angular distance from 0.133-0.200 degrees. *Bottom Right panel:* The emission time distribution in region C which covers the angular distance from 0.200 to infinite degree and is an area outside the *XMM-Newton* field of view.

Discussion

In this work, the blazar H1426+428, was chosen as a candidate source to simulate an X-ray SEDs because of two main reasons; it has the suitable angular size for observation and this blazar has been observed many times by *XMM-Newton* observatory. The X-ray SEDs expected to emit from the blazar H1426+428 halo that the X-ray SEDs were calculated in 2011 by the model of Eungwanichayapant et al. using the Monte Carlo simulations method for calculation. Here, we divided the halo emission region into region A, B and C in order to study the possibility of detecting the halo from each region. We then calculated the SED of each region of H1426+428 halo. We found that an X-ray photon from region A could give us the highest halo flux while comparing to the region B and C of the H1426+428's regions. This is consistent with our expectation that the X-ray SED of region A could be highest as it is closest to the central AGN. One important point that we need to emphasize is the shape of SEDs from different regions. We found that all SEDs have the similar shape and the emission are almost in the same energy band i.e. $10^1 - 10^4$ eV, suggesting that the halo emission is isotropic and occurs from the same physical mechanism. Thus, we could ensure that if the halo's flux is above the sensitivity limit of the instrument, we can observe it in the same X-ray waveband, regardless of the region or distance from the central AGN.

Then, the X-ray SEDs which were simulated formerly were used to be the emission model to generate the observed spectra of the halo from each different region which are region A, B and C assuming that the H1426+428 halo flux is observed by *XMM-Newton* observatory. We found that 2700 counts of X-ray photon from halo (~80%) could be detected in the divided region A which is the most X-ray photon halo that might detect out of the divided regions, whilst only 580 counts (~17%) and 70 counts (~3%) would be detected in regions B and C, respectively, for pn detector (Atchara Kueathan et al., 2018). For each MOS detector, the halo X-ray photons around 480 counts (~83%) could be detected in region A that the most region to find the halo X-ray photon for MOS detector, 90 counts (~16%) and only 10 counts (~2%) would be detected in region B and C, respectively (Atchara Kueathan et al., 2018). In other words, we might say that

the ~97 - 98% halo X-ray photon from the region A and B would be fall into the *XMM-Newton* detectors. Basically, the halo X-ray photon from region A that given up to 2,700 photon counts for pn detector and 480 photon counts for each MOS which is highest potential region for searching the halo X-ray emission. However, we cannot reject the main fact that the AGN is also located in this region, for this reason that the halo photons from region A are might be much diluted by the AGN photons. Here we used WEBPIMM to predict the photon counts of the AGN. The calculation showed that more than ten million counts photon from this AGN could be dominated in this region (Atchara Kueathan et al., 2018). Therefore, it will be difficult to resolve the halo photons from that of the AGN in the region A, including the analytical methods that might be used to so distinguish the halo X-ray photons from the AGN emission. This are also beyond the scope of this work and we will not do any further analysis for the data obtained from this region.

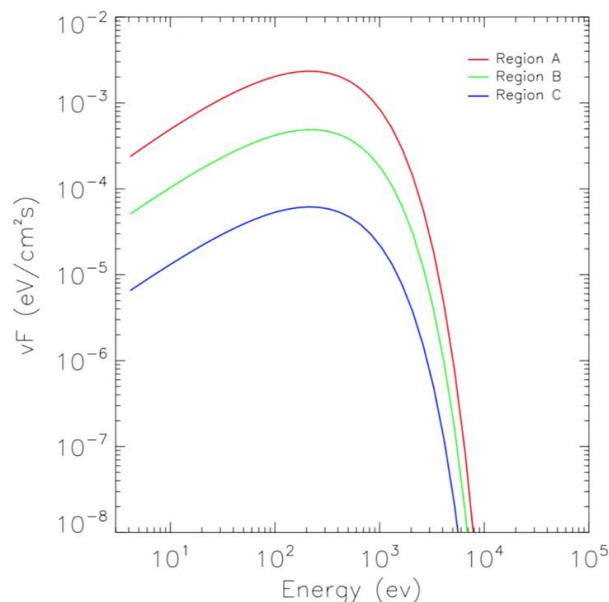


Figure 16 The pair halo X-rays SEDs simulated by assuming the AGN properties following the properties of H1426+428. The simulation was divided into three regions - region A, B and C - for purpose of study of the detection (see text).

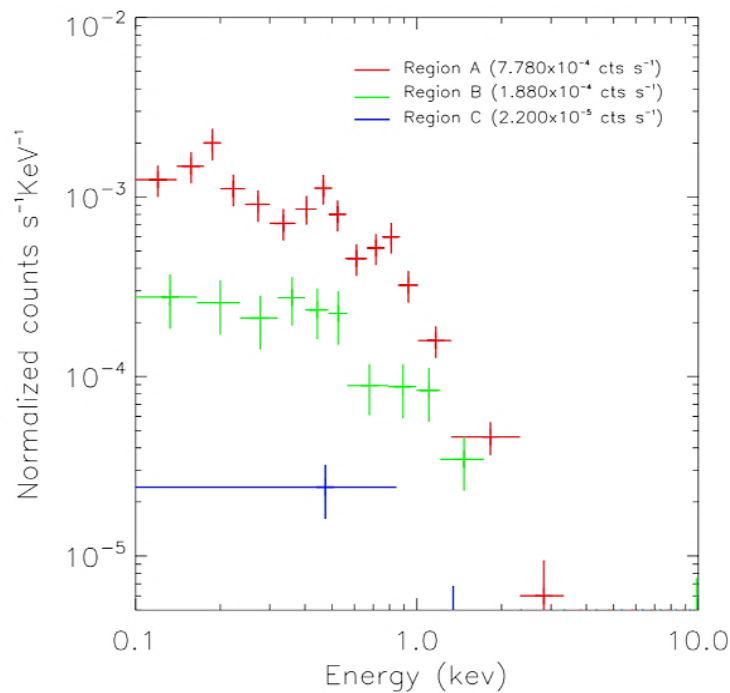


Figure 17 The simulated MOS1 spectra of the halo obtained from H1426+428's halo in region A, B and C.

Given the information of the analysis in region A which is so complicate and beyond for analysis in this work, we forwarded for another chance that might detect the halo X-ray emission. We pointed that chance to search the halo photon from region B instead, even we already known that only 580 halo photons and also only 90 photons from pn and MOS detector respectively could be detected in this region, but it could be confident that the X-ray photons will not be contaminated by the AGN emission. Next step, we will carefully subtract the instrument background from the H1426+428's observed spectra only in region B (Atchara Kueathan et al., 2018). We expected that the resulting spectra of this observed region should provide the opportunity for detecting the existence of electron/positron pair halos and used that resulting spectra for confirm this pair halo as well. We will perform this process in the next chapter.

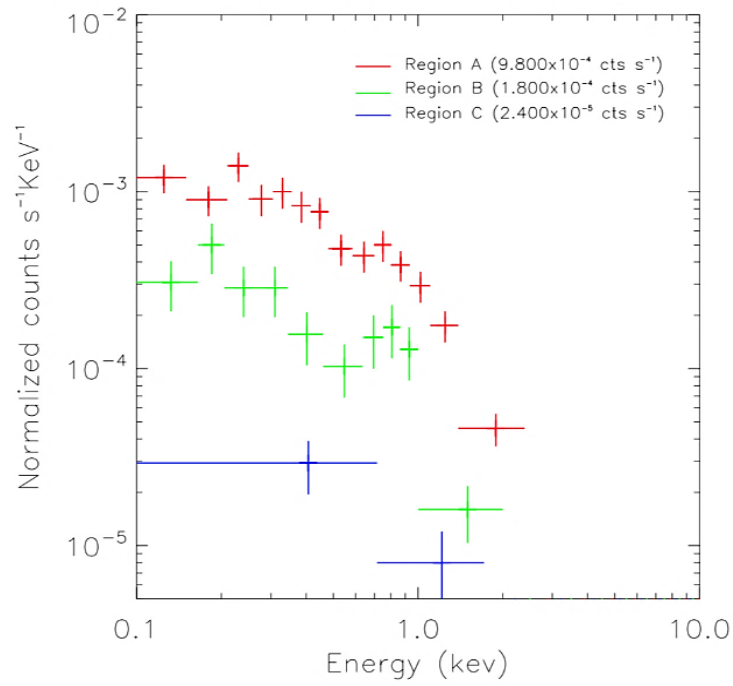


Figure 18 The simulated MOS2 spectra of the halo obtained from H1426+428's halo.

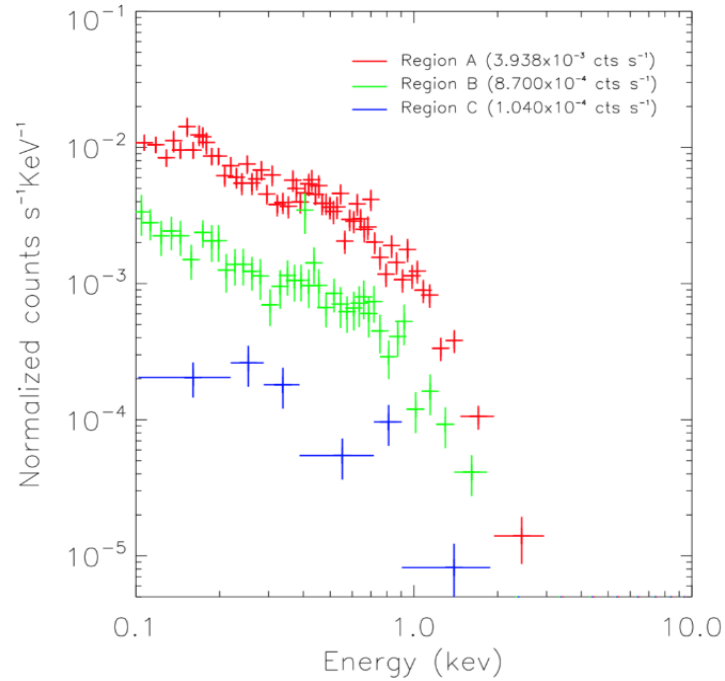


Figure 19 The simulated pn spectra of the halo obtained from H1426+428's halo.

Conclusion

In this chapter, we have computed the X-ray SEDs of H1426+428'halo as an emission model. Our results show an emitted photon of the pair halo that we should obtain if the halo exists. Most of halo's synchrotron energy is emitted in the X-ray waveband and almost falls in region A. These obtained X-ray SEDs were use as emission model to simulate the observed spectra of *XMM-Newton*. The simulation showed that the halo photons $\sim 97 - 98\%$ would be detected in the region A and B which are still in the field of view of *XMM-Newton* telescope. However, we argue that the region A is difficult to detect the halo due to the AGN contamination. Thus, we propose that region B which covers the angular distance from 0.133-0.200 degrees is the best candidate for searching the halo because this area is still in the field of view of the detector and sufficiently far to ignore the AGN emission. We found that $\sim 16-17\%$ of halo photons (~ 580 photons with exposure time of 500 ks) would fall into the region B of detector; although we could lose some halo's photons in this region, with the increment of the exposure time, we argue that it is possible to detect the halo X-ray emission in this region. In the next chapter, we will use the data of H1426+426 obtained from *XMM-Newton* data archive to search for an electron/positron halo of this AGN.

CHAPTER 4

X-RAY SPECTRAL ANALYSIS

Introduction

In the previous chapter, we simulated the X-ray SEDs and *XMM-Newton* observed spectra of H1426+428's halo; the latter was used to estimate the count rate and total counts of halo's photons which we would obtain from our candidate source. However, these X-ray SEDs are theoretical prediction and do not have the observational data to confirm the existence of this phenomenon. In order to confirm this, in this chapter, we will try to search for the emission of the halo in the X-ray waveband from observational data which are obtained from *XMM-Newton* observatory. The spectral of H1426+428 will be analysed to detect the emission of the pair halo that we expect to obtain from our candidate AGN. We will discuss whether the halo is detected in the light of obtained result.

This chapter is laid out as follow. In the Observations and data reduction section, we described how we obtain an X-rays observational data of candidate source and how we reduce these observation data to create the energy spectra. All of these energy spectra were then analysed in Spectral analysis and results section. Our findings are then discussed in the next section and are concluded at the end of this chapter.

Observations and data reduction

In this section, we began by searching for observations of the H1426+428 from *XMM-Newton* science archive. Out of eight observations found, we also skipped one that is off-axis observation because the source is not on the centre of the CCD aimpoint so that we lose high fraction of halo area around the AGN, in particular area B in chapter 3; in this case, the useful area for study the halo emission is insufficient. Therefore, the

on-axis observations selected to study in this work are tabulated in Table 3. We then reduced an *XMM-Newton* data using the Science Analysis System Software (SAS) Version 16.1.0 following the instructions provided in the *XMM-Newton* Extended Source Analysis Software package (XMM-ESAS) web page. In brief, the data reduction steps were presented in Figure 20. We started by setting up a user directory for defining path of observational data. Then, we reduced the observation data files (ODFs) to obtain new, calibrated and reduced all of event files using the scripts EPCHAIN and EMCHAIN for the pn and MOS data, respectively. Then, we filtered these event files for background particle flaring events using the task ESPFILT; this step was to generate the clean pn and MOS event files which is almost free from the background flaring contamination. However, we decided to skip the pn data from our analysis because all pn data have been observed in window mode so that the obtained data are almost in the central area which is the location of AGN. As we have argued in Chapter 3, we would require the observational data of region B; since the pn data in window model provide only the observational data of region A (see Figure 21), these data are not useful for our study in this chapter.

After excluding the pn data, we then continued to analyse the MOS observations by examining the MOS data from each CCD whether they are in anomalous state, or not? This is the effect which some MOS CCD detectors could occasionally operate in anomalous state, where the photon background of energy $E < 1$ keV is strongly enhanced. This identification of data obtained from CCD operating in anomalous state can be performed using MOS-FILTER script. We then exclude data from the anomalous state CCDs from our analysing data because XMM-ESAS does not provide any package to adequately handle the data in this stage. The CCDs which operated in the anomalous state for each MOS observation and so their data were excluded from our analysis are shown in column of 6 Table 3. Next, we detected the point sources presenting in our data in the energy band of 0.1 - 11.0 keV and excised their data from our observations by using task CHEESE (see Figure 22). Therefore, any

point sources detected in the telescope's field of view were removed to minimize the contamination in our halo emission study.

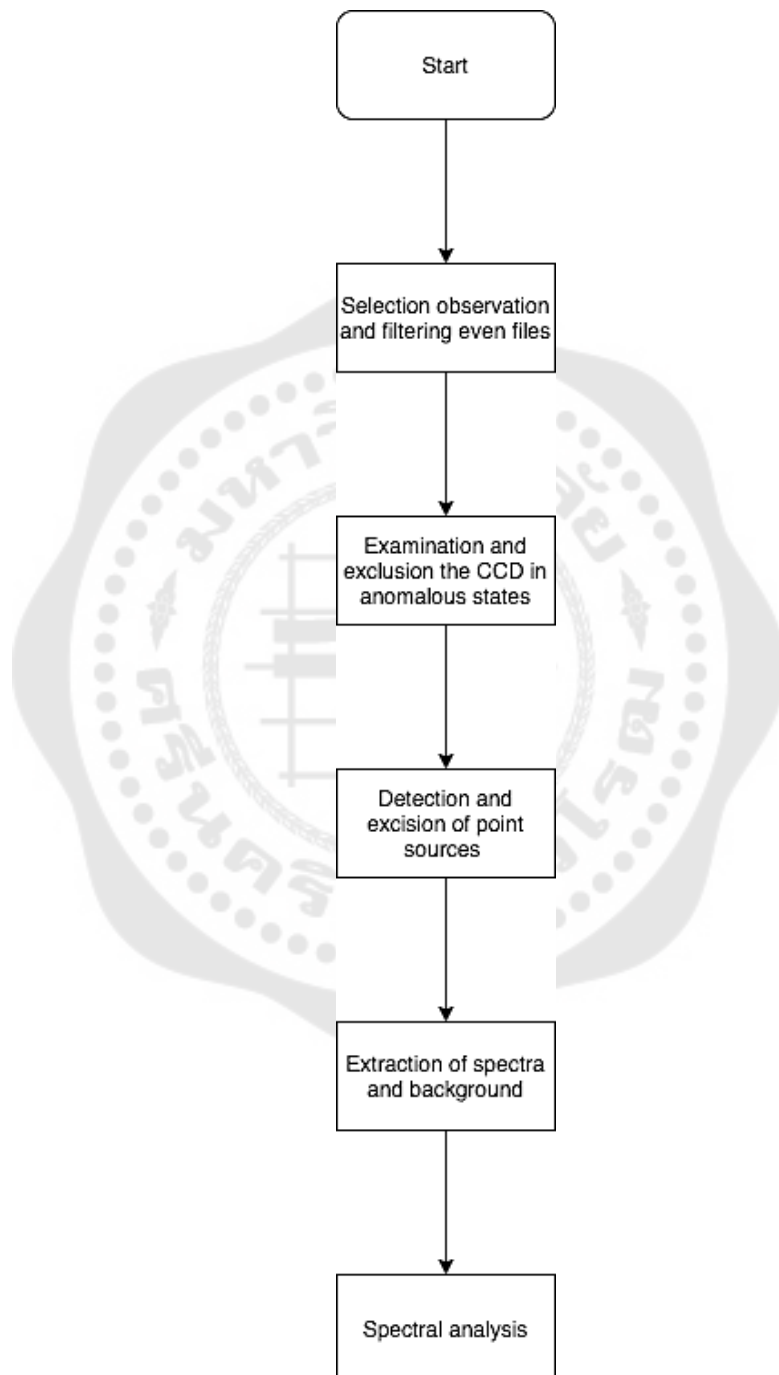


Figure 20 The procedure to reduce the observational data of H1426+428, which follows the instructions in the *XMM-Newton* Extended Source Analysis web page.

Table 3 *XMM-Newton* observational data of H1426+428.

Observation ID ^a	Revolution ^b	Exposure time ^c (ks)	Instrument mode ^d			CCD in Anomalous states ^e		
			MOS1	MOS2	pn	EMOS1	EMOS2	
0111850201	278	68.6	Large Window	Full frame	Small Window	-	-	
0165770101	852	67.9	Small Window	Small Window	Small Window	-	-	
0165770201	853	68.9	Small Window	Small Window	Small Window	-	-	
0212090201	939	30.4	Small Window	Small Window	Small Window	-	CCD5	
0310190101	1012	47.0	Small Window	Small Window	Small Window	CCD6	CCD5	
0310190201	1015	49.5	Small Window	Small Window	Small Window	CCD6	CCD5	
0310190501	1035	47.5	Small Window	Small Window	Small Window	CCD4, CCD6	CCD5	

Notes. ^a*XMM-Newton* observation identity number. ^b*XMM-Newton* revolution. ^cA total observational time of observation. ^dOperating mode of each detector. ^eThe CCD which were in anomalous states during the observation.



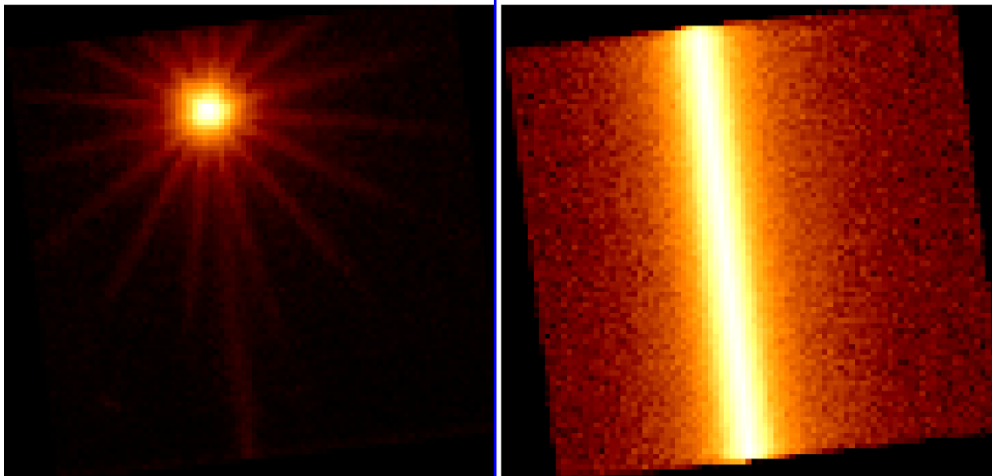


Figure 21 The example of clean pn images.

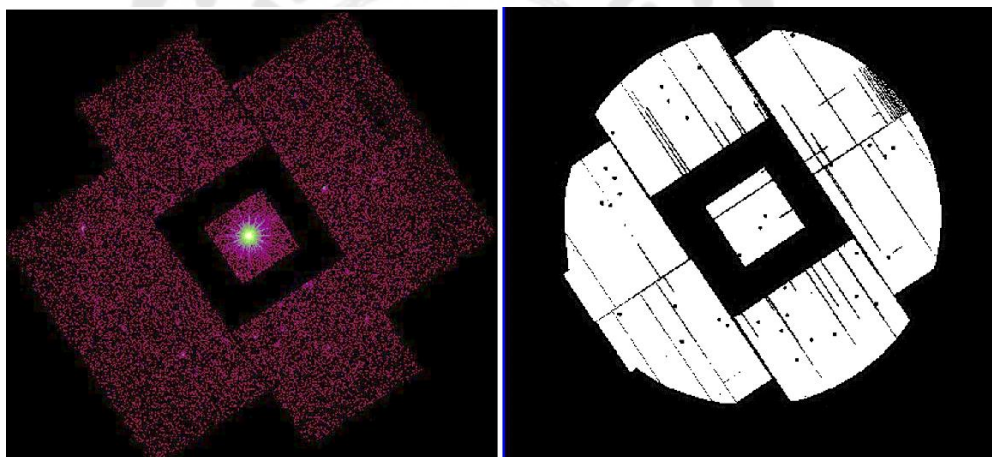


Figure 22 The example MOS image after excising point source using CHEESE script.

The observational data obtained were then used to extract the energy spectra. We extracted the energy spectra using the following method. Recall region B in Chapter 3 in which we have proposed to be used as the region for searching the pair halo (see left panel of Figure 23), we aim to use the data in this region for the analysis. However, to gain maximum data signal to noise, we slightly adjust the boundary of region B to get more analysed area; the inner boundary is the box shape with the size of CCD1 (which means the CCD1, i.e. the central CCD, data were exclude to avoid the

AGN contamination) while the outer edge is nearly the boundary of the telescope field of view (see right panel of Figure 23). Given the inner and outer boundaries of the analysed area, we got the modified version of region B from Chapter 3 for our analysis in this Chapter. However, since our new defined region covers a large angular distance, creating a single spectrum from this area could lead to the problem that there are too much difference between the effective areas of the inner and outer region so that the corresponding RMF and ARF averaged over the entire region could result in under/overestimating the properties of spectrum. To avoid this problem, we divided our new defined region into three sub-regions: region B1, B2 and B3. Region B1 covers the angular distance from 0 - 0.15 degree (0 - 160); Region B2 covers the angular distance from 0.15 - 0.19 (160 - 200) degree; and Region B3 covers the angular distance from 0.19 - 0.22 (200 - 240) degree (see right panel of Figure 23). We then extracted the spectra from these three sub-regions from all observations using the task MOS-SPECTRA. In addition, the background spectra were extracted from the same defined region (i.e. region B1, B2 and B3) by using the task MOS-BACK. Note that, here, the background spectra that we obtained from MOS-BACK is the quiescent particle background (QPB), which mainly consist of two components of background: instrument background and cosmic background. The former could obtain during the instrument calibration.

Indeed, the individual observation was obtained from the *XMM-Newton*s observation consisted of two data sets which one was given from MOS1 camera whilst another one was given by MOS2 camera, so we totally got six spectra from each X-ray observatory. Then, we gained the maximum S/N of the observed spectra for more analysis in next step by grouping all of spectra with the same area included the same camera together. Finally, all of spectra were combined within each group using the package ADDSPEC (A Kueathan, Luangtip, & Eungwanichayapant, 2019); however, in this step we also lost some of data from the MOS1 and/or MOS2 in each observations due to some the data in each observation that has anomalous state which was happened in some of CCDs of instrument. So, we divided the spectra from

each group into two sub-groups, for instance, ones affected by anomalous states and another one is not affected by anomalous state. Using these criteria, we finally got 12 spectra (see details of 12 spectra which were stacked together in order to obtain high S/N spectra in Table 4). Then, each combined spectrum was grouped to have a minimum of 25 counts per bin to utilize the χ^2 minimization method during the spectral fitting and were then used as the basis for analysis in the next section. The example spectra are shown in Figure 24.

Table 4 The stacked spectra of H1426+428 used in this study

Name ^a	Revolution ^b	CCDs used ^c	Region ^d
Detector: EMOS1			
M1-B1	278, 852, 853, 939	2, 3, 4, 5, 6, 7	Region B1
M1-B2	278, 852, 853, 939	2, 3, 4, 5, 6, 7	Region B2
M1-B3	278, 852, 853, 939	2, 3, 4, 5, 6, 7	Region B3
M1-B1-ANO ^z	1012, 1015	2, 3, 4, 5, 7	Region B1
M1-B2-ANO	1012, 1015	2, 3, 4, 5, 7	Region B2
M1-B3-ANO	1012, 1015	2, 3, 4, 5, 7	Region B3
Detector: EMOS2			
M2-B1	278, 852, 853	2, 3, 4, 5, 6, 7	Region B1
M2-B2	278, 852, 853	2, 3, 4, 5, 6, 7	Region B2
M2-B3	278, 852, 853	2, 3, 4, 5, 6, 7	Region B3
M2-B1-ANO	939, 1012, 1015, 1035	2, 3, 4, 6, 7	Region B1
M2-B2-ANO	939, 1012, 1015, 1035	2, 3, 4, 6, 7	Region B2
M2-B3-ANO	939, 1012, 1015, 1035	2, 3, 4, 6, 7	Region B3

Notes. ^aCalled name of the stacked spectra. Here M1 and M2 stand for MOS1 and MOS2, respectively, while B1, B2 and B3 represent the regions that spectra belong to (see Figure 23). ^bThe revolutions of the observations of the spectrum. ^cThe column indicating that the data from the indicating CCD number are included in the spectra. ^dThe region that were used to extract the spectrum.

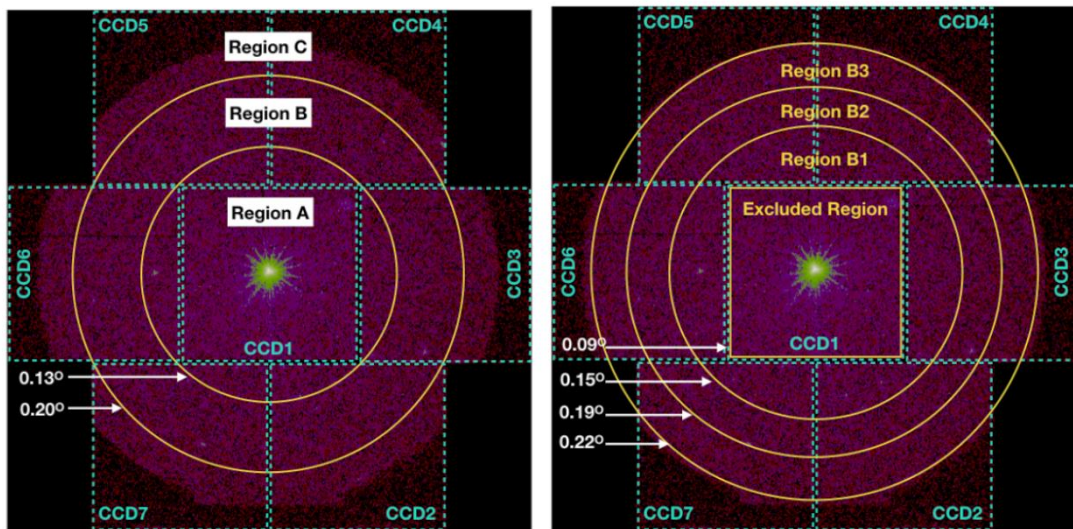


Figure 23 The comparison between analysing regions used in Chapter 3 and this chapter. *Left panel:* The overlaying yellow lines divide the observation into the region A, B and C used in the analysis in Chapter 3. The angular distance of each line from the centre is indicated in white. *Right panel:* The overlaying yellow lines divide the observation into region B1, B2 and B3 used in the analysis of this chapter; the angular distance of each line from the centre is indicated in white. The blue dashed line indicated the boundary of each CCD

Spectral analysis and results

In this work, we also used an X-Ray Spectral Fitting Package (XSPEC) for modeling the obtain X-ray spectra, which is the same package that we used to simulated spectra of *XMM-Newton* in chapter 3. All 12 spectra obtained from previous section will be fitted simultaneously to gain maximum S/N over the energy range of 0.5 - 5.0 keV and best constraint the fitting parameters. Although we have removed some of X-ray emission source that we already well known from the observed spectra, for instance, the central of blazar H1426+428 and detectable bright point source. However,

the X-ray photons were obtained from the defined in each region; region B1, B2 and B3 still are expected that should be also dominated by the two components of X-ray emission which are the instrument background and unsolved cosmic X-ray background. Thus, according to the XMM-ESAS cookbook suggestions (Kuntz & Snowden, 2008), we constructed the model with eight components to explain the spectra: (1) GAUSS + (2) GAUSS + (3) APEC + (4) ABS*APEC + (5) ABS*APEC + (6) ABS*POW + (7) GAUSS + (8) ABS*BB (A Kueathan et al., 2019). In brief, the first two gaussian (GAUSS) which is components that were accounted to represent both of the Al $K\alpha$ and Si $K\alpha$ instrumental emission lines (Kuntz & Snowden, 2008), respectively. The third component – APEC - represents the X-ray emission of the plasma which was emitted from the Local Hot Bubble or heliosphere (Kuntz & Snowden, 2008). The fourth and fifth components of ABS*APEC, this component is the absorbed plasma emission that was represented the clusters or intergalactic medium, and the hot plasma emission from unresolved component such as that of AGN (Kuntz & Snowden, 2008), respectively. The sixth absorbed power-law component (ABS*POW) is used to explain the main unresolved point source of an X-ray binaries or AGN that were not excluded (Kuntz & Snowden, 2008), especially during the point source exclusion step. The seventh gaussian component is the empirical component that was used for accounting the line-like feature that present X-ray emission line in the spectra. Finally, the eighth absorbed blackbody component (ABS*BB) which is the expected component that we used to represent the thermal-like emission from any other components including some of an X-ray emission of an electron/positron pair halo (if exist) (A Kueathan et al., 2019). Here we argue that the absorbed blackbody component could describe well the spectra of the halo since the absorbed blackbody spectral shape is similar to the shape of absorbed halo spectra which we simulated in Chapter 3. To confirm this, we fit the simulated, absorbed halo spectra obtained from Chapter 3 with the the absorbed blackbody component. The result is shown in Figure 25. It can be seen that the model fitted well with the simulated halo's spectra, especially at the energy below 1 keV which is the energy band that the observed halo flux dominates. This means that if a pair halo exists and could be

observed by *XMM-Newton*, we should be able to replicate the absorbed halo spectrum using the absorbed blackbody component, at least for the first order approximation. The last step, we also added the constant component to the model to account a small difference values between MOS1 and MOS2 data due to that data are given the imperfectly detectors identical and also for the normalizing the data obtained from difference regions of B1, B2 and B3.

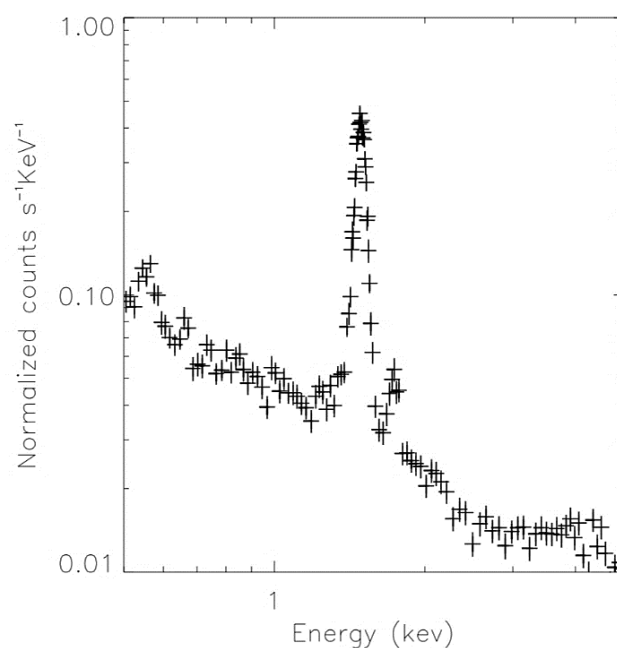


Figure 24 The example spectra of stacked MOS1 from Region B1.

In addition to the model defined above, the broken power-law (BKNPOW) model was also used to account for the residue of soft photon (SP) contamination which cannot be removed completely. We note that this component cannot be added as the ninth component of the above model directly since, unlike the other components, the flux from the SP contamination is not a function of off-axis angle so that the normal RMF used for the spectra does not work. Here we separately added the broken power-law component with the diagonal RMF provided in the ESAS-CCF distribution to represent

the remaining SP contamination. These models was fit simultaneously with the above model to best describe the obtained spectra.

With so many parameters from all model components, we aim to freeze or link the related parameters together as much as possible, in order to reduce the number of free parameters in the model components. Also, some model components may not be added at the beginning since this would dramatically increase the number of free parameters at the same time; in fact, the model component need to be added orderly (which described below) to get the global minimum χ^2 . Furthermore, our strategy is also freezing most parameters and thawing just a few parameters a time to find the best values of the free parameters; then we freeze the previous free parameters and free some new few parameters and find the best fit values of these free parameter. By repeating this step several times, we ended up with the nearly best fit values of all free parameter. Finally, we fit all free parameters again to get their best fit values. The detail of fitting steps is described below.

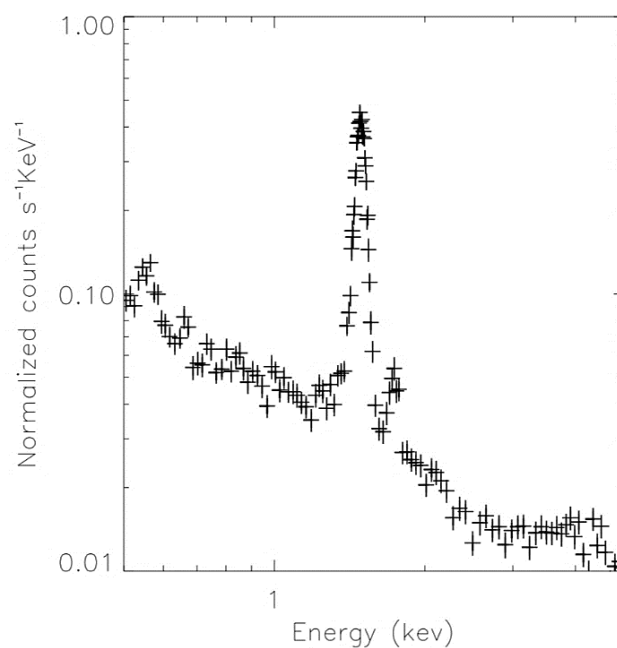


Figure 25 The example spectra of stacked MOS1 from Region B1.

To begin the spectral fitting, we start with the two gaussian components (GAUSS + GAUSS) which represented the MOS instrumental emission lines. We freed the normalisations for the Al $K\alpha$ and Si $K\alpha$ lines which could vary with detector and location for an individual CCD, while the energies and line widths were also allowed to be a free parameter which could vary only in the reasonable range following the suggestion in XMM-ESAS cookbook. Next, to fit spectra with the next four components of APEC + ABS*APEC + ABS*APEC + ABS*POW, we linked the plasma temperatures and normalisations of all spectra together and fit the model to the spectra to obtain the best fitted parameters. After that, we added the absorbed blackbody component (ABS*BB) to the model and also linked the model free parameters of all spectra together to find the best fit values.

For the broken power law components (BKNPOW), as described above, we fitted them as separate models and assigned separate RMF. We assumed the initial guess value of the power-law slopes and breaking point following XMM-ESAS cookbook suggestions, linked this parameter together for all spectra and fit to find the best parameter values. Finally, we decided to add another gaussian component (GAUSS) to account for line-like feature at ~ 0.5 keV; we thawed the central line energy, line width, and normalisation parameters of all spectra and fit. After finishing the spectral fitting and get the appropriate parameters, we calculated the blazar flux of each spectra from the absorbed blackbody component as the last step.

The spectral fitting result is shown in the Figure 26, 27, 28 and 29 and the best fitted values are reported in Table 7 and Table 8 for MOS1 and MOS2 spectra, respectively. Both of the result in Figure 27-29 indicates that the observed spectra were well explained by these model, although the reduced χ^2 value of 1.11 its look seems a little bit higher than unity (A Kueathan et al., 2019); honestly, since all spectra are fitted simultaneously, the high number of spectral bins (6279 bins) could lead to this results and we regard this as the statistical acceptable results. Furthermore, as all best fitting parameters were reported in Table 5 that the parameters are suitable

consistent with the values suggested in the XMM - ESAS cookbook, obviously the parameter from the component 1, 2, 3, 4, 5 and 6 (Kuntz & Snowden, 2008), this could help to ensure that we got the reasonable parameter values, and we will, next, explain further the values of these parameters. To begin, the first and second components represented the Al $K\alpha$ and Si $K\alpha$ instrumental line of MOS detector which should have the gaussian line at 1.49 keV and 1.75 keV (Kuntz & Snowden, 2008). The plasma temperatures of third, fourth and fifth components - i.e. $E \sim 0.32$, $E \sim 0.27$ keV and $E \sim 2.49$ keV, respectively - represented the cosmic background. In fact, it has been suggested that the plasma temperature could be about $\sim 0.25 - 0.70$ keV (Kuntz & Snowden, 2008). Hence, the third and fourth component temperatures are compatible with the values XMM-Newton cookbook suggested, albeit the fifth component seems to be a little bit higher than that we expect. The sixth component was used to explain the unresolved X-ray point source. We found that the best fitted photon index value is ~ 1.18 ; indeed, this values seem to be steeper than a suggestion since it should be ~ 1.46 (Marshall & Ricketts, 1980). In case of the seventh component, we found the gaussian emission line with central energy of ~ 0.56 keV. Although the physical origin of this model component is still unclear whether it arise from the instruments or the cosmic background, but we regard that the adding of this component does not affect the detection of the pair halo due to the spectral energy distribution of the halo are thermal-like still rather than the line-like (Atchara Kueathan et al., 2018). Finally, the eighth component is defined to represent the extra unresolved thermal-like emission that might have not been detected yet, including the pair halo emission (A Kueathan et al., 2019). Interestingly, the best fitted model suggests us that there could be some photons originating from this component. We will discuss this component in more details in the next section. Finally, for the broken power-law component which we added as the separated model, the best fitted model also suggest the break energy at ~ 3.32 keV and ~ 3.11 keV for MOS1 and MOS2, respectively; these values are well consistent with the value suggested by XMM-ESAS webpage (Kuntz & Snowden, 2008).

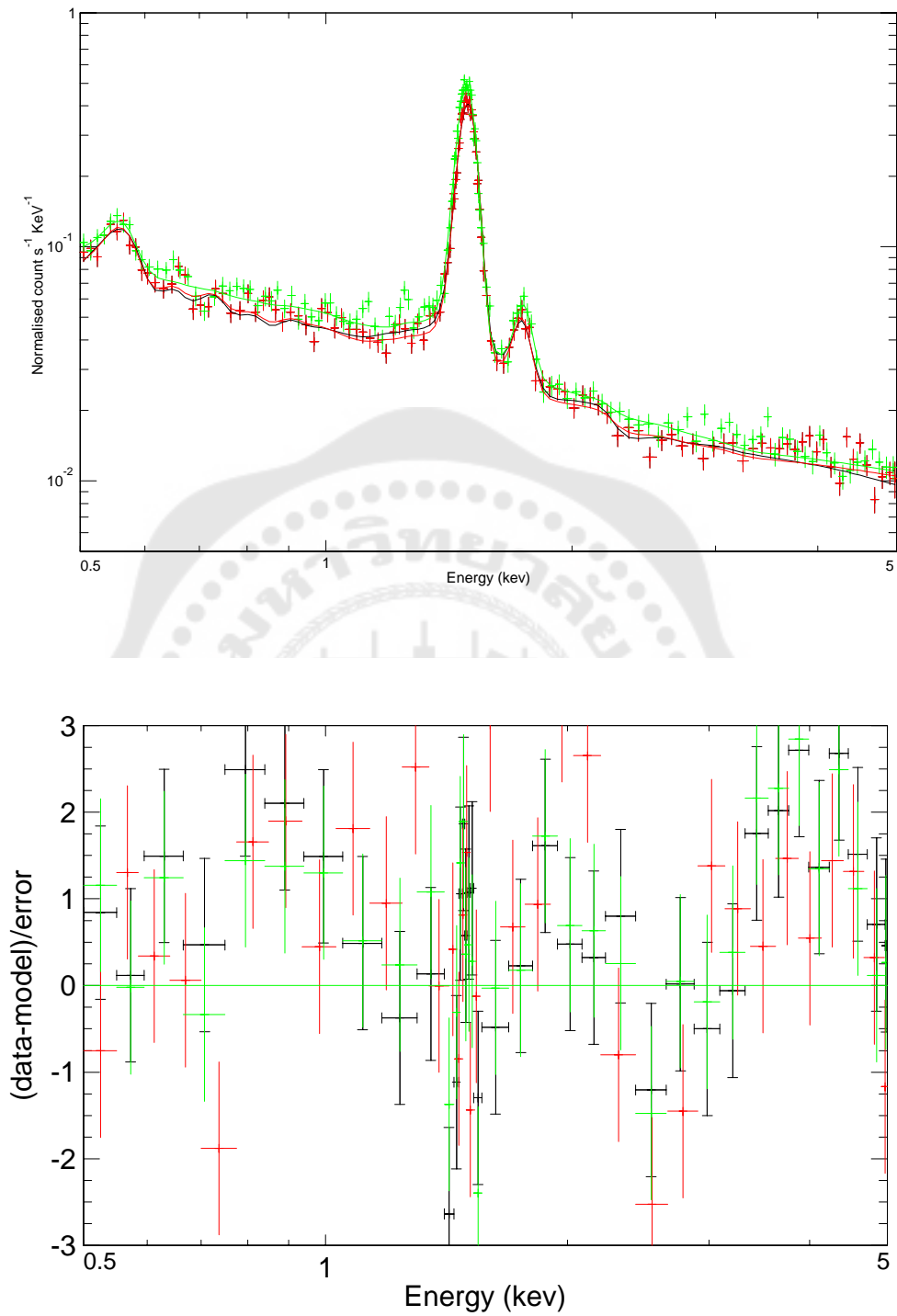


Figure 26 *Top panel:* The model data best fitting with M1-B1 (black), M1-B2 (red) and M1-B3 (green) spectra. *Bottom panel:* The residue plot of with M1-B1 (black), M1-B2 (red) and M1-B3 (green) spectra.

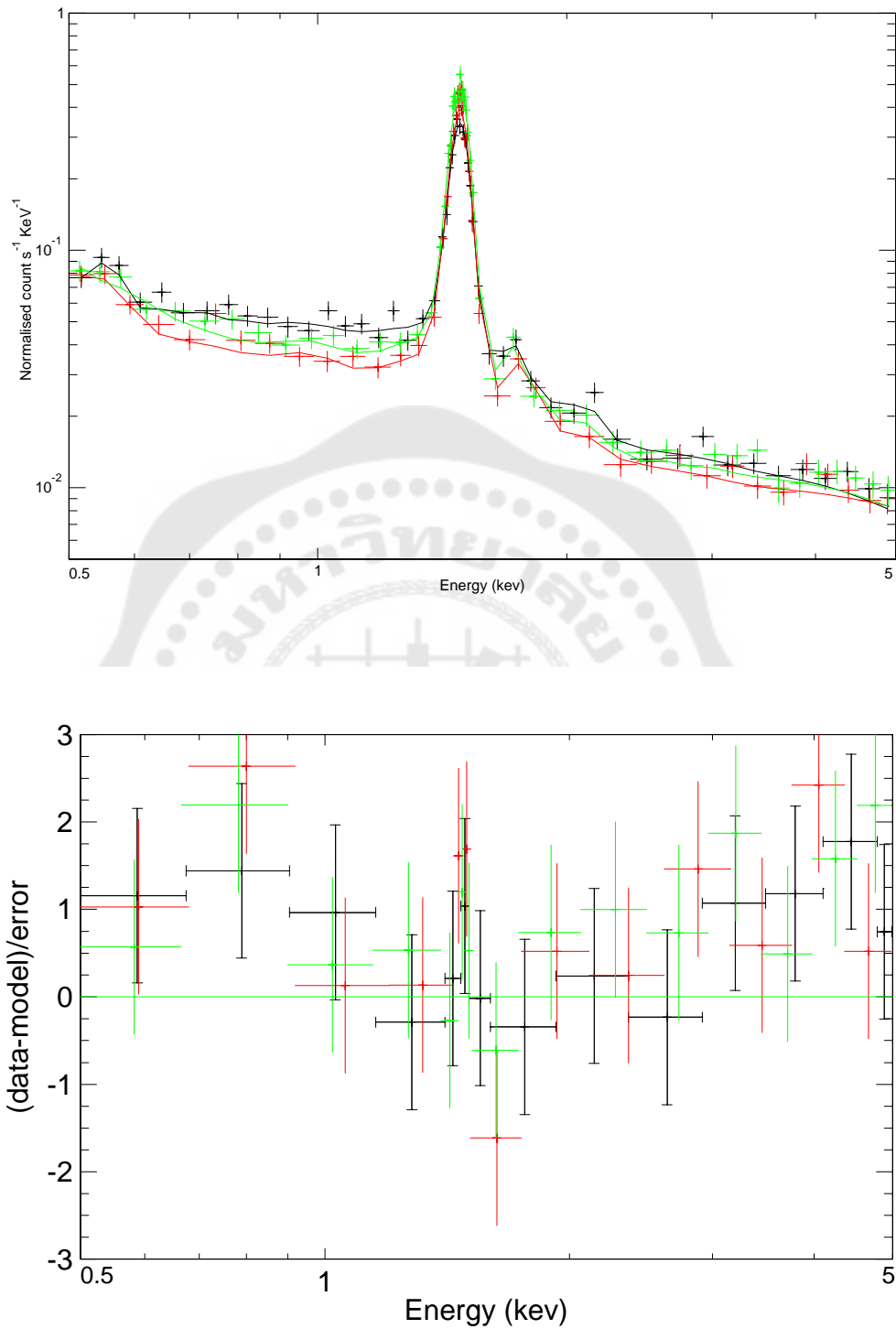


Figure 27 *Top panel:* The model data best fitting with M1-B1-ANO (black), M1-B2-ANO (red) and M1-B3-ANO (green) spectra. *Bottom panel:* The residue plot of with M1-B1-ANO (black), M1-B2-ANO (red) and M1-B3 -ANO (green) spectra.

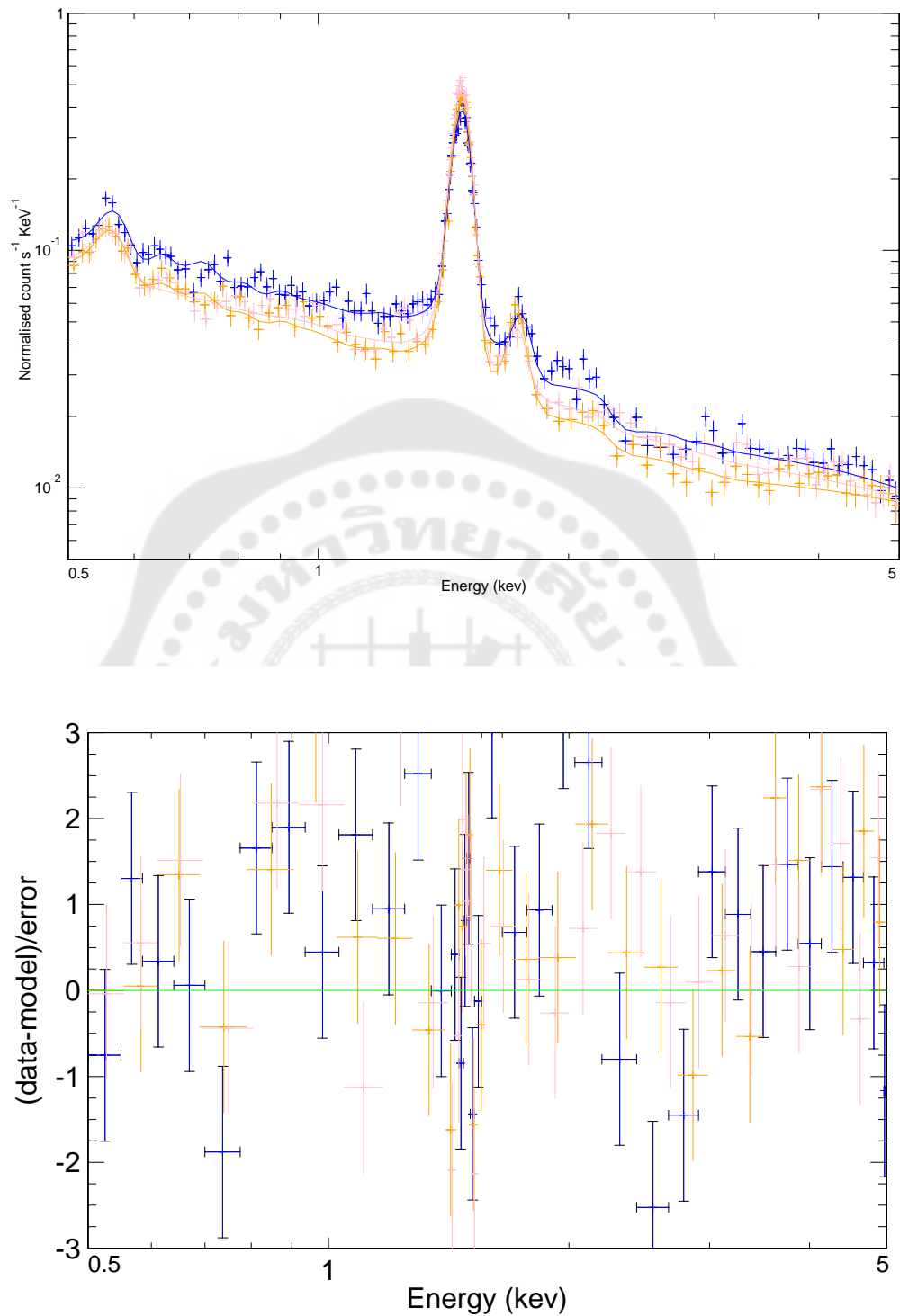


Figure 28 *Top panel:* The model data best fitting with M2-B1 (blue), M2-B2 (orange) and M2-B3 (pink) spectra. *Bottom panel:* The residue plot of with M2-B1 (blue), M2-B2 (orange) and M2-B3 (pink) spectra.

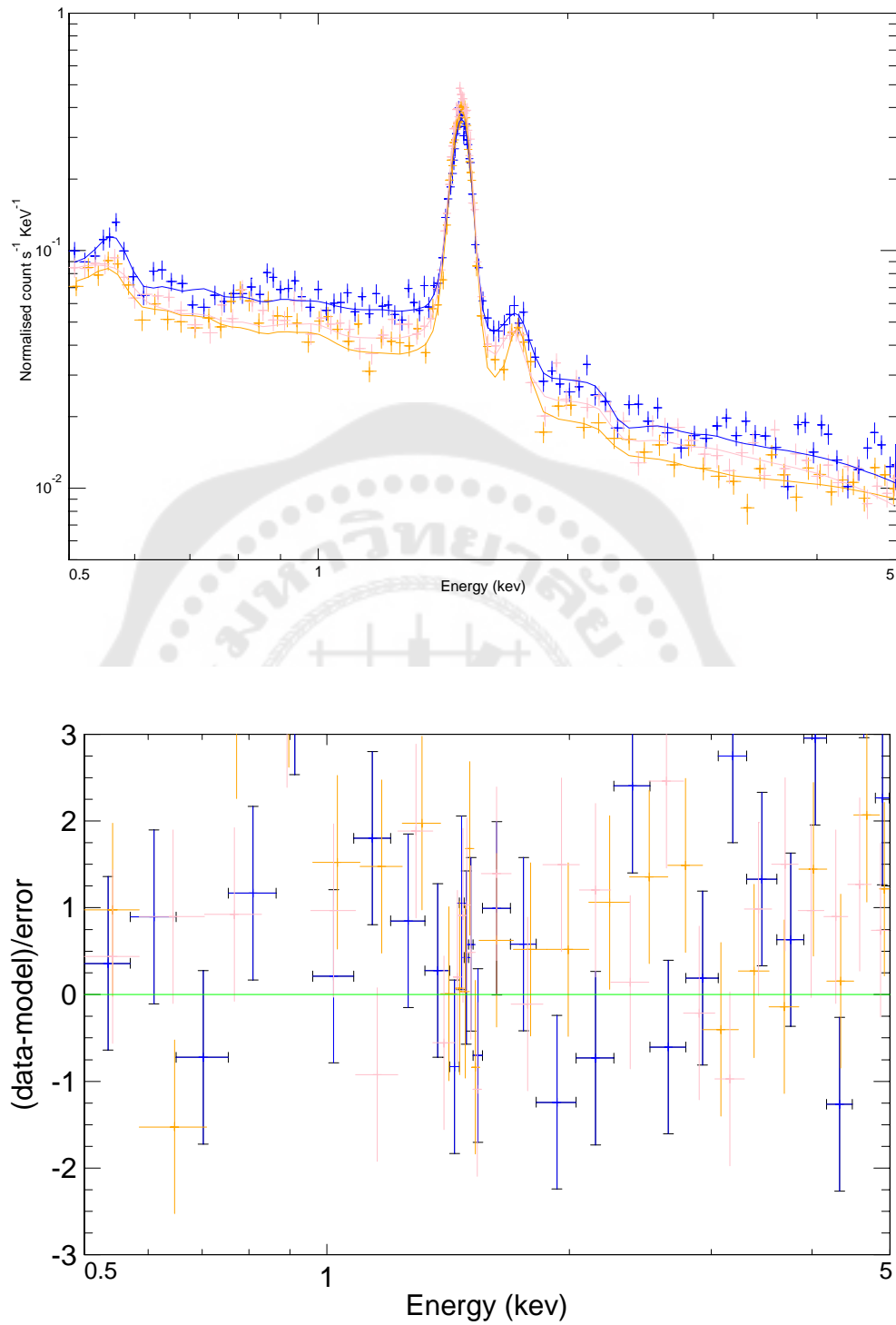


Figure 29 *Top panel:* The model data best fitting with M2-B1-ANO (blue), M2-B2-ANO (orange) and M2-B3-ANO (pink) spectra. *Bottom panel:* The residue plot of with M2-B1-ANO (blue), M2-B2-ANO (orange) and M2-B3-ANO (pink) spectra.

Table 5 The fitting result of MOS1 spectra with the eighth component model.

Model component (parameter [unit])	Spectrum							
	M1-B1	M1-B2	M1-B3	M1-B1-ANO	M1-B2-ANO	M1-B3-ANO	M1-B2-ANO	M1-B3-ANO
(1) GAUSS (line energy [keV])	1.49	1.49	1.49	1.49	1.49	1.49	1.49	1.49
(2) GAUSS (line energy [keV])	1.74	1.74	1.75	1.75	1.75	1.75	1.75	1.75
(3) APEC (temperature [keV])	0.32 ± 0.01							
(4) ABS*APEC (temperature [keV])	$0.27^{+0.03}_{-0.04}$	$0.27^{+0.03}_{-0.04}$	$0.27^{+0.03}_{-0.04}$	$0.27^{+0.03}_{-0.04}$	$0.27^{+0.03}_{-0.04}$	$0.27^{+0.03}_{-0.04}$	$0.27^{+0.03}_{-0.04}$	$0.27^{+0.03}_{-0.04}$
(5) ABS*APEC (temperature [keV])	≤ 2.49							
(6) ABS*POW (photon index)	$1.18^{+0.03}_{-0.01}$	$1.18^{+0.03}_{-0.01}$	$1.18^{+0.03}_{-0.01}$	$1.18^{+0.03}_{-0.01}$	$1.18^{+0.03}_{-0.01}$	$1.18^{+0.03}_{-0.01}$	$1.18^{+0.03}_{-0.01}$	$1.18^{+0.03}_{-0.01}$
(7) GAUSS (line energy [keV])	0.56	0.56	0.56	0.56	0.56	0.56	0.56	0.56
(8) ABS*BB (temperature [keV])	≥ 2.21							
(8) ABS*BB (logflux [$\text{erg} \cdot \text{s}^{-1} \text{cm}^{-2}$])	$-12.89^{+0.04}_{-0.14}$	$-12.88^{+0.04}_{-0.14}$	$-12.39^{+0.04}_{-0.14}$	$-12.89^{+0.04}_{-0.14}$	$-12.88^{+0.04}_{-0.14}$	$-12.39^{+0.04}_{-0.14}$	$-12.88^{+0.04}_{-0.14}$	$-12.39^{+0.04}_{-0.14}$
CONSTANT	1.00	1.00	1.00	1.00	1.00	1.00	1.00	1.00
BROKEN POWER-LAW (breaking energy [keV])	3.32	3.32	3.32	3.32	3.32	3.32	3.32	3.32
$\chi^2/\text{degree of freedom}$	6762/6103							

Notes. See text for the explanation of each model component and parameter.

Table 6 The fitting result of MOS2 spectra with the eighth component model.

Model component (parameter [unit])	Spectrum					
	M1-B1	M1-B2	M1-B3	M1-B1-ANO	M1-B2-ANO	M1-B3-ANO
(1) GAUSS (line energy [keV])	1.49	1.49	1.49	1.49	1.49	1.49
(2) GAUSS (line energy [keV])	1.75	1.75	1.75	1.75	1.75	1.75
(3) APEC (temperature [keV])	0.32 ± 0.01					
(4) ABS*APEC (temperature [keV])	$0.27^{+0.03}_{-0.04}$	$0.27^{+0.03}_{-0.04}$	$0.27^{+0.03}_{-0.04}$	$0.27^{+0.03}_{-0.04}$	$0.27^{+0.03}_{-0.04}$	$0.27^{+0.03}_{-0.04}$
(5) ABS*APEC (temperature [keV])	≤ 2.49					
(6) ABS*POW (photon index)	$1.18^{+0.03}_{-0.01}$	$1.18^{+0.03}_{-0.01}$	$1.18^{+0.03}_{-0.01}$	$1.18^{+0.03}_{-0.01}$	$1.18^{+0.03}_{-0.01}$	$1.18^{+0.03}_{-0.01}$
(7) GAUSS (line energy [keV])	0.56	0.56	0.56	0.56	0.56	0.56
(8) ABS*BB (temperature [keV])	≥ 2.21					
(8) ABS*BB (logflux [$\text{erg} \cdot \text{s}^{-1} \text{cm}^{-2}$])	$-12.89^{+0.04}_{-0.14}$	$-12.88^{+0.04}_{-0.14}$	$-12.39^{+0.04}_{-0.14}$	$-12.89^{+0.04}_{-0.14}$	$-12.88^{+0.04}_{-0.14}$	$-12.39^{+0.04}_{-0.14}$
CONSTANT	0.93	0.94	0.90	1.25	1.12	1.11
BROKEN POWER-LAW (breaking energy [keV])	3.11	3.11	3.11	3.11	3.11	3.11
$\chi^2/\text{degree of freedom}$	6762/6103					

Notes. ^aThe Gaussian line in KeV unit. ^bThe unsolved thermal and ^cthe seed photon of the ABS*APEC component (in unit of keV). ^dThe power-law photon index of ABS*POW component. ^eThe absorbed photon of blackbody component and also calculate the flux energy with $\text{erg} \cdot \text{s}^{-1} \text{cm}^{-2}$ unit. ^fThe constant of model between MOS1 and MOS2 data. ^gMinimum $\chi^2/\text{degree of freedom}$ from the fit.

Discussion

In previous section, 12 halo spectra were fitted with the eight model components of (1) GAUSS+ (2) GAUSS + (3) APEC + (4) ABS*APEC + (5) ABS*APEC + (6) ABS*POW + (7) GAUSS + (8) ABS*BB (A Kueathan et al., 2019), in which the first seven components represented both instrumental background and cosmic background following the suggestion in XMM - ESAS cookbook while the last component was added to represent the extra emission, including that of the pair halo (if exist). In the previous section, we explain the physical meaning of the first seven components, and we have argued that the value is reasonable. Therefore, in this section, we will discuss only the implication of the eighth component to determine whether we detect the halo X-ray emission?

As we demonstrated in the section “the simulated *XMM-Newton* spectra” of Chapter 3 that the exposure time of 500 ks would provide ~ 4500 halo photons obtained from pn, MOS1 and MOS2 detectors, this number of photons could be sufficient for detecting the halo at the statistical significant level of 3σ . However, since in this chapter, we analyzed only the data from MOS1 and MOS2 detectors, so we re-calculated the required exposure for detecting the halo at the statistical significant level of 3σ by using the WEBPIMM; the exposure time of ~ 4600 ks was required in this case. Although the total exposure time that was used in this Chapter (~ 400 ks) seems to be ~ 10 times lower than the required exposure time for detecting the halo, this number also depends on the physical parameters of the halo. In other words, we would require the exposure time of ~ 4600 ks for detecting the halo that has the seed gamma-ray energy of 100 TeV and 1000 nG IGMF. In fact, it has been shown that the halos occurring with some physical conditions would require the exposure time as low as a couple of ks for detection (A Eungwanichayapant et al., 2019). Therefore, since we don't know exactly the physical parameter of H1426+428 halo, we cannot conclude that our exposure time is insufficient for detection the halo.

If the detection is possible, we then checked whether the blackbody component added into the model to represent the halo emission improve the spectral

fitting? We compare the residue of the fitting obtained from the models with and without the blackbody component as shown in Figure 30. It was found that adding the blackbody component slightly improve the fitting result. To be more confident, we checked whether this component is statistical preferred using F-statistic. The statistical test indicates that adding the blackbody component could improve the χ^2 by ~ 20 for four degree of freedom losing, corresponding to 1-F probability of 99.79% (the probability that adding the component help to improve the fit) (A Kueathan et al., 2019). Therefore, it seems that we need this component to explain the spectra. Then, we calculated the flux of the blackbody component and the values are shown in the Table 5 and Table 6. The values from these table that indicates that the flux of the halo component, the unresolved thermal-like emission, is in the level of $\approx 10^{-13} \text{ erg} \cdot \text{cm}^{-2} \cdot \text{s}^{-1}$. Crucially, this could imply that at least, there might be the excess photons that could not be explained by the known components in the literatures.

The next question is that if the flux from the blackbody component is genuine, is this the emission of the pair halo, or not? If not, one possibility is that it can be contaminate from another object that located nearby object. We checked the nearest bright source that might be affect to X-ray emission, in our case, the blazar H1426+428 is only one of the bright sources that located nearby object. Even we already moved the central of blazar region from our analysis in the reduction process, it is possible that we did not removed all of photon from this AGN completely. In fact, the removed AGN of the very bright source, fraction of the blazar point spread function (PSF) wing might affect our spectra, especially in the closely AGN region which is region B1 in our case due to the excess flux from the AGN. For this reason, we inquired into the level of blazar contamination on our spectra using the estimating fraction of the blazar flux that might fall down to the analysed regions. Given an information from the *XMM-Newton* user handbook, $\lesssim 1\%$ of point source flux would contribute to the region at angular radius $> 0.04^\circ$ off from the centre of PSF. Assuming that the flux of the blazar H1426+428 is $5.1 \times 10^{-11} \text{ erg} \cdot \text{cm}^{-2} \cdot \text{s}^{-1}$ (Ghisellini et al., 2010). In analysed regions that mostly close to the central of the AGN, region B1, that have the inner radius is 0.09° off from the

AGN centre. This inner radius indicated that radius is so much less than $5 \times 10^{-13} \text{ erg} \cdot \text{cm}^{-2} \cdot \text{s}^{-1}$ blazar flux could contribute to the region B1 and also in region B2 and B3, and so we confident that our analyzing region should not contaminate from the nearby object emission.

Thus, if we confident that the detected excess flux is genuine and also the excess flux is not a dominated flux from the nearby object emission, we might argue that the excess flux might be some of fraction that could arise from the pair halo emission of the blazar H1426+428 (A Kueathan et al., 2019). In fact, it is theoretically has predicted that SED of H1426+428's pair halos would seem similarly with the thermal-like emission as shown in Figure 4.3, so it is reasonable that the blackbody component was represented as the halo emission as we discussed above. Moreover, the simulated emission flux (A Eungwanichayapant et al., 2019) that we obtained from the H1426+428 show the possible level flux was generated from the seed gamma ray energy $\sim 70 - 100 \text{ TeV}$ that gyrated in the ambient magnetic field $\sim 1000 \text{ nG}$ will give the emission flux in the the order of $10^{-13} \text{ erg} \cdot \text{cm}^{-2} \cdot \text{s}^{-1}$, obviously which this level flux is broadly consistent with our detection. However, we cannot confident that the excess flux is only some fraction of the halo, this is still caveat with this interpretation. Actually, the analyzed *XMM-Newton* background is more complicate tasks and need carefully perform. Here, we carefully follow the suggested steps for analyzing our data, we regard this excess flux that we found as the first order approximation; the deeper analyses which examine every model component carefully are required in the future work to confirm the results. In addition, we accepted that fact that the blackbody component was used to represent the halo emission, it might be one of high risk of misinterpretation due to two reasons (A Kueathan et al., 2019); (i) it could not explain well the halo spectra above $\sim 1 \text{ keV}$ and (ii) the thermal emission is one of the common emissions of astronomical objects. For the latter reason, we cannot neglect the fact that the detected thermal-like emission might be the combined emissions from many types of astronomical object, including the pair halo also. However, this also means that we

cannot reject the scenario which this thermal-like emission could be the emission of the halo. More data as well as other method would be needed to confirm this.

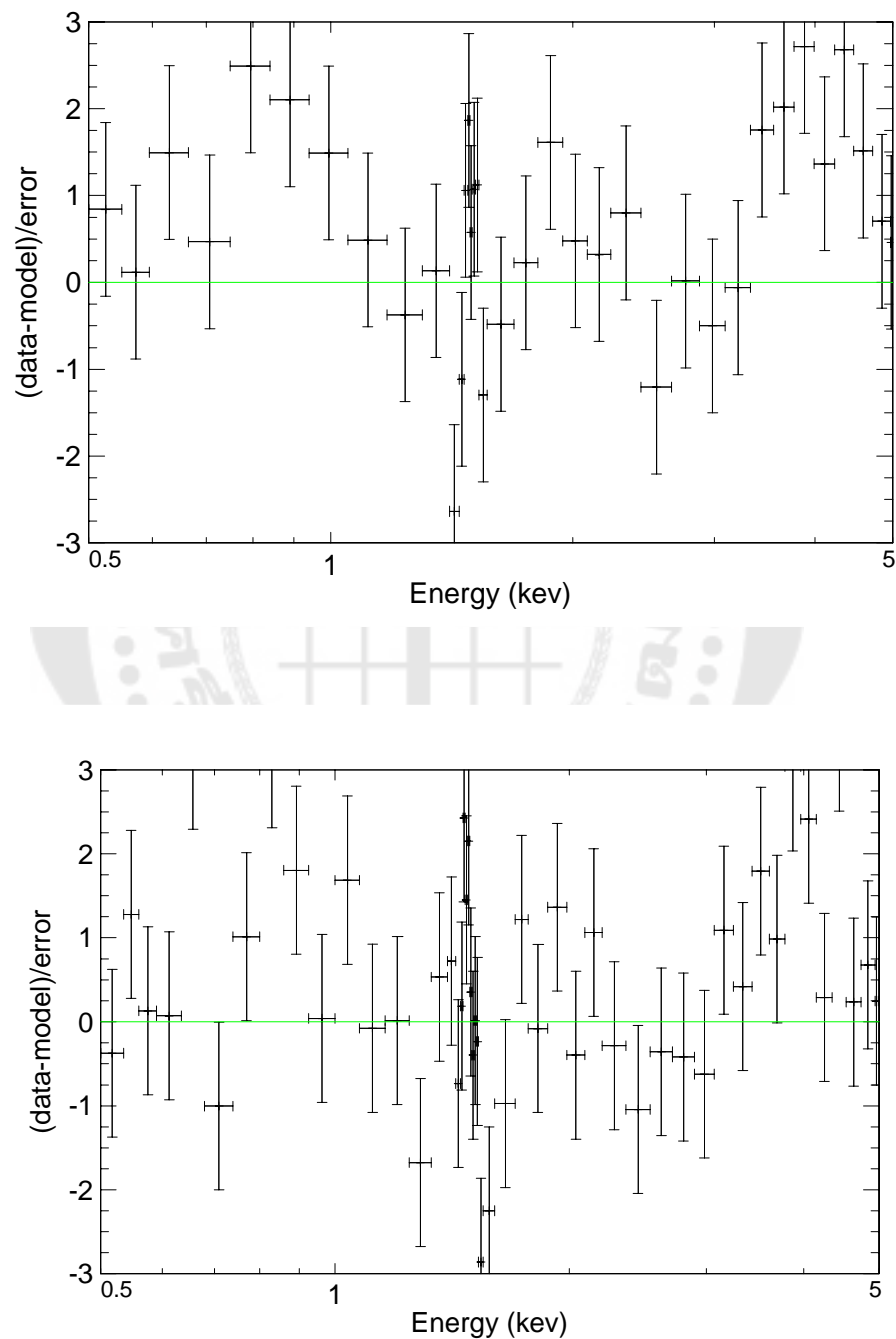


Figure 30 The fitting residue obtained from the model without (top panel) and with blackbody (bottom panel) component.

Conclusion

In this chapter, we analyzed the X-ray emission flux which obtained from the observed area's H1426+428, this is for searching the X-ray photons from an electron/positron pair halo. We end up twelve good quality spectra which were carefully created from the seven H1426+426's observations following the standard steps by the *XMM-Newton* cookbook suggestion. We mainly modelled these observed spectra using the suggested eight components model that including the absorbed blackbody component which represented the pair halo emission flux of our source. The mainly background, instrument and unresolved cosmic background (Kuntz & Snowden, 2008), were accounted by these eight components including the extra emission flux, here is pair halo component. The excess flux of $\approx 10^{-13} \text{ erg} \cdot \text{cm}^{-2} \cdot \text{s}^{-1}$ has been detected from the absorbed blackbody component, we also discuss that the possibility emission whether this excess flux could be intrinsic of the pair halo emission from the blazar H1426+428, and finally, we also argue that at least, some fraction of detected flux could be the X-ray emission of the halo as the first order approximation and require the further analysis to confirm this.

CHAPTER 5

CONCLUSION

Throughout this thesis, we have attempted to search for an electron/positron pair halo using the *XMM-Newton* observatory. In this chapter, we will summarise the key results found in this thesis; the properties of X-ray SEDs of H1426+428, the simulated X-ray spectral results, and the possibility whether the detected X-ray flux could be intrinsic to the halo emission, based on the results found in previous chapters. Also, at the end of this chapter, we will suggest further works for studying and searching for the electron/positron pair halo.

Conclusion

In this thesis, we have chosen the blazar H1426+428 as candidate source for searching an electron/positron pair halo. We computed the X-ray SEDs of H1426+428's halo and used these SEDs as emission model of the halo. This emission model was computed using the parameters obtained from the properties of H1426+428's: the monoenergetic, intrinsic gamma-ray photon energy of 100 TeV, source luminosity of $10^{45} \text{ erg} \cdot \text{s}^{-1}$ and a magnetic field of $1 \mu\text{G}$. In this work, the calculation of X-ray SEDs were obtained from three different angular areas in which we used size the *XMM-Newton* field of view for dividing: region A (covering the angular distance from 0 – 0.133 degrees), region B (covering the angular distance from 0 – 0.133 degrees) and region C (covering the angular distance from 0.200 to infinite degree); note that the region A was defined as the region with has high contamination from the central AGN. Our X-ray SED results show an emitted photon of the pair halo in the X-ray waveband that we should obtain if the halo with our assumed properties exists. We found that most halo photons fall in region A which is the area that is closest to the central AGN, comparing to the region B and region C.

Then, we used these obtained X-ray SEDs as an emission model to simulate the observed spectra of *XMM-Newton*. As we expected, we found that $\sim 97 - 98\%$ of halo photons could be detected in the region A and B, which are still in the field of view of *XMM-Newton* telescope. Moreover, we also found that the halo photons could be detected in region A rather than in the region B; however, we argued that the area in region A is too difficult to study the halo emission because there would be high contamination from AGN. Therefore, in this work, we only focused on the halo photons from Region B which cover the angular distance from 0.133 - 0.200 degrees. We have reasoned that this region is the best candidate area for searching the halo because this is the area that is still in the field of view of the *XMM-Newton*, and is sufficiently far so that we can ignore the AGN emission. In fact, our calculation showed that $\sim 16 - 17\%$ of all halo photons (or around 580 photons with an exposure time of 500 ks) would detect in this area.

After that, we analysed the observed spectra of H1426+428 obtained from *XMM-Newton* to estimate whether we could detect the halo photons from the data. We began to search for the observations of H1426+428 from the *XMM-Newton* data archive. Subsequently, we carefully reduced and then analysed these data, in particular that from the region B; this is to be confident that the analysed area were not contaminated from the flux of AGN. However, we also avoid to create a single spectrum from the area of region B since this could lead to the problem of too much difference between the effective areas of the inner and outer regions. Therefore, we divide our analysed region into three sub-regions: region B1, B2, and B3; region B1 covers the angular distance from 0 - 0.15 degree which also excluded the data from CCD1; region B2 covers the angular distance from 0.15 - 0.19 degree; region B3 covers the angular distance from 0.19 - 0.22 degree. Using these criteria, all of twelve good quality spectra from seven observations of the blazar H1426+428 have been created following the instruction provided in the XMM-ESAS webpage. The eight component model were fitted with the twelve spectra which were accounted for all instrument backgrounds, unresolved cosmic backgrounds, and the extra, pair halo component. The result from

the modeling suggested the excess flux around the candidate source which is in order $10^{-13} \text{ erg} \cdot \text{cm}^{-2} \cdot \text{s}^{-1}$. We discussed the origin of this excess flux whether this flux could be intrinsic to the halo emission. Three main reasons which might cause the observed excess photons has been discussed: (i) too much components and free parameters in the model, (ii) contamination from the nearby object, especially AGN, and (iii) the flux that could arise from the pair halo emission of the blazar H1426+428. We argue that the first reason is unlikely since we performed the statistical test to calculate the confidential level of adding the model component. For the second reason – the contamination from AGN, our calculation showed that the fraction of AGN photons fall into the region B should be very small and ignorable. Therefore, we argued that at least some fraction of detected flux could be the X-ray emission of the halo.

Future work

Given the scope of this work, we have calculated for only one condition of the halo - the monoenergetic, intrinsic the gamma-ray photon energy of 100 TeV, source luminosity of $10^{45} \text{ erg} \cdot \text{s}^{-1}$ and a magnetic field of $1 \mu\text{G}$ – to obtain the X-ray SEDs of H1426+428 halo, in order to estimate the pair halo emission. In fact, since the halo could occur with various initial conditions. Simulating the halo emission using other conditions could also be useful. In this section, we will suggest some additional and further works for studying and searching for pair halos.

The simulation of X-ray SEDs of pair halos with other conditions

As we stated above, we have not computed the X-ray SEDs of pair halo in other conditions such as at different magnetic field (B) and different intrinsic gamma-ray photon energy. The X-ray SEDs from several cases of the difference magnetic fields and intrinsic gamma-ray photon energy would present the halo emission from the various sources, other than H1426+428. Another further work is that the simulation of the X-ray SEDs of pair halo using the power-law distribution of the gamma-ray photon, instead of

the monoenergetic distribution. This assumption would be more realistic distribution of the gamma-ray emission from blazars. (Anant Eungwanichayapant, 2003). The results from these will help to constrain the range of parameters of the halo which make the halo observable.

The search for X-rays from pair halo using other current and future X-ray observatories

To gain more information data to search the pair halo, the observed X-ray data from other current X-ray observatories --i.e. *Chandra*, *Swift*, *NuSTAR* and *Suzaka*-- could be used, which might provide more opportunity to search the pair halo. These X-rays detector that we talked before, given us to observe the pair halo in difference energy band depend on these sensitivities of X-ray detector, therefore, we also detect whether the X-ray emission from pair halo theoretically proposed in this thesis will be examined by the current generation. In addition, in the near future, we might use the X-ray data from higher sensitivity observatories such as from that of Advanced Telescope for High-ENERgy Astrophysics (*Athena*). It is aimed that the *Athena* satellite will be operated in the energy range of 0.2 – 12.0 keV (Nandra et al., 2014) and will offer spectroscopic and imaging capabilities exceeding the currently operating X-ray astronomy satellites - e.g. the *Chandra* X-ray observatory and *XMM-Newton* observatory - by at least one order of magnitude on several parameter spaces simultaneously. We expected that, with the data from *Athena*, we might have more possibility to detect the halos.

The observations of pair halo in gamma-ray waveband using future generation detectors

As we have known that the pair halo emission was initially searched in gamma-ray waveband and there has been such an attempt in this band until now. Therefore, detecting the halo in this traditional waveband is still a challenge. In the near future, the search for the pair halo could be performed using Cherenkov Telescope Array (CTA), which is the next generation ground-based observatory for VHE gamma-ray astronomy.

The CTA will be capable of detecting gamma rays in the energy range from 20 GeV to more than 300 TeV with unprecedented precision in energy (Mazin, 2019). With sensitivity of CTA, the search for the halo gamma-ray emission could be performed at lower flux level, comparing to the current instruments.





APPENDIX

Appendix B

The result of X-ray SEDs of H1426+428's pair halo.

The X-ray SEDs from pair halos were simulated using the emission time distribution in Appendix A. The SEDs were simulated following the pre-defined region: Region A, Region B and Region C. The values of SEDs are shown below.

The X-ray SEDs from pair halo in Region A:

0.000289	0.000289	0.000289	0.000289	0.000289	0.000289
0.000289	0.000350	0.000350	0.000350	0.000350	0.000350
0.000350	0.000350	0.000423	0.000423	0.000423	0.000423
0.000423	0.000423	0.000423	0.000508	0.000508	0.000508
0.000508	0.000508	0.000508	0.000508	0.000607	0.000607
0.000607	0.000607	0.000607	0.000607	0.000607	0.000721
0.000721	0.000721	0.000721	0.000721	0.000721	0.000721
0.000852	0.000852	0.000852	0.000852	0.000852	0.000852
0.000852	0.000998	0.000998	0.000998	0.000998	0.000998
0.000998	0.000998	0.001159	0.001159	0.001159	0.001159
0.001159	0.001159	0.001159	0.001334	0.001334	0.001334
0.001334	0.001334	0.001334	0.001334	0.001517	0.001517
0.001517	0.001517	0.001517	0.001517	0.001517	0.001705
0.001705	0.001705	0.001705	0.001705	0.001705	0.001705
0.001888	0.001888	0.001888	0.001888	0.001888	0.001888
0.001888	0.002057	0.002057	0.002057	0.002057	0.002057
0.002057	0.002057	0.002198	0.002198	0.002198	0.002198
0.002198	0.002198	0.002198	0.002298	0.002298	0.002298
0.002298	0.002298	0.002298	0.002298	0.002343	0.002343
0.002343	0.002343	0.002343	0.002343	0.002343	0.002318
0.002318	0.002318	0.002318	0.002318	0.002318	0.002318
0.002214	0.002214	0.002214	0.002214	0.002214	0.002214

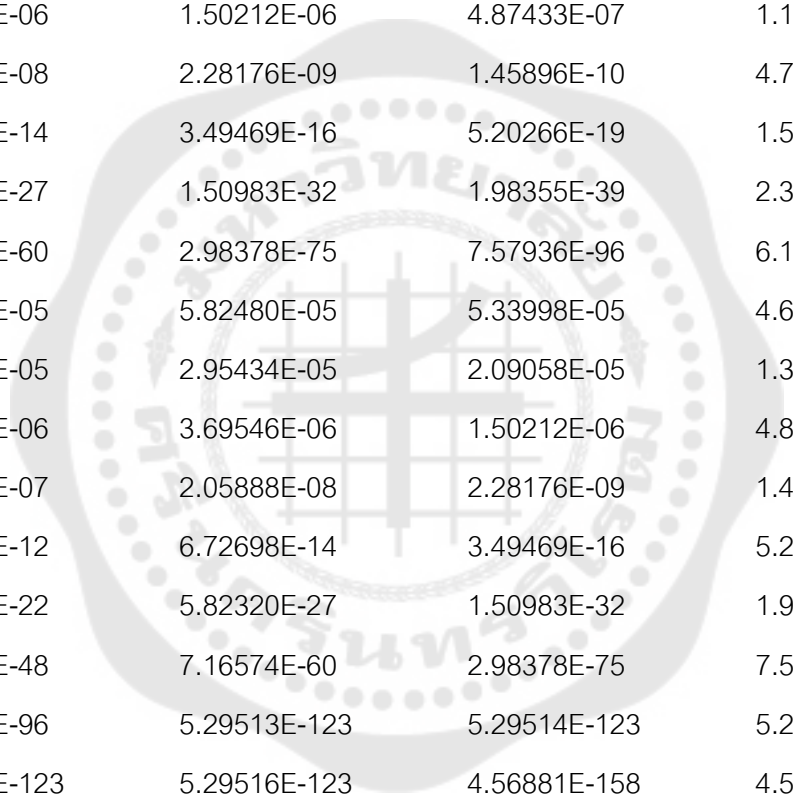
0.000000	0.000000	0.000000	0.000000	0.000000	0.000000
0.000000	0.000000	0.000000	0.000000	0.000000	0.000000
0.000000	0.000000	0.000000	0.000000	0.000000	0.000000
0.000000	0.000000	0.000000	0.000000	0.000000	0.000000
0.000000	0.000000	0.000000	0.000000	0.000000	0.000000
0.000000	0.000000	0.000000	0.000000	0.000000	0.000000
0.000000	0.000000	0.000000	0.000000	0.000000	0.000000
0.000000	0.000000	0.000000	0.000000	0.000000	0.000000
0.000000	0.000000	0.000000	0.000000	0.000000	0.000000
0.000000	0.000000	0.000000	0.000000	0.000000	0.000000
0.000000	0.000000	0.000000	0.000000	0.000000	0.000000
0.000000	0.000000	0.000000	0.000000	0.000000	0.000000

The X-ray SEDs from pair halo in region B:

6.155195E-05	6.155195E-05	6.155195E-05	6.155195E-05
6.155195E-05	7.415657E-05	7.415657E-05	7.415657E-05
7.415657E-05	7.415657E-05	8.903406E-05	1.064703E-04
1.267377E-04	1.500710E-04	1.766333E-04	2.064713E-04
2.394563E-04	2.752145E-04	3.130491E-04	3.518588E-04
3.900685E-04	4.255877E-04	4.558243E-04	4.778001E-04
4.883984E-04	4.847592E-04	4.648163E-04	4.279093E-04
3.753522E-04	3.107914E-04	2.401007E-04	1.705809E-04
1.094566E-04	6.202374E-05	3.017464E-05	1.216949E-05
3.896171E-06	9.389389E-07	1.596482E-07	1.769891E-08
1.162381E-09	4.015445E-11	6.268248E-13	3.610199E-15
5.820971E-18	8.903406E-05	1.064703E-04	1.267377E-04
1.500710E-04	1.766333E-04	2.064713E-04	2.394563E-04
2.752145E-04	3.130491E-04	3.518588E-04	3.900685E-04
4.255877E-04	4.558243E-04	4.778001E-04	4.883984E-04

4.847592E-04	4.648163E-04	4.279093E-04	3.753522E-04
3.107914E-04	2.401007E-04	1.705809E-04	1.094566E-04
6.202374E-05	3.017464E-05	1.216949E-05	3.896171E-06
9.389389E-07	1.596482E-07	1.769891E-08	1.162381E-09
4.015445E-11	6.268248E-13	3.610199E-15	5.820971E-18
8.903406E-05	1.064703E-04	1.267377E-04	1.500710E-04
1.766333E-04	2.064713E-04	2.394563E-04	2.752145E-04
3.130491E-04	3.518588E-04	3.900685E-04	4.255877E-04
4.558243E-04	4.778001E-04	4.883984E-04	4.847592E-04
4.648163E-04	4.279093E-04	3.753522E-04	3.107914E-04
2.401007E-04	1.705809E-04	1.094566E-04	6.202374E-05
3.017464E-05	1.216949E-05	3.896171E-06	9.389389E-07
1.596482E-07	1.769891E-08	1.162381E-09	4.015445E-11
6.268248E-13	3.610199E-15	5.820971E-18	8.903406E-05
1.064703E-04	1.267377E-04	1.500710E-04	1.766333E-04
2.064713E-04	2.394563E-04	2.752145E-04	3.130491E-04
3.518588E-04	3.900685E-04	4.255877E-04	4.558243E-04
4.778001E-04	4.883984E-04	4.847592E-04	4.648163E-04
4.279093E-04	3.753522E-04	3.107914E-04	2.401007E-04
1.705809E-04	1.094566E-04	6.202374E-05	3.017464E-05
1.216949E-05	3.896171E-06	9.389389E-07	1.596482E-07
1.769891E-08	1.162381E-09	4.015445E-11	6.268248E-13
3.610199E-15	5.820971E-18	8.903406E-05	1.064703E-04
1.267377E-04	1.500710E-04	1.766333E-04	2.064713E-04
2.394563E-04	2.752145E-04	3.130491E-04	3.518588E-04
3.900685E-04	4.255877E-04	4.558243E-04	4.778001E-04
4.883984E-04	4.847592E-04	4.648163E-04	4.279093E-04
3.753522E-04	3.107914E-04	2.401007E-04	1.705809E-04
1.094566E-04	6.202374E-05	3.017464E-05	1.216949E-05

7.89418E-06	9.48901E-06	1.13709E-05	1.35769E-05
1.61425E-05	1.90989E-05	2.24676E-05	2.62551E-05
3.04445E-05	3.49866E-05	3.97888E-05	4.47054E-05
4.95286E-05	5.39852E-05	5.77396E-05	6.04103E-05
7.89418E-06	9.48901E-06	1.13709E-05	1.35769E-05
1.61425E-05	1.90989E-05	2.24676E-05	2.62551E-05
3.04445E-05	3.49866E-05	3.97888E-05	4.47054E-05
4.95286E-05	5.39852E-05	5.77396E-05	6.04103E-05
7.89418E-06	9.48901E-06	1.13709E-05	1.35769E-05
1.61425E-05	1.90989E-05	2.24676E-05	2.62551E-05
3.04445E-05	3.49866E-05	3.97888E-05	4.47054E-05
4.95286E-05	5.39852E-05	5.77396E-05	6.04103E-05
6.16035E-05	6.09643E-05	5.82480E-05	5.33998E-05
4.66241E-05	3.84188E-05	2.95434E-05	2.09058E-05
1.33771E-05	7.57476E-06	3.69546E-06	1.50212E-06
4.87433E-07	1.19454E-07	2.05888E-08	2.28176E-09
1.45896E-10	4.73560E-12	6.72698E-14	3.49469E-16
5.20266E-19	1.55646E-22	5.82320E-27	1.50983E-32
1.98355E-39	2.31015E-48	7.16574E-60	2.98378E-75
6.16035E-05	6.09643E-05	5.82480E-05	5.33998E-05
4.66241E-05	3.84188E-05	2.95434E-05	2.09058E-05
1.33771E-05	7.57476E-06	3.69546E-06	1.50212E-06
4.87433E-07	1.19454E-07	2.05888E-08	2.28176E-09
1.45896E-10	4.73560E-12	6.72698E-14	3.49469E-16
5.20266E-19	1.55646E-2	2.82320E-27	1.50983E-32
1.98355E-39	2.31015E-48	7.16574E-60	2.98378E-75
7.57936E-96	6.16035E-05	6.09643E-05	5.82480E-05
5.33998E-05	4.66241E-05	3.84188E-05	2.95434E-05
2.09058E-05	1.33771E-05	7.57476E-06	3.69546E-06



1.50212E-06	4.87433E-07	1.19454E-07	2.05888E-08
2.28176E-09	1.45896E-10	4.73560E-12	6.72698E-14
3.49469E-16	5.20266E-19	1.55646E-22	5.82320E-27
1.50983E-32	1.98355E-39	2.31015E-48	7.16574E-60
2.98378E-75	7.57936E-96	6.16035E-05	6.09643E-05
5.82480E-05	5.33998E-05	4.66241E-05	3.84188E-05
2.95434E-05	2.09058E-05	1.33771E-05	7.57476E-06
3.69546E-06	1.50212E-06	4.87433E-07	1.19454E-07
2.05888E-08	2.28176E-09	1.45896E-10	4.73560E-12
6.72698E-14	3.49469E-16	5.20266E-19	1.55646E-22
5.82320E-27	1.50983E-32	1.98355E-39	2.31015E-48
7.16574E-60	2.98378E-75	7.57936E-96	6.16035E-05
6.09643E-05	5.82480E-05	5.33998E-05	4.66241E-05
3.84188E-05	2.95434E-05	2.09058E-05	1.33771E-05
7.57476E-06	3.69546E-06	1.50212E-06	4.87433E-07
1.19454E-07	2.05888E-08	2.28176E-09	1.45896E-10
4.73560E-12	6.72698E-14	3.49469E-16	5.20266E-19
1.55646E-22	5.82320E-27	1.50983E-32	1.98355E-39
2.31015E-48	7.16574E-60	2.98378E-75	7.57936E-96
7.57936E-96	5.29513E-123	5.29514E-123	5.29511E-123
5.29514E-123	5.29516E-123	4.56881E-158	4.56889E-158
4.56882E-158	4.56884E-158	4.56880E-158	2.18285E-202
2.18288E-202	2.18289E-202	2.18282E-202	2.18282E-202
2.58728E-257	2.58727E-257	2.58729E-257	2.58729E-257
2.58729E-257	0.000000000	0.000000000	0.000000000
0.000000000	0.000000000	0.000000000	0.000000000
0.000000000	0.000000000	0.000000000	0.000000000
0.000000000	0.000000000	0.000000000	0.000000000
0.000000000	0.000000000	0.000000000	0.000000000

0.000000000	0.000000000	0.000000000	0.000000000
0.000000000	0.000000000	0.000000000	0.000000000
0.000000000	0.000000000	0.000000000	0.000000000
0.000000000	0.000000000	0.000000000	0.000000000
0.000000000	0.000000000		



Appendix C

Research publications

In this work, we published the resulting of an electron/positron pair halo that might observe using *XMM-Newton* observatory. One of our publication published, The search for X-ray emission from electron/positron pair halos using the *XMM-Newton* observatory, that explain the possibility of an electron/positron pair halo which might happen in our candidate source, H1426+428, including a chance to observe them from the *XMM-Newton* observatory we they exist (see more details in Chapter3). Another one, we published the resulting of the observed an X-ray emission flux of H1426+428 that obtained the observed data from *XMM-Newton* observatory -Searching for the electron/positron pair halo of the Blazar H1426+428 using *XMM-Newton*- that shown an opportunity to search electron/positron pair halo from X-ray waveband (see more processing to observe and analysis pair halo in Chapter4). Here, we attracted our two publications below;

PAPER · OPEN ACCESS

Searching for the electron/positron pair halo of the Blazar H1426+428 using XMM-Newton

To cite this article: A Kueathan *et al* 2019 *J. Phys.: Conf. Ser.* **1380** 012117

View the [article online](#) for updates and enhancements.



IOP ebooksTM

Bringing you innovative digital publishing with leading voices to create your essential collection of books in STEM research.

Start exploring the collection - download the first chapter of every title for free.

Searching for the electron/positron pair halo of the Blazar H1426+428 using XMM-Newton

A Kueathan¹, W Luangtip^{1,2*} and A Eungwanichayapant^{3,2}

¹ Department of physics, Faculty of Science, Srinakharinwirot University, Bangkok 10110, Thailand

² National Astronomical Research Institute of Thailand, Chiangmai 50180, Thailand

³ School of Science, Mae Fah Luang University, Chiang Rai 57100, Thailand

*E-mail: wasutep@g.swu.ac.th

Abstract. Electron/positron pair halo is a physical phenomenon in which the very high energy gamma rays emitted from Blazar interact with cosmic infrared background (CIB) so that produce the electron/positron pairs; the produced electron/positron pairs could up-scatter the cosmic microwave background (CMB) reproducing the gamma-rays, thus these form the cascade process of producing the electron/positron pairs appearing as an halo around the blazar. In case that the halo presents in the ambient strong magnetic field, the electron/positron pairs could emit X-ray light via synchrotron process providing another opportunity to detect the halo. In this work, we search for the X-ray emission from the halo of the Blazar H1426+428 using the observed X-ray data from *XMM-Newton* observatory. The X-ray spectra of the halo are carefully extracted from the annulus, source free regions around the Blazar to avoid the X-ray contaminations from the Blazar itself and the nearby point sources. These spectra were fitted using the physical model which takes into account the emissions from the unresolved cosmic X-ray and instrument backgrounds. The unresolved flux of $\approx 10^{-13}$ erg s⁻¹ cm⁻² have been detected in the regions, and we argue that, at least, some fraction of the flux might be the emission from the halo.

1. Introduction

Active Galactic Nuclei (AGN) have been known as extragalactic sources of very high energy (VHE, $E \gg 100$ GeV) gamma-rays. During traveling in the cosmological scale, some of these gamma-rays cannot reach to us because they interact with infrared photons in Extragalactic Background Light (EBL) via $\gamma\gamma$ -pair production (PP). The absorption of the gamma-rays has been reported [1] and expected as an indirect tool for probing the EBL. The products of the absorption are pairs of energetic electron/positron that, in turn, can interact with microwave photons in Cosmic Microwave Background (CMB) to be VHE gamma-rays via inverse Compton scattering (IC). These second gamma-rays will redo the same processes as their ancestor did until their energies are not enough to be absorbed by the EBL photons. These processes are called the electromagnetic cascades. The study of the cascades neglect the effect of extragalactic magnetic fields (EGMFs) until the model of electron/positron pair halos was proposed in 1994 [2]. In the model, the EGMFs gyrate the electron/positron pairs in the cascades several rounds before proceed the cascades. As a result, the cascades develop isotropically around the AGN and create electron/positron pairs that can emit observable photons. Gamma-ray from inverse Compton scattering is the first type of the observable photons that people used for searching the pair halos.



The spectral energy distribution (SED) and the spatial distribution of gamma-ray predicted in 2009 [3] were used to find the signal of the pair halo. Searching pair halos with gamma-ray is very challenging because there are still no strong evidence from observation gamma-rays [4–5]. On the other hand, X-ray photons from synchrotron radiation of the electron/positron pairs could provide another promising window of opportunity for searching pair halos. It has been shown by [6] that the simulated SEDs of X-ray pair halos and the sensitivity of the XMM-Newton are comparable, suggesting the possibility of detecting a pair halo signal.

Blazar H1426+428 is one of the best candidates for searching a pair halo at least in the gamma ray regime. The redshift $z = 0.129$ of this object is the suitable distance for forming a pair halo. Moreover, this blazar has been reported the EBL absorption features in its SED [7–8], which means the electromagnetic cascades have already triggered. In this work, we will analysis the stacked X-ray data to search for the extended components of H1426+428, which could be the radiation from the pair halo.

2. Observations and data reduction

We searched for the X-ray data of the blazar H1428+428 from XMM-Newton science archive [9]. Out of eight observations found, we skipped one that is off-axis observation, and proceeded to study with only on-axis observations tabulated in table 1. Since the halo is theoretically predicted to radiate as a sphere around the central blazar (i.e. the halo) up to scale of Mpc [10], we skipped analysing the data obtained from the central CCD (see figure 1) to avoid the contamination from the central blazar, and focused on the data obtained from the other CCDs as shown in figure 1. We performed the data reduction and data analysis following the method suggested for analysing XMM-Newton observations of extended sources (XMM-ESAS cookbook) using XMM-ESAS package [11]. In brief, the observational data were reprocessed using the latest instrument calibration. Then, the observing periods which were highly affected by soft proton background flaring were removed to get the clean observational data. We also removed the data from CCDs which were in anomalous state (see column 4-5 of table 1 and figure 1). Finally, any point sources detected in the telescope's field of view were removed to minimise the contamination. The observational data created by these steps were then used to extract the energy spectra. In fact, we divided the observational data into three regions – region A, B and C – defined in figure 1 and extract the spectra from these individual regions, instead of extracting single spectrum from the entire region. This is to avoid creating the spectrum from the single area which varies in response matrix largely from inner edge to outer edge. Indeed, since each individual observation always had two data sets obtained from the MOS1 and MOS2 cameras, so we got six spectra in total from each observation. Finally, to gain S/N of the spectra for further analysis, we grouped the spectra of every observation obtained from the same region and camera together, and combined the spectra within each group using the package ADDSPEC [12]; however, since we lost the MOS1 and/or MOS2 data of some observations due to the anomalous state, so the spectra from each group were also divided into two sub-groups: i.e. ones affected and not affected by anomalous state. Using these criteria, we end up with 12 spectra. Each spectrum was grouped to have a minimum of 25 counts per bin to utilise the χ^2 minimisation method during the spectral fitting and were then used as the basis for further analysis.

3. Spectral analysis and discussion

Here, we used an X-Ray Spectral Fitting Package (XSPEC) [13] to model the obtained X-ray spectra over the energy range of 0.5 - 5.0 keV. Since we had already removed all well know sources of X-ray emission, i.e. the central blazar H1426+428 and any significant point sources,

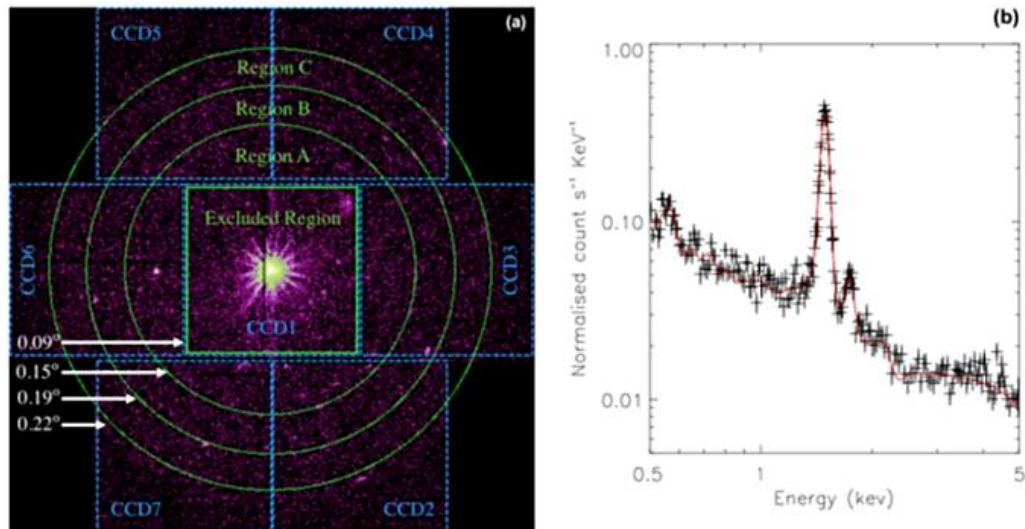


Figure 1. (a): the example MOS observation of the H1428+428. The overlaying green lines indicate the region A, B and C used in the analysis; the angular distance of each line from the centre is indicated by the white arrow. The blue dashed lines indicate the boundary of each CCD. (b): The model data (red) best fitted with the observed spectra (black) obtained from region A of MOS1 camera.

Table 1. XMM-Newton observational data of H1426+428.

Observation ID	Observing date	Exposure time (ks)	CCD# being in anomalous state	
			MOS1	MOS2
0111850201	2001-06-16	68.6	-	-
0165770101	2004-08-04	67.9	-	-
0165770201	2004-08-06	68.9	-	-
0212090201	2005-01-24	30.4	-	5
0310190101	2005-06-19	47.0	6	5
0310190201	2005-06-25	49.5	6	5
0310190501	2005-08-04	47.5	4,6	5

one might expect that the X-ray photons obtained from the region A, B and C should be dominated by instrument background and the unresolved cosmic background. Thus, according to the XMM-ESAS cookbook, we constructed the model with eight components to explain the spectra: (1)GAUSS + (2)GAUSS + (3)APEC + (4)ABS*APEC + (5)ABS*APEC + (6)ABS*POW + (7)GAUSS + (8)ABS*BB. The first two gaussian (GAUSS) components are to account for the Al K α (E~1.49 keV) and Si K α (E~1.75 keV) instrumental emission lines, respectively [14]. The third APEC component represents the plasma emission from the Local Hot Bubble or heliosphere. The fourth and fifth ABS*APEC components are the absorbed plasma emission that represent the emission from the clusters or intergalactic medium, and the hot plasma from unresolved component such as that of AGN, respectively. The sixth absorbed power-law component (ABS*POW) is used to explain the unresolved point source such as X-ray binaries or AGN.

The seventh gaussian component is used to account for the line-like feature obviously seen in the spectra at $E \sim 0.56$ keV (see figure 1 (b)). Finally, the eighth absorbed blackbody component (ABS*BB) is used to represent the extra, thermal-like emission from any other components, including electron/positron pair halo (if exist). In addition to this, the broken power-law were also add to the model to account for the residue of soft photon contamination which cannot remove completely.

All 12 spectra were fitted simultaneously to get the best statistical constraint of fitted parameters. In fact, we also add the constant component to the model to allow for a small difference between MOS1 and MOS2 data (given that the detectors are not perfectly identical), and also for normalising the data obtained from region A, B and C. The spectral fitting result are illustrated in table 2 and the right panel of figure 1. We note the that the fitting value obtained from all spectra are well consistent and, here, we show only the fitting results obtained from the region A of MOS1 which were not affected by anomalous state. From figure 1, it is obvious that the model could explain well the data even though the reduced χ^2 value of 1.11 seems to be a little higher than unity; in fact, since all spectra are fitted simultaneously, the high number of spectral bins (6279 bins) could lead to this results and we regard this as the statistical acceptable results. In addition, as all best fitting parameters of the component 1, 2, 3, 4, 5 and 6 reported in table 2 are broadly consistent with the values suggested in the XMM-ESAS cookbook, here, we will skip discussing further the values of these parameters (albeit the upper bound temperature of the fifth component seems to be higher than that we expect). In case of the gaussian component (7) added to the model to improve the fit, although the physical origin is still unclear whether it arise from the instruments or the cosmic background, we regard that adding this component does not affect the detection of the pair halo since the spectral energy distribution of the halo are thermal-like rather than the line-like [6].

Table 2. Fitting results of region A spectrum obtained from MOS1.

Model component (parameter)	Value (unit)
(1)GAUSS (line energy)	1.49 (keV)
(2)GAUSS (line energy)	1.75 (keV)
(3)APEC (temperature)	0.32 ± 0.01 (keV)
(4)ABS*APEC (temperature)	$0.27^{+0.03}_{-0.04}$ (keV)
(5)ABS*APEC (temperature)	≤ 2.49 (keV)
(6)ABS*POW (photon index)	$1.18^{+0.03}_{-0.01}$
(7)GAUSS (line energy)	0.56 (keV)
(8)ABS*BB (temperature)	≥ 2.21 (keV)
(8)ABS*BB (log flux)	$-12.89^{+0.04}_{-0.14}$ ($\text{erg s}^{-1} \text{cm}^{-2}$)
$\chi^2 / \text{degree of freedom}$	6762.92/6103

As defined in the model, the absorbed blackbody component is used to represent the extra unresolved thermal-like emission that might have not been detected yet, including the pair halo emission. Thus, the detected blackbody-like flux of $\approx 10^{-13} \text{ erg s}^{-1} \text{ cm}^{-2}$ could imply that at least, there might be the excess photons that could not be explained by the known components in the literatures. However, one might not be surprised to see the excess photons since, mathematically, adding more component is simply the increment of free parameters. Thus we check whether this component is statistical preferred using F-statistic; adding the blackbody

component improve the χ^2 by ~ 20 for four degree of freedom losing, corresponding to 1-F probability of 99.79% (the probability that adding the component help to improve the fit). Therefore, it is unlikely that the flux detected is spurious.

The next question is that if the flux is genuine, can it be the contamination from the nearby object. In fact, the nearest, bright source in our case is the blazar H1426+428. Although the central blazar region were removed from our analysis, as the source is very bright, some fraction of the blazar point spread function wing might affect our spectra, especially that of the region A, causing the contamination. We simply check the level of blazar contamination on our spectra by estimating the fraction of the blazar flux falling into our analysing regions. From the XMM-Newton user handbook [15], $\lesssim 1\%$ of point source flux would contribute to the region at angular radius $>0.04^\circ$ off from the source centre. Assuming that the flux of the blazar H1426+428 is $5.1 \times 10^{-11} \text{ erg s}^{-1} \text{ cm}^{-2}$ [16] and the inner radius of the region A is 0.09° off from the source centre, so much less than $5 \times 10^{-13} \text{ erg s}^{-1} \text{ cm}^{-2}$ blazar flux could contribute to the region A, B and C, and so we regard that this contamination should not dominate the emission in our analysing region.

Thus, if the detected excess flux is genuine and not dominated by the blazar emission, we might argue that the flux (at least some fraction) could arise from the pair halo emission of the blazar H1426+428. In fact, it is theoretically predicted that the spectral energy distribution of halos would seem nearly as the thermal-like emission [6], so that it is reasonable to represent the halo emission using the blackbody component. Moreover, our simulations (Eungwanichayapant et al. in prep.) show that the flux of H1426+428 halo generated from the seed blazar gamma ray energy of $\sim 70 - 100 \text{ TeV}$ surrounded by $\sim 1000 \text{ nG}$ ambient magnetic field could be in the order of $10^{-13} \text{ erg s}^{-1} \text{ cm}^{-2}$, broadly consistent with our detection. However, there are still caveats with this interpretation. In fact, analysing the XMM-Newton background is the complicate tasks and need to perform very carefully (see [17] and references therein). In this work, as we follow the standard steps for analysing the data, we regard this as the first order approximation; the deeper analyses which examine every model components carefully are required in the future work to confirm the results. In addition, using the blackbody component to represent the halo emission might be at risk of misinterpretation since the thermal emission is one of the common emissions of astronomical objects. In fact, the detected thermal-like emission might be the combined emissions from many types of astronomical objects, including the pair halo. Thus, as discussed above, one must carefully examine the model components before interpret the emission as pair halo.

4. Conclusion

In this work, we analysed the X-ray data obtained from the areas around the blazar H1426+428 in order to search for the pair halo emission. Twelve good quality spectra had been created from seven observations of the blazar H1426+428. We modeled the spectra using eight components model which were accounted for all instrument backgrounds, unresolved cosmic backgrounds and the extra pair halo component. The excess flux of $\approx 10^{-13} \text{ erg s}^{-1} \text{ cm}^{-2}$ has been detected and we discuss the possibility whether this flux could be intrinsic to the halo emission. We regard that the results are an first order approximation; the further analysis are required to confirm this.

Acknowledgments

AK acknowledges financial support in the form of funding for a postgraduate studentship from the Research Professional Development Project under the Science Achievement Scholarship of Thailand. This work is supported by grants from National Astronomical Research Institute of Thailand (NARIT). The data used in this work are based on observations obtained with XMM-Newton, an ESA science mission with instruments and contributions directly funded by ESA

Member States and NASA.

References

- [1] Abdalla H *et al* 2017 *Astron. Astrophys.* **606** 59–69
- [2] Aharonian F A, Coppi P S and Völk H J 1994 *Astrophys. J.* **423** 5–8
- [3] Eungwanichayapant A and Aharonian F 2009 *Int. J. Mod. Phys.* **18** 911–27
- [4] Aharonian F A *et al* 2001 *Astron. Astrophys.* **366** 746–51
- [5] Neronov A, Semikoz D V, Tinyakov P G and Tkachev I I 2011 *Astron. Astrophys.* **526** 90–3
- [6] Kueathan A, Luangtip W, Maithong W and Eungwanichayapant A 2018 *J. Phys.: Conf. Ser.* **1144** 012131–4
- [7] Aharonian F *et al* 2002 *Astron. Astrophys.* **384** 23–6
- [8] Aharonian F *et al* 2003 *Astron. Astrophys.* **403** 523–8
- [9] European Space Agency (ESA) *XMM-Newton Science Archive* Online: <https://nxs.a.esac.esa.int/nxs.a-web>
- [10] Eungwanichayapant A, Aharonian F A and Voelk H J 2005 *Proc. the 9th Asian-Pac. Regional IAU Meet.* pp 145–6
- [11] Snowden S and Kuntz K 2014 *Cookbook for Analysis Procedures for XMM-Newton Epic Observations of Extended Objects and the Diffuse Background* Online: <https://heasarc.gsfc.nasa.gov/docs/xmm/esas/cookbook/xmm-esas.html>
- [12] George I M 1995 *ADDSPEC(Aug95)* Online: <https://heasarc.gsfc.nasa.gov/ftools/caldb/help/addspec.txt>
- [13] National Aeronautics and Space Administration (NASA) *Xspec: An X-ray Fitting Spectral Package* Online: <https://heasarc.gsfc.nasa.gov/xanadu/xspec/>
- [14] Kuntz K D and Snowden S L 2008 *Astron. Astrophys.* **478** 575–96
- [15] National Aeronautics and Space Administration (NASA) *XMM-Newton Users Handbook* Online: <https://heasarc.nasa.gov/docs/xmm/uhb/onaxisxraypsf.html>
- [16] Tavecchio F, Ghisellini G, Ghirlanda G, Foschini L and Maraschi L 2010 *Mon. Notices Royal Astron. Soc.* **401** 1570–86
- [17] European Space Agency (ESA) *Background Analysis* Online: <https://www.cosmos.esa.int/web/xmm-newton/background>

PAPER · OPEN ACCESS

The search for X-ray emission from electron/positron pair halos using the *XMM-Newton* observatory

To cite this article: A Kueathan *et al* 2018 *J. Phys.: Conf. Ser.* **1144** 012131

View the [article online](#) for updates and enhancements.



IOP ebooks™

Bringing you innovative digital publishing with leading voices to create your essential collection of books in STEM research.

Start exploring the collection - download the first chapter of every title for free.

The search for X-ray emission from electron/positron pair halos using the *XMM-Newton* observatory

A Kueathan¹, W Luangtip¹, W Maithong² and
 A Eungwanichayapant³

¹ Department of Physics, Faculty of Science, Srinakharinwirot University,
 114 Sukhumvit 23, Bangkok 10110, Thailand

² Department of Physics and General Science, Faculty of Science and Technology, Chiang Mai
 Rajabhat University, Chiang Mai 50300, Thailand

³ School of Science, Mae Fah Luang University, Chiang Rai 57100, Thailand

E-mail: wasutep@g.swu.ac.th

Abstract. An electron/positron pair halo is formed by electromagnetic cascades that initiate when high energy gamma-rays from extragalactic sources – i.e. Blazar AGN – interact with the cosmic infrared background (CIB), and are then absorbed via the electron/positron pair production process. The high energy electron/positron pairs produced could up-scatter the cosmic microwave background (CMB) and become gamma rays which can interact with CIB again. Thus, the process could happen continuously until the produced gamma-rays have insufficient energy to interact with the CIB. Indeed, given the presence of intergalactic magnetic field, the produced electron/positron pairs could gyrate before scattered with the CMB photons so that they emit X-ray photons via the synchrotron radiation process. In this work, we determine whether the predicted X-ray photons emitted from the halo can be detected by the current generation X-ray observatory: *XMM-Newton*. The Spectral Energy Distributions (SEDs) of the synchrotron radiation of the pair halo predicted to be obtained from the AGN H1426+428 are simulated by the Monte Carlo simulations method; these are used as a source model for simulating observed spectra. The spectra of the halo virtually observed by *XMM-Newton* are generated in three different regions: the inner region, outer region and the region out of the *XMM-Newton's* field of view. The resulting spectra suggest that the outer region spectra could provide the best opportunity to detect and confirm the existence of electron/positron pair halos.

1. Introduction

An electron/positron pair halo was first proposed in 1994 by Aharonian [1]; it is formed by electromagnetic cascades that initiate when high energy gamma-rays from an AGN are absorbed by the cosmic infrared background (CIB) via the electron/positron pair production process. The produced high energy electron/positron pairs could up-scatter the cosmic microwave background (CMB) and become gamma rays which can interact with the CIB again. Thus, the process can occur continuously until the produced gamma-rays have insufficient energy to interact with the CIB. According to the model, the calculated size of electron/positron pair halos is in the order of ~ 10 Mpc and appear to enclose the central AGN [2]; the gamma rays which have energy in the range of 0.1 - 10 TeV are predicted to be emitted from the halo [1]. Indeed, given the presence of the intergalactic magnetic field (IGMF), the produced electron/positron pairs could gyrate

before being scattered with the CMB photons so that the halo also emits X-ray photons via the synchrotron radiation process [3]. Importantly, the discovery of pair halo emission would provide a new tool to probe the CIB and the IGMF around AGNs. The first attempt to observe the pair halo was in 2001. The High-Energy Gamma Ray Astronomy (HEGRA) team [4] attempted to detect gamma rays from the halo using the its gamma-ray telescope; however, no detection was claimed. Later, in 2009, Eungwanichayapant and Aharonian [5] further calculated the angular distribution of the gamma ray emission; the detectable distance of the AGN has been proposed. A year later, Ando and Kusendo [6], reported the detection of the electron/positron pair halo from the AGN which has a magnetic field of ~ 1 fG. However, it was argued by Neronov [7] that the detection is artificial due to systematic errors of the telescope instruments. Nevertheless, the SEDs and angular distribution of the halo in the X-ray waveband were proposed in 2011 [3]. Until now, there has still not yet been an attempt to search for such an emission in this regime. Among the current generation of X-ray observatories, *XMM-Newton* cameras – EPIC pn, MOS1 and MOS2¹ – are the best instruments for hunting the halo X-ray emission, given that they have the largest effective areas [8]. In this research, we will demonstrate whether the current generation of X-ray telescope – *XMM-Newton* – will be able to detect such an emission. The paper is laid out as follows. In Section 2, we explain how the SEDs in the X-ray waveband are generated; then the method used to simulate *XMM-Newton* spectra is shown in Section 3. We then discuss and conclude these in light of the obtained results in Section 4.

2. Simulation of SEDs

In this work, we simulated the X-ray SEDs expected to be obtained from the AGN H1426+428 which is a BL Lacertae object with a luminosity in the order of 10^{45} erg s⁻¹ [9] and located at $z = 0.129$. This object has been observed the absorption feature in the gamma-ray spectra [10] and is expected to have a gamma pair halo [11]. Given the source properties, we simulated the X-ray SEDs using parameters similar to that of the AGN: the monoenergetics, intrinsic gamma ray photon energy of 100 TeV, source luminosity of 10^{45} erg s⁻¹ and a magnetic field of $1 \mu\text{G}$. The SEDs were calculated using Monte Carlo simulations following the model of Eungwanichayapant et al. 2011 [3]. All electromagnetic cascades from the AGN were simulated to get the energy and spatial distributions of the electrons/positrons to compute the energy and angular distributions of the X-ray photons from the pair halo. However, to search for the X-ray emission from the halo using the *XMM-Newton* observatory, we should consider the X-ray flux from the central AGN. Therefore, in this work we separated the observed radiation regions of the AGN H1426+428 into three regions: region A, B and C. Region A covers the angular distance from $0 - 0.133$ degrees. This is the area that the contamination of X-ray emission from the AGN could dominate the X-ray emission from the pair halo. Region B covers the angular distance from $0.133 - 0.200$ degrees. This part is still in the field of view of *XMM-Newton* but sufficiently far away that we can ignore the AGN X-ray emission. Region C covers the angular distance from 0.200 to infinite degree which is an area outside the telescope's field of view.

The simulated SED of the X-ray emission from each region is shown in figure 1.

3. Simulation of *XMM-Newton* spectra

In order to simulate the halo spectra of the AGN H1426+428, assuming that the source is observed by the *XMM-Newton* telescope, the three SEDs generated in Section 2 were used as the emission models of the H1426+428 halo. The simulation was performed by the X-ray spectral fitting package (XSPEC) version 12.9.² Firstly, the SED data obtained from Section 2 was converted into the FIT file format (i.e. XSPEC table models) to make them readable by XSPEC.

¹ https://xmm-tools.cosmos.esa.int/external/xmm_user_support/documentation/uhb/epic.html

² <https://heasarc.gsfc.nasa.gov/xanadu/xspec/>

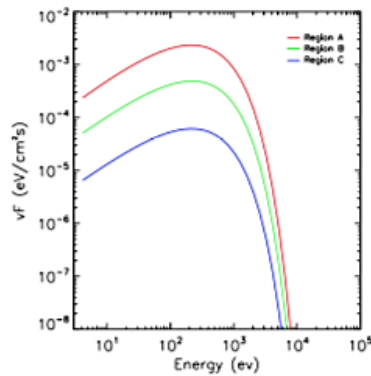


Figure 1. The pair halo X-ray SEDs simulated by assuming the monoenergetics, intrinsic gamma ray photon energy of 100 TeV, source luminosity of 10^{45} erg s^{-1} and the magnetic field of $1 \mu G$.

In addition, we also added the absorption column (N_H) of 1.11×10^{20} atoms cm^{-2} into all the SED models to account for galactic absorption along the direction to the AGN H1426+428 [12]. Thus, the multiplicative models of N_H absorption and SED were used as a basis for the observed spectral simulations. After the models were well defined in XSPEC, the *XMM-Newton* spectra were simulated using the XSPEC command FAKEIT for all three *XMM-Newton* detectors: pn, MOS1 and MOS2; while the Response Matrix File (RMF) and Ancillary Response File (ARF) of each instrument at the current telescope cycle used in the simulation were obtained from the observatory's official webpage.³ The spectra were generated using counting statistic, assuming the source exposure time of 500 ks.

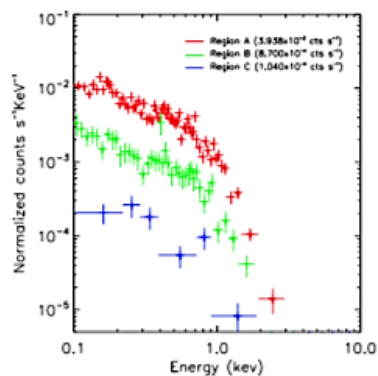


Figure 2. The simulated pn spectra of the pair halo obtained from the AGN H1426+428. The observed count rates are also shown in the plot legend.

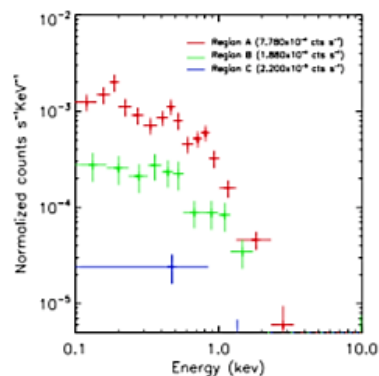


Figure 3. As for figure 2., the simulated MOS spectra.

The simulated spectra as well as the corresponding observed count rate of the AGN H1426+428 that is virtually observed by *XMM-Newton* are shown in figure 2 (for pn spectra) and figure 3 (for MOS1 and MOS2 spectra). As expected, the observed halo flux from region A is highest while regions B and C are relatively in the middle and lowest respectively, since

³ <https://heasarc.gsfc.nasa.gov/docs/xmm/xmmhp-prop-tools.html>

the halo flux should be reduced as a function of the distance from the central AGN. Assuming that the AGN H1426+428 is simultaneously observed by *XMM-Newton* pn, MOS1 and MOS2 detectors for 500 ks, a total photon counts of 2700, 580 and 70 should be expected to be obtained from regions A, B and C, respectively.

4. Discussion and Conclusion

In this work, the X-ray SEDs expected to be emitted from the AGN H1426+428 halo were calculated by Monte Carlo simulations following the proposed model [3]. Then, the observed spectra of the halo from the three different regions – region A, B and C – were simulated. Obviously, most of the halo X-ray photons (2700 counts, ~80%) could be detected in region A, whilst only 580 counts (~17%) and 70 counts (~3%) were detected in regions B and C, respectively. In other words, up to ~97% of the halo photons would fall into the *XMM-Newton* detectors. In fact, given that up to 2700 photon counts would be detected in region A, this might be a region with good potential to search for the halo X-ray emission. However, since the AGN is also located in this region, the halo photons could be much diluted by the AGN photons; indeed, more than ten million counts could be obtained from the AGN so that it is difficult to resolve the halo photons from that of the AGN. Although it is not impossible to perform an analysis in this region, the analytical methods that might be used to distinguish the halo X-ray photons from the AGN emission are outside the scope of this work and are not discussed here.

Given the complication of the analysis in region A, another chance to detect the halo emission could lie in region B. Although only 580 halo photons were detected in this region, we could be confident that the spectra will not be contaminated by the AGN emission. Thus, by carefully subtracting the instrument background from the observed spectra of the AGN H1426+428 in region B, the resulting spectra should provide the opportunity to detect and confirm the existence of electron/positron pair halos.

Acknowledgments

AK acknowledges financial support in the form of funding for a postgraduate studentship from the Research Professional Development Project under the Science Achievement Scholarship of Thailand. WL and AE would also like to thank the National Science and Technology Development Agency for the research funding support that they offered.

References

- [1] Aharonian F A, Coppi P S and Völk H J 1994 *Astrophys. J.* **423** L5–L8
- [2] Eungwanichayapant A, Aharonian F A and Voelk H J 2005 *APRIM 2005 Proceedings of the 9th Asian-Pacific Regional IAU Meeting* pp 145–146
- [3] Eungwanichayapant A, Maithong W and Ruffolo D 2011 *Proc. Int. Astron. Union* vol 7 pp 417–419
- [4] Aharonian F A *et al.* 2001 *Astron. Astrophys.* **366** 746
- [5] Eungwanichayapant A and Aharonian F 2009 *Int. J. Mod. Phys.* **18** 911
- [6] Ando S and Kusenko A 2010 *Astrophys. J.* **722** L39–L44
- [7] Neronov A, Semikoz D V, Tinyakov P G and Tkachev I I 2011 *Astron. Astrophys.* **526** A90
- [8] Eungwanichayapant A, Luangtip W, Maithong W and Ruffolo D in prep
- [9] Razzaque S, Dermer C D and Finke J D *Astrophys. J.* 196 ISSN 0004-637X
- [10] H E S S Collaboration 2017 *Astron. Astrophys.* **606**
- [11] Abramowski A *et al.* *Astron. Astrophys.* A145 ISSN 0004-6361 (*Preprint* 1401.2915)
- [12] Kalberla P M W *et al.* 2005 *Astron. Astrophys.* **440** 775–782 (*Preprint astro-ph/0504140*)

REFERENCES

- Abdalla, H., Abramowski, A., Aharonian, F., Benkhali, F. A., Akhperjanian, A., Andersson, T., . . . Backes, M. (2017). Gamma-ray blazar spectra with HESS II mono analysis: The case of PKS 2155-304 and PG 1553+113. *Astronomy & Astrophysics*, 600, A89.
- Abramowski, A., Acero, F., Aharonian, F., Akhperjanian, A., Anton, G., Balenderan, S., . . . Tjus, J. B. (2013). Measurement of the extragalactic background light imprint on the spectra of the brightest blazars observed with HESS. *Astronomy & Astrophysics*, 550, A4.
- Abramowski, A., Aharonian, F., Benkhali, F. A., Akhperjanian, A., Angüner, E., Anton, G., . . . Barnacka, A. (2014). Search for extended γ -ray emission around AGN with HESS and Fermi-LAT. *Astronomy & Astrophysics*, 562, A145.
- Aharonian, F., Akhperjanian, A., Barrio, J., Bellicke, M., Bernlöhr, K., Börst, H., . . . Cornils, R. (2002). TeV gamma rays from the blazar H 1426+428 and the diffuse extragalactic background radiation. *Astronomy & Astrophysics*, 384(3), L23-L26.
- Aharonian, F., Akhperjanian, A., Barrio, J., Bernlöhr, K., Börst, H., Bojahr, H., . . . Denninghoff, S. (2001). Evidence for TeV gamma ray emission from Cassiopeia A. *Astronomy & Astrophysics*, 370(1), 112-120.
- Aharonian, F., Coppi, P., & Völk, H. (1993). Very High Energy Gamma-Rays from AGN: Cascading on the Cosmic Background Radiation Fields and the Formation of Pair Halos. *arXiv preprint astro-ph/9312045*.
- Aharonian, F., Konopelko, A., Völk, H., & Quintana, H. (2001). 5@5—a 5 GeV energy threshold array of imaging atmospheric Cherenkov telescopes at 5 km altitude. *Astroparticle Physics*, 15(4), 335-356.
- Alonso, M. F., Supanitsky, A. D., & Rovero, A. C. (2015). Detecting extended gamma-ray emission with the next generation Cherenkov telescopes. *arXiv preprint arXiv:1509.01289*.
- Ando, S. i., & Kusenko, A. (2010). Evidence for gamma-ray halos around active galactic

- nuclei and the first measurement of intergalactic magnetic fields. *The Astrophysical Journal Letters*, 722(1), L39.
- Chen, W., Buckley, J. H., & Ferrer, F. (2015). Search for GeV γ -ray pair halos around low redshift blazars. *Physical Review Letters*, 115(21), 211103.
- Coppi, P. S., & Aharonian, F. A. (1997). Constraints on the very high energy emissivity of the universe from the diffuse GeV gamma-ray background. *The Astrophysical Journal Letters*, 487(1), L9.
- Costamante, L., Aharonian, F., Ghisellini, G., & Horns, D. (2003). The SED of the TeV BLLac 1ES 1426+ 428 after correction for the TeV–IR absorption. *New Astronomy Reviews*, 47(6-7), 677-680.
- Eungwanichayapant, A. (2003). *Giant Pair Halos Surrounding Non-thermal Extragalactic Objects*.
- Eungwanichayapant, A., & Aharonian, F. (2009). Very High Energy Gamma Rays from e^\pm Pair Halos. *International Journal of Modern Physics D*, 18(06), 911-927.
- Eungwanichayapant, A., Luangtip, W., Maithong, W., & Ruffolo, D. (2019). X-Rays from e^\pm Pair Halos. *The Astrophysical Journal*, 880(2), 124.
- Eungwanichayapant, A., Maithong, W., & Ruffolo, D. (2011). Synchrotron radiation from giant e^\pm pair halos. *Proceedings of the International Astronomical Union*, 7(S284), 417-419.
- Finke, D. (2010). *European integration and its limits: intergovernmental conflicts and their domestic origins*: ECPR Press.
- Finke, J. D., Razzaque, S., & Dermer, C. D. (2010). Modeling the extragalactic background light from stars and dust. *The Astrophysical Journal*, 712(1), 238.
- Ghisellini, G., Tavecchio, F., Foschini, L., Ghirlanda, G., Maraschi, L., & Celotti, A. (2010). General physical properties of bright Fermi blazars. *Monthly Notices of the Royal Astronomical Society*, 402(1), 497-518.
- Gould, R., & Rephaeli, Y. (1978). The effective penetration distance of ultrahigh-energy electrons and photons traversing a cosmic blackbody photon gas. *The Astrophysical Journal*, 225, 318-324.

Gould, R. J., & Schröder, G. (1966). Opacity of the universe to high-energy photons.

Physical Review Letters, 16(6), 252.

Johnson, M., Cruddace, R., Ulmer, M., Kowalski, M., & Wood, K. (1983). A survey by HEAO 1 of clusters of galaxies. III-The complete Abell catalog. *The Astrophysical Journal*, 266, 425-445.

Kueathan, A., Luangtip, W., & Eungwanichayapant, A. (2019). *Searching for the electron/positron pair halo of the Blazar H1426+ 428 using XMM-Newton*. Paper presented at the Journal of Physics: Conference Series.

Kueathan, A., Luangtip, W., Maithong, W., & Eungwanichayapant, A. (2018). *The search for X-ray emission from electron/positron pair halos using the XMM-Newton observatory*. Paper presented at the Journal of Physics: Conference Series.

Kuntz, K., & Snowden, S. (2008). The EPIC-MOS particle-induced background spectra. *Astronomy & Astrophysics*, 478(2), 575-596.

Marshall, N., & Ricketts, M. J. (1980). Determination of a binary period for the variable X-ray source A1907+ 09. *Monthly Notices of the Royal Astronomical Society*, 193(1), 7P-13P.

Mazin, D. (2019). The Cherenkov Telescope Array. *arXiv preprint arXiv:1907.08530*.

Nandra, K., Barcons, X., Barret, D., Fabian, A., den Herder, J., Piro, L., & Watson, M. (2014). ATHENA: The Advanced Telescope for High-Energy Astrophysics. *Mission proposal*, <http://www.the-athena-x-ray-observatory.eu>.

Neronov, A., Semikoz, D., Tinyakov, P., & Tkachev, I. (2011). No evidence for gamma-ray halos around active galactic nuclei resulting from intergalactic magnetic fields. *Astronomy & Astrophysics*, 526, A90.

Nikishov, A. (1961). Absorption of High Energy Photons in the Universe. *Zhur. Eksptl'. i Teoret. Fiz.*, 41.

Ong, R. A., & Collaboration, V. (2014). Highlights from VERITAS on VHE gamma-ray sources in our Galaxy. *Advances in Space Research*, 53(10), 1483-1491.

Remillard, R., Tuohy, I., Brissenden, R., Buckley, D., Schwartz, D., Feigelson, E., & Tapia, S. (1989). Two X-ray-selected BL Lacertae objects observed with the HEAO 1

- scanning modulation collimator. *The Astrophysical Journal*, 345, 140-147.
- Schlickeiser, R. (1996). Models of high-energy emission from active galactic nuclei. *Astronomy and Astrophysics Supplement Series*, 120, 481-489.
- Stecker, F. W., De Jager, O. C., & Salamon, M. (1992). TeV gamma rays from 3C 279-A possible probe of origin and intergalactic infrared radiation fields. *The Astrophysical Journal*, 390, L49-L52.
- Strüder, L., Briel, U., Dennerl, K., Hartmann, R., Kendziorra, E., Meidinger, N., . . . Bornemann, W. (2001). The European photon imaging camera on XMM-Newton: the pn-CCD camera. *Astronomy & Astrophysics*, 365(1), L18-L26.
- Tkaczyk, W., Wdowczyk, J., & Wolfendale, A. (1975). Extragalactic heavy nuclei in cosmic rays? *Journal of Physics A: Mathematical and General*, 8(9), 1518.
- Turner, M. J., Abbey, A., Arnaud, M., Balasini, M., Barbera, M., Belsole, E., . . . Boer, M. (2001). The European photon imaging camera on XMM-Newton: the MOS cameras. *Astronomy & Astrophysics*, 365(1), L27-L35.
- Wood, R. D., & Hutchinson, F. (1984). Non-targeted mutagenesis of unirradiated lambda phage in Escherichia coli host cells irradiated with ultraviolet light. *Journal of molecular biology*, 173(3), 293-305.

VITA

NAME ATCHARA KUEATHAN

DATE OF BIRTH 15 MAY 1994

PLACE OF BIRTH UBONRACHATHANI

INSTITUTIONS ATTENDED 2013-2016 Bachelor of Science in Physics Program
From Srinakharinwirot University
2016 Master of Science in Physics Program
From Srinakharinwirot University

HOME ADDRESS 48/1 Soi Ratchada Phisek 20, Sam Saen Nok, Huai Khwang,
Bangkok, 10320

PUBLICATION 2018 The search for X-ray emission from electron/positron
pair halos using the XMM-Newton observatory
2019 Searching for the electron/positron pair halo of the
Blazar H1426+428 using XMM-Newton

AWARD RECEIVED -

